Master's thesis

NTNU
Norwegian University of Science and Technology
Faculty of Engineering
Department of Mechanical and Industrial Engineering

Didrik Fjeld Elset

Crane Payload Stabilization using Lagrangian Kinematics and Euler Angles

Position Control of Crane Payload with Moving Attachment Point and Hoisting

Master's thesis in Mechanical Engineering
Supervisor: Olav Egeland
June 2019

NTNU
Kunnskap for en bedre verden

Didrik Fjeld Elset

Crane Payload Stabilization using Lagrangian Kinematics and Euler Angles

Position Control of Crane Payload with Moving Attachment Point and Hoisting

Master’s thesis in Mechanical Engineering
Supervisor: Olav Egeland
June 2019

Norwegian University of Science and Technology
Faculty of Engineering
Department of Mechanical and Industrial Engineering

NTNU
Kunnskap for en bedre verden

Contents

List of Figures

List of Tables

Preface

This is the concluding Master's thesis written with guidance from the department of Mechanical Engineering at the Norwegian University of Science and Technology (NTNU), Trondheim. The work was carried out from January to June 2019.

My specialisation has been Production and Quality Engineering with Manufacturing Technology as my main profile. I would like to thank my supervisor Professor Olav Egeland who has been very helpful over the course of this project. Without his knowledge and ability to explain the matter this project would not be possible to complete.

I would also like to thank PhD candidate Geir Ole Tysse for his helpful insights in crane theory and for his Simulink and Matlab assistance. Him opening his office door to me was truly appreciated.

A thank you should also be sent to my coworkers in the office who have been open to discussions and contributed with a great working environment.

Last but not least I would like to thank my parents who have been supporting me my whole life.

Trondheim, June 11, 2019

Didrik Fjeld Elset

Abstract

This thesis is testing a controller's ability to stabilize a payload while moving along a preset trajectory for a wide selection of scenarios. It presents the equations of motion for a spherical pendulum with moving attachment point by using Euler angles and Lagrangian kinematics. Damping of the pendulum payload is done by feedback control and the stability analysis is done with Lyapunov's second method and LaSalle's invariance principle. The damping is then expanded into a feedback system consisting of a position loop and a velocity loop to ensure the stability of the pendulum alongside with the desired movement of the attachment point. A second velocity loop is added to prevent the need for measuring the acceleration of the attachment point.

Further, the attachment point is set as the end-effector of a 3 DOF knuckle boom crane. Rotation and transformation matrices, Denavit-Hartenberg convention, and the Jacobian are used to describe the cranes kinematics. The relationship between the joint angles and the linear actuators are found using trigonometry. A trajectory is planned to ensure a smooth path from an initial position to a desired final position within a preset amount of time. The trajectory is chosen to resemble a potential crane routine with hoisting, motion from one position to another in the horizontal plane, and lowering the payload to its initial height.

The results are presented through plots using Simulink and Matlab for a magnitude of parameter values and trajectories. The robustness of the controller is strong for most of the scenarios which make a promising basis for a practical implementation.

Sammendrag

Denne oppgaven har som formål å teste en kontrollers evne til å stabilisere en nyttlast samtidig som kranen skal bevege seg i en forhåndsinnstilt bane for en rekke ulike situasjoner. Den presenterer bevegelsesligningene for en sfærisk pendel med et bevegelig opphengspunkt ved bruk av Euler-vinkler og Lagrange-mekanikk. Dampingen av svingningene til nyttelasten er gjort ved en tilbakekoblet kontroller og systemets stabilitet er beskrevet ved bruk av Lyapunovs andre metode i samspill med LaSalles teorem for invariante mengder. Dempingen blir så ekspandert til et tilbakekoplet system der både opphengspunktets posisjon og hastighet blir matet tilbake til kontrolleren og brukt sammen med proporsjonalkonstanter for å sikre kranens bevegelse i tillegg til stabilisering av pendelen. Grunnet praktiske utfordringer ved å måle opphengspunktets akselerasjon blir en hastighetssløyfe introdusert.

Videre blir kontrolleren koblet sammen med en såkalt “knuckle boom-kran” eller jibb-kran med tre frihetsgrader. Kinematikken til kranen er beskrevet gjennom bruk av robotkinematikk, Denavit-Hartenberg-konvensjonen og Jacobian til kranen. Forholdet mellom vinklene i leddene til kranen og de lineære aktuatorene er funnet gjennom bruk av cosinussetningen og andre trigonometriske forhold. En bane opphengspunktet skal følge fra en initiell posisjon til et endepunkt innen en gitt tid. Denne banen er valgt slik at den skal ligne en potensiell løfteoperasjon med et begynnende løft etterfulgt av en bevegelse i det horisontale planet, før den senkes til sin initielle høyde.

Resultatene er presentert gjennom simuleringer gjort i Simulink og Matlab for en rekke parameterverdier og baner. Kontrolleren viser seg å være robust for de fleste scenarioer og danner et lovende grunnlag for integrering i en fysisk kran.

Chapter 1.

Introduction

1.1. Background

Heavy-lifting cranes are utilized in factories, harbours and oil platforms all over the world. They are often involved in hazardous environments and the swaying and unintended movement of the payload is a constant challenge and potential hazard. Disturbances like waves, wind and other noise can make a crane operation tedious and dangerous. The reduction of these undesired motions is an important task by many means.

For a crane to be able to perform its various task like gripping, lifting, and transport in a feasible manner is it paramount that the payload stay in an easily controllable position. A way to achieve this is by adding passive damping devices to the system like dashpots and viscous damping[2]. Active approaches are also common where feedback or feed-forward systems are integrated to ensure stability[16]. Fuzzy control systems have been thoroughly tested with promising results [25][24][8], but will not be tested in this thesis.

Several mathematical models have been made to describe cranes, and the use of Lagrangian equation of motion has been used especially for gantry cranes [19][15]. Knuckle boom cranes are typically used on ships or for construction [16] and there has been research done on these, specifically[20][5][21], also with the use of Lagrangian equations of motion [4]. In [6], screw theory is used to perform dynamic modelling and force analysis on a knuckle boom crane which is an approach that will not be reviewed here.

A crane operator needs to be extensively trained and highly skilled to manually steer the crane without getting unwanted motion in the payload. It is not uncommon that an assigned task is aborted in order to prevent possible hazardous situations [16]. A controller that can ensure efficient damping of the payload and at the same time get the payload to its desired location would decrease the duration of each operation, and therefore, work more efficiently and therefore save money. In addition to this the probability of accidents would decrease, and lives could be saved.

1.2. Objective

The objectives of this thesis are

- Describe the theory behind the damping of oscillations excited by a spherical pendulum.
- Describe the the motion of a 3 DOF knuckle boom crane using forward and backward kinematics.
- Create a controller that damps the oscillations as well as follows a desired trajectory.
- Test the robustness of the controller on various trajectories and parameter values.
- Present and discuss the results using Simulink/Matlab
- Present potential further developments on the controller.

1.3. Outline

The thesis is focusing on the theory behind and testing of the controller and a substantial part of it is used to describe the mathematics behind the system and present the results for a wide range of situations.

- Chapter 1 presents the background and objective of this thesis.
- Chapter 2 describes the theory of Lagrangian equations of motion, Lyapunov stability analysis, basic robotics, and trajectory planning.
- Chapter 3 describes the modeling and control of this particular system using Lagrangian kinematics, Lyapunov stability analysis, damping by feedback control for a simple and a spherical pendulum. The Lagrangian is executed for all scenarios, progressively adding new features to the system.
- Chapter 4 describes the knuckle boom crane, using Denavit-Hartenberg, homogeneous transformation matrix and the Jacobian.
- The results are described and presented in Chapter 5 where a multitude of plots are shown to explore the range of which the controller is working.

- The results from Chapter 5 are discussed in Chapter 6.
- Chapter 7 presents and discusses the Simulink model with reference to the matlab files in the Appendix A.
- Finally, concluding remarks and a discussion regarding potential future work is presented in Chapter 8.

Chapter 2.

Theory

2.1. Lagrangian Equations of Motion

Lagrangian analysis [12] is used to generate the dynamic equations, as in [14] where the energy of mechanical systems makes the base for computation. Let F_i be the force applied to the ith particle of a system of particles which obey Newton's second law. This law cam them be written as

$$F_i = m_i \ddot{r}_i \quad r_i \in \mathbb{R}^3, \quad i = 1, ..., n \tag{2.1}$$

where m_i and r_i are the particle's mass and position, respectively, and the total amount of particles is n. Now, to apply this on an object consisting of an assembling of these particles, with limited degrees of freedom, are some constraints added between the positions of the particles. Each constraint is represented by a function $g_i : \mathbb{R}^{3n} \to \mathbb{R}$ such that

$$g_j(r_1, ...r_n) = 0 \quad j = 1, ..., k. \tag{2.2}$$

A constraint of this type is called a holonomic constraint. It is applied to the system through constraint forces, which are determined in a way that ensures that Equation 2.2 is satisfied at all times. If the constraint is viewed as a smooth surface in $\mathbb{R}^n$, the constraint forces are normal to this and restrict the velocity of the system to be tangential to the surface. Thus,

$$\begin{bmatrix} m_1 I & & 0 \\ & \ddots & \\ 0 & & m_n I \end{bmatrix} \begin{bmatrix} \ddot{r}_i \\ \dots \\ \ddot{r}_n \end{bmatrix} + \sum_{j=1}^{k} \Gamma_j \lambda_j, \tag{2.3}$$

where $\Gamma_1, ...\Gamma_k \in \mathbb{R}^{3n}$ are a basis for the constraint forces and λ_j is the scale factor and is called the Lagrangian multiplier. This is formally found by solving the $3n + k$ equation in Equation 2.2 and Equation 2.3 for the $3n + k$ variables

$r \in \mathbb{R}^{3n}$ and $\lambda \in \mathbb{R}^k$. This approach is demanding computationally, it is therefore common to describe the motion of the system in terms of a smaller set of variables. Consider a system of n particles and k constraints. The desired set is of $m = 3n - k$ variables $q_1, ..., q_m$ and smooth functions $f_1, ...f_n$. The q_i's are called the generalized coordinates for the system.

The Lagrangian, $\mathcal{L}$, is defined as the difference between the kinetic and the potential energy of a system, K and U, respectively.

$$\mathcal{L}(q, \dot{q}) = K(q, \dot{q}) - U(q) \tag{2.4}$$

both written in generalized coordinates. Lagrange's equations of motion with generalized coordinates $q \in \mathbb{R}^m$ are given by

$$\frac{\mathrm{d}}{\mathrm{d}t}\left(\frac{\partial \mathcal{L}}{\partial \dot{q}_i}\right) - \frac{\partial \mathcal{L}}{\partial q} = \Upsilon_i \quad i = 1, ..., m \tag{2.5}$$

where Υ_i is the external force acting on the ith element. If the system has no constraints q is considered components of r making $K = \frac{1}{2} m_i \dot{\boldsymbol{r}}^2$, where $\boldsymbol{r}$ is on a vector form and Equation 2.5 is reduced to Equation 2.1. Then, Equation 2.5 can be written as

$$\frac{\mathrm{d}}{\mathrm{d}t}\left(\frac{\partial \mathcal{L}}{\partial \dot{\boldsymbol{r}}}\right) = \frac{\partial \mathcal{L}}{\partial \boldsymbol{r}} + \Upsilon_i \tag{2.6}$$

where the left side of the equation is the derivative of the momentum, and the right side is the applied forces. This is Newton's second law in generalized coordinates.

2.2. Lyapunov Stability

Lyapunov proposed two methods for stability in [13]. The first method defines three types of stability of an equilibrium for a autonomous nonlinear dynamic system. Conceptually it states that an equilibrium is Lyapunov stable if a solution starts a certain distance from the equilibrium will it always remain within this distance. It is asymptotically stable if the solution, in addition to being Lyapunov stable, converges towards the equilibrium. Finally, the solution is exponentially stable if it is asymptotically stable and converges faster than a particular known rate.

The second method uses the so-called Lyapunov function. Consider a system $\dot{\boldsymbol{x}} = f(\boldsymbol{x})$, where $\boldsymbol{x}$ is a vector of variables with an equilibrium point at $\boldsymbol{x} = 0$.

Then, consider a function $V(\boldsymbol{x}) : \mathbb{R}^n \rightarrow \mathbb{R}$ such that

$$\begin{aligned} V(\boldsymbol{x}) &= 0, && \text{if and only if} \quad \boldsymbol{x} = 0 \\ V(\boldsymbol{x}) &> 0, && \text{if and only if} \quad \boldsymbol{x} \neq 0 \\ \dot{V}(\boldsymbol{x}) &\leq 0, && \text{for} \quad \boldsymbol{x} \leq 0 \end{aligned} \tag{2.7}$$

then the system is Lyapunov stable and the function $V(\boldsymbol{x})$ is called the Lyapunov function. The system is asymptotically stable if $\dot{V} < 0$ for $x \neq 0$.

There is a way to show that a system is asymptotically stable, even though $\dot{V}(\boldsymbol{x}) = 0$ when $\boldsymbol{x} = 0$. Again, consider a system where $\dot{\boldsymbol{x}} = f(\boldsymbol{x})$, where $\boldsymbol{x}$ is a vector of variables and $f(0) = 0$. Let $V(\boldsymbol{x})$ be a differentiable function with a continuous derivative, a so-called C^1 function, such that $\dot{V} \leq 0$ for all x. Now, a union of trajectories that is made out of the set $\{\boldsymbol{x} : \dot{V}(\boldsymbol{x}) = 0\}$ is defined as I. If it is shown that the only trajectory within I is the trivial case where $\boldsymbol{x} = 0$, then the origin is asymptotically stable. The requirements of $V(\boldsymbol{x}) > 0$ if and only if $\boldsymbol{x} \neq 0$ and $V(0) = 0$ must still satisfied for this to be applicable. This theorem is called LaSalle's invariance principle [10].

2.3. The Rotation Matrix and the Homogeneous Transformation Matrix

A rotation matrix is a common method to describe a transformation from one coordinate system to another with the same origin and is widely used in robotics [22][9]. The rotations are described as an angle about the respective axes. Rotations about the x, y, and z axis are defined as in[7]

$$\boldsymbol{R}_x(\phi_x) = \begin{bmatrix} 1 & 0 & 0 \\ 0 & c_x & -s_x \\ -0 & s_x & c_x \end{bmatrix} \tag{2.8}$$

$$\boldsymbol{R}_y(\phi_y) = \begin{bmatrix} c_y & 0 & s_y \\ 0 & 1 & 0 \\ -s_y & 0 & c_x \end{bmatrix} \tag{2.9}$$

$$\boldsymbol{R}_z(\phi_z) = \begin{bmatrix} c_z & -s_z & 0 \\ s_z & c_z & 0 \\ 0 & 0 & 1 \end{bmatrix} \tag{2.10}$$

If the origin of the two frames are in different position, a translation has to be done in addition to the rotation. This translation, often called $\boldsymbol{r}$ is the vector that represents the origin of the new frame in the coordinates of the base frame.

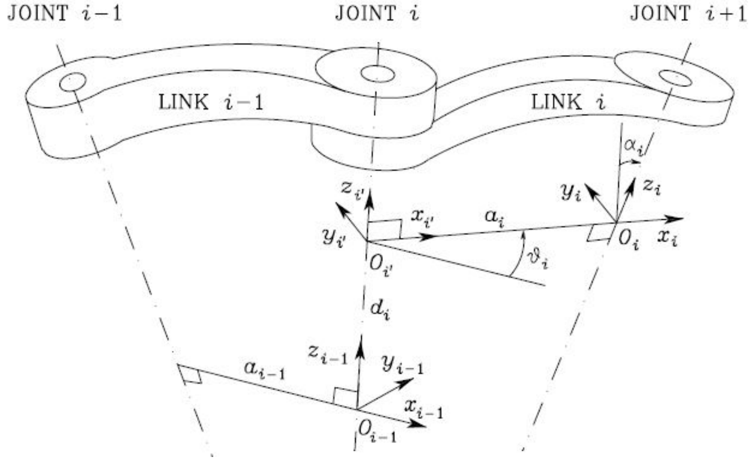

Figure 2.1.: Denavit-Hartenberg kinematic parameters [18]

Consider a base frame $\{a\}$ which is translated and rotated to frame $\{b\}$ can the transformation be described as $\boldsymbol{t}_b^a = \boldsymbol{r}_b^a + \boldsymbol{R}_b^a$ [18]. The homogeneous transformation matrix is a matrix that describes a transformation from one frame to another. A transformation from frame a to b, that is a rotation $\boldsymbol{R}_b^a$ and a translation $\boldsymbol{r}_b^a$, is

$$\boldsymbol{T}_b^a = \begin{bmatrix} \boldsymbol{R}_b^a & \boldsymbol{r}_b^a \\ \boldsymbol{0}^{\mathrm{T}} & 1 \end{bmatrix} \tag{2.11}$$

2.4. Denativ-Hartenberg Convention

To find the intermediate transformation matrices a systematic, general method is derived to define the relative position and orientation of two consecutive links. [18] describes the process with reference to Figure 2.1:

- Choose axis z_i along the axis of Joint $i + 1$.
- Locate the origin O_i at the intersection of axis z_i with the common normal to axis z_{i-1} and z_i. Also locate the origin $O_{i'}$ at the intersection of the common normal with axis z_{i-1}.
- Choose axis x_i along the common normal til axis z_{i-1} and z_i with positive direction from Joint i to Joint $i + 1$.
- Choose axis y_i so as to complete a right-handed frame.

Once the link frames has been chosen, the position and orientation of Frame i relative to Frame $i - 1$ can be described using four parameters unique for the system. The parameters are a_i, α_i, d_i and θ_i. The transformation from one joint to another consist of two homogeneous transformation matrices. Initially a rotation, θ, about the current z axis is done followed by a translation, d, along the same axis which gives the matrix

$$\mathrm{Rot}_z(\theta_i)\mathrm{Trans}_z(d_i) = \begin{bmatrix} c_{\theta_i} & -s_{\theta_i} & 0 & 0 \\ s_{\theta_i} & c_{\theta_i} & 0 & 0 \\ 0 & 0 & 1 & d_i \\ 0 & 0 & 0 & 1 \end{bmatrix} \tag{2.12}$$

Then, a rotation, α, about the current x axis and a translation, a, along the same axis gives the matrix

$$\mathrm{Rot}_x(\alpha_i)\mathrm{Trans}_x(a_i) = \begin{bmatrix} 1 & 0 & 0 & a_i \\ 0 & c_{\alpha_i} & -s_{\alpha_i} & 0 \\ 0 & s_{\alpha_i} & c_{\alpha_i} & 0 \\ 0 & 0 & 0 & 1 \end{bmatrix} \tag{2.13}$$

The two parameters a_i and α_i is constant and only depentant of the geometry of the system. If the joint is rotary the joint variable is θ_i and d_i if the joint is prismatic. The homogeneous transformation matrix between Frame i to Frame $i-1$ is given as

$$\begin{aligned} \boldsymbol{T}_i^{i-1}(q_i) &= \mathrm{Rot}_z(\theta_i)\mathrm{Trans}_z(d_i)\mathrm{Rot}_x(\alpha_i)\mathrm{Trans}_x(a_i) \\ &= \begin{bmatrix} c_{\theta_i} & -s_{\theta_i} & 0 & 0 \\ s_{\theta_i} & c_{\theta_i} & 0 & 0 \\ 0 & 0 & 1 & d_i \\ 0 & 0 & 0 & 1 \end{bmatrix} \begin{bmatrix} 1 & 0 & 0 & a_i \\ 0 & c_{\alpha_i} & -s_{\alpha_i} & 0 \\ 0 & s_{\alpha_i} & c_{\alpha_i} & 0 \\ 0 & 0 & 0 & 1 \end{bmatrix} \\ &= \begin{bmatrix} c_{\theta_i} & -s_{\theta_i}c_{\alpha_i} & s_{\theta_i}s_{\alpha_i} & a_i c_{\theta_i} \\ s_{\theta_i} & c_{\theta_i}c_{\alpha_i} & -c_{\theta_i}s_{\alpha_i} & a_i s_{\theta_i} \\ 0 & s_{\alpha_i} & c_{\alpha_i} & d_i \\ 0 & 0 & 0 & 1 \end{bmatrix} \end{aligned} \tag{2.14}$$

2.5. Differential Kinematics

The geometric Jacobian is a function that finds the relationship between the joint velocities end the linear and angular velocity of the end-effector and is defined as

$$\begin{bmatrix} \dot{\boldsymbol{p}}_e \\ \boldsymbol{\omega}_e \end{bmatrix} = \boldsymbol{J}(\boldsymbol{q})\dot{\boldsymbol{q}} \tag{2.15}$$

where $\dot{\boldsymbol{p}}_e$ and $\boldsymbol{\omega}_e$ is the linear velocity and the angular velocity of the end-effector, respectively. $\boldsymbol{J}$ can be divided into two parts, one for the linear velocity, $\boldsymbol{J}_P$, and one for the angular velocity, $\boldsymbol{J_O}$.The Jacobian can then be described as

$$J = \begin{bmatrix} J_{P1} & \dots & J_{Pn} \\ J_{O1} & \dots & J_{On} \end{bmatrix} \tag{2.16}$$

where

$$\begin{bmatrix} J_{Pi} \\ J_{Oi} \end{bmatrix} = \begin{cases} \begin{bmatrix} z_{i-1} \\ 0 \end{bmatrix} & \text{for a prismatic joint} \\ \begin{bmatrix} z_{i-1} \times (\boldsymbol{p}_e - \boldsymbol{p}_{i-1}) \\ z_{i-1} \end{bmatrix} & \text{for a revolute joint} \end{cases} \tag{2.17}$$

z_{i-1} is given by the third column of the rotation matrix $\boldsymbol{R}^0_{i-1}$ and $\boldsymbol{p}_e$ is given by the first three elements of the fourth column of the transformation matrix $\boldsymbol{T}^0_e$.

2.6. Trajectory Planning

In a point-to-point motion, the manipulator has to move from an initial position within a time t_f. The path the manipulator takes is not defined, but the planning algorithm should be chosen so that the following features are in place [18].

- the computation needed should not be too demanding,
- the joint positions and velocities should be continuous functions of time,
- undesirable effects should be minimized.

Choosing the motion primitive can be done from an incremental motion problem. Consider the moment of inertia of a rigid body about its rotation axis I. The path consists of rotating the angle q from an initial value q_i to a final value q_f within a time t_f. To find a suitable solution among the infinite amount of solutions that exist is it assumed that the rotation is excited through a torque τ supplied by a motor, and that a solution can be found from minimizing the energy consumed by the motor. The optimization problem is set as follows. If the derivative of the angle q is defined as $\dot{q} = \omega$, the solution to the differential equation

$$I\dot{\omega} = \tau \tag{2.18}$$

subject to the condition

$$\int_0^{t_f} \omega\,(t)\,dt = q_f - q_i \tag{2.19}$$

so as to minimize the performance index

$$\int_0^{t_f} \tau^2 dt. \tag{2.20}$$

It can be shown that the solution to this optimization problem is

$$\omega\left(t\right) = at^2 + bt + c \tag{2.21}$$

This brings the basis of using a third-order polynomial function to generate the trajectory. The joint motion can therefore be found from the cubic polynomial

$$q\left(t\right) = a_3t^3 + a_2t^2 + a_1t + a_0 \tag{2.22}$$

can be chosen, giving the parabolic velocity profile

$$\dot{q}\left(t\right) = 3a_3t^2 + 2a_2t + a_1 \tag{2.23}$$

and a linear acceleration profile

$$\ddot{q}\left(t\right) = 6a_3t + 3a_2. \tag{2.24}$$

To solve for the coefficients the initial and final position q_i and q_f is used together with the initial and final velocity $\dot{q}_i$ and $\dot{q}_f$ which are usually set to zero. This is done by using the following system of equations

$$\begin{aligned} a_0 &= q_i \\ a_1 &= \dot{q}_i \\ a_3t^3 + a_2t^2 + a_1t + a_0 &= q_f \\ 3a_3t^2 + 2a_2t + a_1 &= \dot{q}_f \end{aligned} \tag{2.25}$$

In order to ensure that the manipulator can handle the motion in practice, a trapezoidal velocity profile is assigned, which consists of a constant acceleration initially that turns into a cruising face with constant velocity and a constant deceleration to finish the motion Figure 2.2. Notice the symmetry in the velocity profile assuming that the initial acceleration is the same in magnitude as the finishing deceleration and that the initial velocity and the final velocity is set to zero. For the transition from q_i to q_f to happen in time t_f some constraints must be satisfied by the trajectory. The velocity at the end of the parabolic segment must be equal to the velocity of the linear segment, i.e.,

$$\ddot{q}_c = \frac{q_m - q_c}{t_m - t_c} \tag{2.26}$$

where q_c is the value of q at the end of the parabolic segment at time t_c. q_m is the average point $q_m = \left(q_f + q_i\right)/2$ at time $t_m = t_f/2$. q_c is then

$$q_c = q_i + \frac{1}{2}\ddot{q}_c t_c^2 \tag{2.27}$$

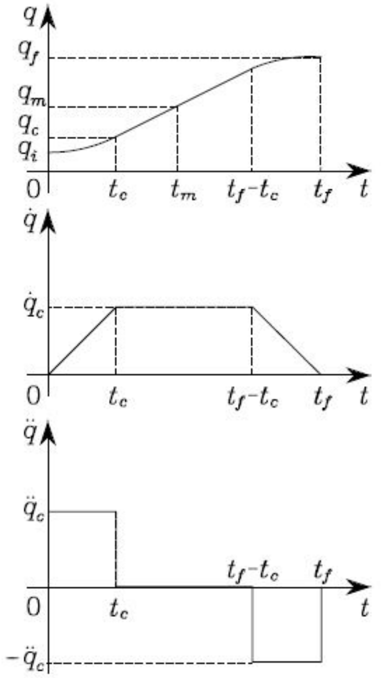

Figure 2.2.: Trapezoidal velocity profile [18]

combining (2.26) and (2.27) gives

$$\ddot{q}_c t_c^2 - \ddot{q}_c t_f t_c + q_f - q_i = 0 \tag{2.28}$$

It is common that $\ddot{q}_c$ is specified with the constraint that $\operatorname{sgn}(\ddot{q}_c) = \operatorname{sgn}(q_f - q_i)$, where sgn is the signum function. t_c can then be found from (2.28) as

$$t_c = \frac{t_f}{2} - \frac{1}{2}\sqrt{\frac{t_f^2 \ddot{q}_c - 4(q_f - q_i)}{\ddot{q}_c}} \tag{2.29}$$

it is noted that $t_c \leq t_f/2$. The acceleration is therefore under the constraint

$$|\ddot{q}_c| \geq \frac{4|q_f - q_i|}{t_f^2} \tag{2.30}$$

If the acceleration is set to equal the expression in (2.30), the constant velocity segment is not featured in the trajectory and has thus a triangular profile. This also means that $t_c = t_f/2$ If q_i, q_f and t_f is given, t_c can be found from

Equation 2.29 and the following is generated

$$q\left(t\right)=\begin{cases}q_i+\frac{1}{2}\ddot{q}_c t^2 & 0\leq t\leq t_c\\ q_i+\ddot{q}_c t_c\left(t-t_c/2\right) & t_c<t\leq t_f-t_c\\ q_f-\frac{1}{2}\ddot{q}_c\left(t_f-t\right)^2 & t_f-t_c<t\leq t_f.\end{cases}\tag{2.31}$$

Chapter 3.

Modelling and Control of Pendulum

3.1. Kinematics of a Simple Pendulum

Consider a horizontal xy plane where the z axis is pointing vertically upwards. A point mass m is attached at $(0,0,0)$ with a mass-less rope with length L. The pendulum moves in the xz plane, the position of the mass can therefore be described as $(x,0,z)$. The motion of the pendulum is defined by the angle made from the vertical z axis and the rope, called θ. Consider the distance s on the arc from the bottom $(\theta = 0)$ and the position of the mass. The tangential force is $mg\sin\theta$ and Newton's second law gives

$$m\frac{\mathrm{d}^2 s}{\mathrm{d}t^2} = -mg\sin\theta \tag{3.1}$$

The relation between s and θ is $s = L\theta$. Inserted in the equation above gives

$$\frac{\mathrm{d}^2\theta}{dt^2} = -\frac{g}{L}\sin\theta \tag{3.2}$$

which gives the known pendulum model

$$\ddot{\theta} + \omega_0^2 \sin\theta = 0 \tag{3.3}$$

where $\omega_0 = \sqrt{\frac{g}{L}}$ is the frequency of the pendulum.

3.2. Lagrangian Kinematics for a Simple Pendulum

The Lagrangian formulation of these equations of motion is found from subtracting the potential energy from the kinetic energy as, described in section 2.1. differentiating the holonomic constraints for the simple pendulum, $x = -L\sin\theta$ and $z = -L\cos\theta$, gives the velocity components $\dot{x} = -L\dot{\theta}\cos\theta$ and $\dot{z} = L\dot{\theta}\sin\theta$. This gives the expressions for the kinematic and potential energy as

$$K = \frac{1}{2}m(\dot{x}^2 + \dot{z}^2) = \frac{1}{2}mL^2\dot{\theta}^2 \tag{3.4}$$

$$U = mg(L + z) = mgL(1 - \cos\theta) \tag{3.5}$$

The Lagrangian function is given as in Equation 2.4 where the generalized coordinate being θ

$$\mathcal{L} = K - U = \frac{1}{2}mL^2\dot{\theta}^2 + mgL(\cos\theta - 1) \tag{3.6}$$

The Lagrangian equation of motion is defined as in Equation 2.5. Since there are no applied forces becomes the expression

$$\frac{\mathrm{d}}{\mathrm{d}t}\left(\frac{\partial\mathcal{L}}{\partial\dot{\theta}}\right) - \frac{\partial\mathcal{L}}{\partial\theta} = 0 \tag{3.7}$$

For this system

$$\frac{\partial\mathcal{L}}{\partial\dot{\theta}} = mL^2\dot{\theta} \tag{3.8}$$

which gives

$$\frac{\mathrm{d}}{\mathrm{d}t}\left(\frac{\partial\mathcal{L}}{\partial\dot{\theta}}\right) = \frac{\mathrm{d}}{\mathrm{d}t}\left(mL^2\dot{\theta}\right) = mL^2\ddot{\theta} \tag{3.9}$$

and

$$\frac{\partial\mathcal{L}}{\partial\theta} = -mgL\sin\theta \tag{3.10}$$

which inserted into (3.7) gives

$$mL^2\ddot{\theta} + mgL\sin\theta = 0 \tag{3.11}$$

3.3. Damping by Feedback Control

A damper can be made by the feedback velocity loop

$$\ddot{x}_0 = -2L\zeta\omega_0\dot{\theta} \tag{3.12}$$

where ζ is the damping ratio and is set to a certain value. In practice this feedback means that if the angular velocity $\dot{\theta}$ being fed back is large, will the acceleration of the attachment point be proportionally large. Inserting this into (3.20) gives

$$\ddot{\theta} + 2\zeta\omega_0\dot{\theta}\cos\theta + \omega_0^2\sin\theta = 0 \tag{3.13}$$

Using the small angle approximation which states that for small angles $\sin\theta \approx \theta$ and $\cos\theta \approx 1$ gives

$$\ddot{\theta} + 2\zeta\omega_0\dot{\theta} + \omega_0^2\theta = 0 \tag{3.14}$$

which is a linear damped oscillator with undamped natural frequency ω_0 and a damping ratio ζ. The damping ratio ζ is in [3] defined as the proximity to critical damping. $\zeta = 1$ means that a system is critically damped. If $\zeta < 1$ the system is said to be underdamped and overdamped if $\zeta > 1$. For a second order system, the value $\zeta = \frac{1}{\sqrt{2}}$ is the smallest value of damping ratio for which the system shows no amplification at any input frequence [1].

3.4. Moving Attachment Point

If the attachment point is able to move in the x direction, it can be defined as $(x_0, 0, 0)$. The holonomic constraints are now $x = x_0 - L\sin\theta$ and $z = -L\cos\theta$, which gives the velocity components $\dot{x} = \dot{x}_0 - L\dot{\theta}\cos\theta$ and $\dot{z} = L\dot{\theta}\sin\theta$. The kinetic energy is

$$\begin{aligned} K &= \frac{1}{2}m(\dot{x}^2 + \dot{z}^2) \\ &= \frac{1}{2}m\left((\dot{x}_0 - L\dot{\theta}\cos\theta)^2 + (L\dot{\theta}\sin\theta)^2\right) \\ &= \frac{1}{2}mL^2\dot{\theta}^2 - mL\dot{x}_0\dot{\theta}\cos\theta + \frac{1}{2}m\dot{x}_0^2 \end{aligned} \tag{3.15}$$

while the potential energy is still $U = mgL(1 - \cos\theta)$. The Lagrangian function ($\mathcal{L} = K - U$) then becomes

$$\mathcal{L} = \frac{1}{2}mL^2\dot{\theta}^2 - mL\dot{x}_0\dot{\theta}\cos\theta + \frac{1}{2}m\dot{x}_0^2 + mgL(\cos\theta - 1) \tag{3.16}$$

The equations of motion is then

$$\begin{aligned} \frac{\mathrm{d}}{\mathrm{d}t}\left(\frac{\partial\mathcal{L}}{\partial\dot{\theta}}\right) &= \frac{\mathrm{d}}{\mathrm{d}t}\left(mL^2\dot{\theta} - mL\dot{x}_0\cos\theta\right) \\ &= mL^2\ddot{\theta} - mL\ddot{x}_0\cos\theta + mL\dot{x}_0\dot{\theta}\sin\theta \end{aligned} \tag{3.17}$$

and

$$\frac{\partial\mathcal{L}}{\partial\theta} = mL\dot{x}_0\dot{\theta}\sin\theta - mgL\sin\theta \tag{3.18}$$

(3.7) gives

$$mL^2\ddot{\theta} - mL\ddot{x}_0\cos\theta + mgL\sin\theta = 0 \tag{3.19}$$

which can be written

$$\ddot{\theta} + \omega_0^2 \sin\theta = \frac{1}{L}\ddot{x}_0 \cos\theta \tag{3.20}$$

3.5. Lyapunov Stability Analysis for a Simple Pendulum

The system should be stable for all practical values of θ, the mechanical energy is therefore set as the Lyapunov function from section 2.2

$$V = K + U = \frac{1}{2}mL^2\dot{\theta}^2 + mgL(1 - \cos\theta) \tag{3.21}$$

Lyapunov's second method for stability states that the Lyapunov must satisfy $V(\theta) = 0$ if and only if $\theta = 0$. $\theta = 0$ inserted into Equation 3.21 gives $V = 0$, which is intuitive since the pendulum then hangs straight down and has now energy. The second requirement is $V(\theta) > 0$ if and only if $\theta \neq 0$. Neither of the terms in Equation 3.21 can be negative which means that this is met. Finally, the last requirement is $\dot{V}(\theta) \leq 0$ for all values of $\theta \neq 0$. The time derivative of the function is

$$\dot{V} = \dot{\theta}(mL^2\ddot{\theta} + mgL\sin\theta) \tag{3.22}$$

From (3.19) this can be written as

$$\dot{V} = mL\ddot{x}_0 \cos\theta\dot{\theta} \tag{3.23}$$

Inserting $\ddot{x}_0$ from (3.12) gives

$$\dot{V} = -2\zeta mL^2\omega_0\dot{\theta}^2 \cos\theta \tag{3.24}$$

It is seen that this $\dot{V} \leq 0$ when $-\frac{\pi}{2} < \theta < \frac{\pi}{2}$ and is therefore Lyapunov stable for all values of θ. For the system to be asymptotically stable, must the LaSalle's invariance principe be checked. Let the set of trajectories $I = \{\theta, \dot{\theta} : \dot{V}(\theta) = 0\}$ which is the same as $I = \{\theta, \dot{\theta} : \dot{\theta} = 0\}$ which means that there are no trajectories within I which again means that the equilibrium is asymptotically stable.

3.6. Pendulum with Moving Attachment point in the x and z Direction

The attachment point is now able to move in both x and y direction and can be defined as $(x_0, 0, z_0)$, which gives the following holonomic constraints. In the x direction nothing is changed, $x = x_0 - L\sin\theta$, but the equation for the z direction becomes $z = z_0 - L\cos\theta$. These give the velocity components $\dot{x} = \dot{x}_0 - L\dot{\theta}\cos\theta$

and $\dot{z} = \dot{z}_0 + L\dot{\theta}\sin\theta$. Kinetic energy is

$$\begin{aligned} K &= \frac{1}{2}m(\dot{x}^2 + \dot{z}^2) \\ &= \frac{1}{2}m\left((\dot{x}_0 - L\dot{\theta}\cos\theta)^2 + (\dot{z}_0 + L\dot{\theta}\sin\theta)^2\right) \\ &= \frac{1}{2}mL^2\dot{\theta}^2 - mL\dot{x}_0\dot{\theta}\cos\theta - mL\dot{z}_0\dot{\theta}\sin\theta + \frac{1}{2}m(\dot{x}_0^2 + \dot{z}_0^2) \end{aligned} \tag{3.25}$$

The potential energy remains unchained and is $U = mgL(1 - \cos\theta)$. The Lagrangian function becomes

$$\mathcal{L} = \frac{1}{2}mL^2\dot{\theta}^2 - mL\dot{x}_0\dot{\theta}\cos\theta + mL\dot{z}_0\dot{\theta}\sin\theta + \frac{1}{2}m(\dot{x}_0^2 + \dot{z}_0^2) - mgL(1 - \cos\theta) \tag{3.26}$$

The Lagrangian equations of motion is then

$$\begin{aligned} \frac{\mathrm{d}}{\mathrm{d}t}\left(\frac{\partial\mathcal{L}}{\partial\dot{\theta}}\right) &= \frac{\mathrm{d}}{\mathrm{d}t}\left(mL^2\dot{\theta} - mL\dot{x}_0\cos\theta + mL\dot{z}_0\sin\theta\right) \\ &= mL^2\ddot{\theta} - mL\ddot{x}_0\cos\theta + mL\dot{x}_0\dot{\theta}\sin\theta + mL\ddot{z}_0\sin\theta + mL\dot{z}_0\dot{\theta}\cos\theta \end{aligned} \tag{3.27}$$

$$\frac{\partial\mathcal{L}}{\partial\theta} = mL\dot{x}_0\dot{\theta}\sin\theta + mL\dot{z}_0\dot{\theta}\cos\theta - mgL\sin\theta \tag{3.28}$$

which from (3.7) gives

$$mL^2\ddot{\theta} - mL\ddot{x}_0\cos\theta + mL\ddot{z}_0\sin\theta + mgL\sin\theta = 0 \tag{3.29}$$

3.7. Pendulum with Varying Rope Length

If the rope length is varying, the velocity components become $\dot{x} = \dot{x}_0 - L\dot{\theta}\cos\theta - \dot{L}\sin\theta$ and $\dot{z} = L\dot{\theta}\sin\theta - \dot{L}\cos\theta$. The kinetic energy is then

$$\begin{aligned} K =& \frac{1}{2}m(\dot{x}^2 + \dot{z}^2) \\ =& \frac{1}{2}m\left((\dot{x}_0 - L\dot{\theta}\cos\theta - \dot{L}\sin\theta)^2 + (L\dot{\theta}\sin\theta - \dot{L}\cos\theta)^2\right) \\ =& \frac{1}{2}m(\dot{x}_0^2 + L^2\dot{\theta}^2\cos^2\theta + \dot{L}^2\sin^2\theta) - m\dot{x}_0L\dot{\theta}\cos\theta - m\dot{x}_0\dot{L}\sin\theta \\ &+ mL\dot{L}\dot{\theta}\cos\theta\sin\theta + \frac{1}{2}m(L^2\dot{\theta}^2\sin^2\theta + \dot{L}\cos^2\theta) - mL\dot{L}\dot{\theta}\cos\theta\sin\theta \\ =& \frac{1}{2}mL^2\dot{\theta}^2 - mL\dot{x}_0\dot{\theta}\cos\theta - m\dot{x}_0\dot{L}\sin\theta + \frac{1}{2}m\dot{x}_0^2 + \frac{1}{2}m\dot{L}^2 \end{aligned} \tag{3.30}$$

while the potential energy is $U = mgL(1 - \cos\theta)$. The Lagrangian is

$$\begin{aligned}\mathcal{L} =& \frac{1}{2}mL^2\dot{\theta}^2 - mL\dot{x}_0\dot{\theta}\cos\theta - m\dot{x}_0\dot{L}\sin\theta + \frac{1}{2}m\dot{x}_0^2 \\ &+ \frac{1}{2}m\dot{L}^2 - mgL(1-\cos\theta)\end{aligned} \tag{3.31}$$

Then the Lagrangian equation of motion is found from

$$\begin{aligned}\frac{\mathrm{d}}{\mathrm{d}t}\left(\frac{\partial\mathcal{L}}{\partial\dot{\theta}}\right) &= \frac{\mathrm{d}}{\mathrm{d}t}\left(mL^2\dot{\theta} - mL\dot{x}_0\cos\theta\right) \\ &= mL^2\ddot{\theta} + 2mL\dot{L}\dot{\theta} - mL\ddot{x}_0\cos\theta - m\dot{L}\dot{x}_0\cos\theta + mL\dot{x}_0\dot{\theta}\sin\theta\end{aligned} \tag{3.32}$$

and

$$\frac{\partial\mathcal{L}}{\partial\theta} = mL\dot{x}_0\dot{\theta}\sin\theta - m\dot{x}_0\dot{L}\cos\theta - mgL\sin\theta \tag{3.33}$$

which gives

$$mL^2\ddot{\theta} - mL\ddot{x}_0\cos\theta + 2mL\dot{L}\dot{\theta} + mgL\sin\theta = 0 \tag{3.34}$$

which can be written as

$$\ddot{\theta} - \frac{1}{L}\ddot{x}_0\cos\theta + \frac{g}{L}\sin\theta = -\frac{2}{L}\dot{L}\dot{\theta} \tag{3.35}$$

3.8. Pendulum with Moving Attachment Point and Varying Rope Length

A pendulum that moves in the xz plane with moving attachment point in the x direction and in the z direction together with a varying rope length gives the following velocity components, $\dot{x} = \dot{x}_0 - L\dot{\theta}\cos\theta - \dot{L}\sin\theta$ and $\dot{z} = \dot{z}_0 + L\dot{\theta}\sin\theta - \dot{L}\cos\theta$. The kinetic energy is

$$\begin{aligned}K =& \frac{1}{2}m(\dot{x}^2 + \dot{z}^2) \\ =& \frac{1}{2}m\left((\dot{x}_0 - L\dot{\theta}\cos\theta - \dot{L}\sin\theta)^2 + (\dot{z}_0 + L\dot{\theta}\sin\theta - \dot{L}\cos\theta)^2\right) \\ =& \frac{1}{2}m(\dot{x}_0^2 + L^2\dot{\theta}^2\cos^2\theta + \dot{L}^2\sin^2\theta + \dot{z}_0^2 + L^2\dot{\theta}^2\sin^2\theta + \dot{L}^2\cos^2\theta) \\ &- m\dot{x}_0L\dot{\theta}\cos\theta - m\dot{x}_0\dot{L}\sin\theta + mL\dot{L}\dot{\theta}\sin\theta\cos\theta + m\dot{z}_0L\dot{\theta}\sin\theta \\ &- m\dot{z}_0\dot{L}\cos\theta - mL\dot{L}\dot{\theta}\sin\theta\cos\theta \\ =& \frac{1}{2}m(\dot{x}_0^2 + \dot{z}_0^2 + L^2\dot{\theta}^2 + \dot{L}^2) - m\dot{x}_0L\dot{\theta}\cos\theta - m\dot{x}_0\dot{L}\sin\theta + m\dot{z}_0L\dot{\theta}\sin\theta - m\dot{z}_0\dot{L}\cos\theta\end{aligned} \tag{3.36}$$

The potential energy is still $U = mgL(1 - \cos\theta)$. The Lagrangian is therefore

$$\begin{aligned}\mathcal{L} =& \frac{1}{2}m(\dot{x}_0^2 + \dot{z}_0^2 + L^2\dot{\theta}^2 + \dot{L}^2) - m\dot{x}_0 L\dot{\theta}\cos\theta - m\dot{x}_0\dot{L}\sin\theta + m\dot{z}_0 L\dot{\theta}\sin\theta \\ &- m\dot{z}_0\dot{L}\cos\theta - mgL(1-\cos\theta)\end{aligned} \tag{3.37}$$

The Lagrangian equation of motion is found from

$$\begin{aligned}\frac{\mathrm{d}}{\mathrm{d}t}\left(\frac{\partial\mathcal{L}}{\partial\dot{\theta}}\right) =& \frac{\mathrm{d}}{\mathrm{d}t}\left(mL^2\dot{\theta} - mL\dot{x}_0\cos\theta + mL\dot{z}_0\sin\theta\right) \\ =& mL^2\ddot{\theta} + 2mL\dot{L}\dot{\theta} - mL\ddot{x}_0\cos\theta - m\dot{L}\dot{x}_0\cos\theta + mL\dot{x}_0\dot{\theta}\sin\theta \\ &+ mL\ddot{z}_0\sin\theta + m\dot{L}\dot{z}_0\sin\theta + mL\dot{z}_0\dot{\theta}\cos\theta\end{aligned} \tag{3.38}$$

and

$$\begin{aligned}\frac{\partial\mathcal{L}}{\partial\theta} =& mL\dot{x}_0\dot{\theta}\sin\theta - m\dot{L}\dot{x}_0\cos\theta + mL\dot{z}_0\dot{\theta}\cos\theta \\ &+ m\dot{z}_0\dot{L}\sin\theta - mgL\sin\theta\end{aligned} \tag{3.39}$$

which gives

$$mL^2\ddot{\theta} + 2mL\dot{L}\dot{\theta} - mL\ddot{x}_0\cos\theta + mL\ddot{z}_0\sin\theta + mgL\sin\theta = 0 \tag{3.40}$$

which can be written as

$$\ddot{\theta} = \frac{1}{L}\ddot{x}_0\cos\theta - \frac{1}{L}\ddot{z}_0\sin\theta - \frac{g}{L}\sin\theta - \frac{2}{L}\dot{L}\dot{\theta} \tag{3.41}$$

3.9. Simple Spherical Pendulum with Euler Angles

A frame $\{n\}$ is defined as the inertial frame with the z axis pointing vertically upwards and the x and y axis are both in the horizontal plane (Figure 3.1). The attachment point is in the xy plane with position $\boldsymbol{r}_b^n = [0,0,0]^{\mathrm{T}}$ in the coordinates of frame n, which means the attachment point is fixed. The pendulum is defined as a mass m connected to a mass-less wire of length L. Frame $\{b\}$ is fixed at the attachment point where the z axis is defined as an elongation of the wire. The motion of the point mass is caused by a rotation of angle ϕ_x about the x axis, $\boldsymbol{R}_x(\phi_x)$, and a rotation ϕ_y about the y axis, $\boldsymbol{R}_y(\phi_y)$. These rotation matrices are defined as in section 2.3

$$\boldsymbol{R}_x(\phi_x) = \begin{bmatrix} 1 & 0 & 0 \\ 0 & c_x & -s_x \\ -0 & s_x & c_x \end{bmatrix} \tag{3.42}$$

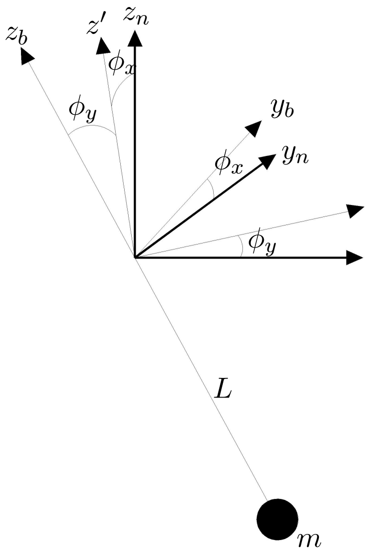

Figure 3.1.: Spherical Pendulum

and

$$\boldsymbol{R}_y(\phi_y) = \begin{bmatrix} c_y & 0 & s_y \\ 0 & 1 & 0 \\ -s_y & 0 & c_x \end{bmatrix} \tag{3.43}$$

The composite rotation from frame $\{n\}$ to frame $\{b\}$ is therefore

$$\boldsymbol{R}_b^n = \boldsymbol{R}_x(\phi_x)\boldsymbol{R}_y(\phi_y) = \begin{bmatrix} c_y & 0 & s_y \\ s_x s_y & c_x & -s_x c_y \\ -c_x s_y & s_x & c_x c_y \end{bmatrix} \tag{3.44}$$

where $s_\alpha = \sin\phi_\alpha$ and $c_\alpha = \cos\phi_\alpha$.

The position of the point mass m is given as $\boldsymbol{r}^n = \boldsymbol{R}_b^n \boldsymbol{r}_r^b$ where $\boldsymbol{r}_r^b = [0, 0, -L]^{\mathrm{T}}$ is the position of the point mass in the coordinates of frame $\{b\}$.

$$\boldsymbol{r}^n = \begin{bmatrix} c_y & 0 & s_y \\ s_x s_y & c_x & -s_x c_y \\ -c_x s_y & s_x & c_x c_y \end{bmatrix} \begin{bmatrix} 0 \\ 0 \\ -L \end{bmatrix} = \begin{bmatrix} -L s_y \\ L s_x c_y \\ -L c_x c_y \end{bmatrix} \tag{3.45}$$

The velocity of the point mass is the derivative with respect to time of the position vector $\boldsymbol{r}^n$

$$\boldsymbol{v}^n = \begin{bmatrix} -L c_y \dot{\phi}_y \\ L c_x c_y \dot{\phi}_x - L s_x s_y \dot{\phi}_y \\ L s_x c_y \dot{\phi}_x + L c_x s_y \dot{\phi}_y \end{bmatrix} \tag{3.46}$$

In the same way as in section 3.2 is Lagrange's equations derived from the energy equations. The kinetic energy for a spherical pendulum is found from $\frac{1}{2}m(\boldsymbol{v}^n)^2$ and is

$$\begin{aligned} K =&\frac{1}{2}m(L^2c_y^2\dot{\phi}_y^2 + L^2c_x^2c_y^2\dot{\phi}_y^2 - 2L^2s_xc_xs_yc_y\dot{\phi}_x\dot{\phi}_y + L^2s_x^2s_y^2\dot{\phi}_y^2 \\ &L^2s_x^2c_y^2\dot{\phi}_x^2 + 2L^2s_xc_xs_yc_y\dot{\phi}_x\dot{\phi}_y + L^2c_x^2s_y^2\dot{\phi}_y^2) \\ =&\frac{1}{2}mL^2\left(\dot{\phi}_x^2c_y^2 + \dot{\phi}_y^2\right) \end{aligned} \tag{3.47}$$

The potential energy is $U = -mgL(c_xc_y - 1)$. The Lagrangian equation of motion for ϕ_x is derived by finding $\frac{\partial \mathcal{L}}{\partial \dot{\phi}_x}$ and differentiating this with respect to time. Then finding $\frac{\partial \mathcal{L}}{\partial \phi_x}$ and setting the difference between the two expressions equal to zero.

$$\mathcal{L} = \frac{1}{2}mL^2\left(\dot{\phi}_x^2c_y^2 + \dot{\phi}_y^2\right) + mgL(c_xc_y - 1) \tag{3.48}$$

This gives

$$\frac{\mathrm{d}}{\mathrm{d}t}\left(\frac{\partial \mathcal{L}}{\partial \dot{\phi}_x}\right) = \frac{\mathrm{d}}{\mathrm{d}t}\left(mL^2\dot{\phi}_xc_y^2\right) = mL^2\left(\ddot{\phi}_xc_y^2 - 2\dot{\phi}_x\dot{\phi}_ys_yc_y\right) \tag{3.49}$$

$$\frac{\mathrm{d}}{\mathrm{d}t}\left(\frac{\partial \mathcal{L}}{\partial \dot{\phi}_y}\right) = \frac{\mathrm{d}}{\mathrm{d}t}\left(mL^2\dot{\phi}_y\right) = mL^2\left(\ddot{\phi}_y\right) \tag{3.50}$$

and

$$\frac{\partial \mathcal{L}}{\partial \phi_x} = -mgLs_xc_y \tag{3.51}$$

and

$$\frac{\partial \mathcal{L}}{\partial \phi_y} = -mL^2\dot{\phi}_x^2s_yc_y - mgLc_xs_y \tag{3.52}$$

The resulting equations of motion are then

$$mL^2\ddot{\phi}_xc_y^2 - 2mL^2\dot{\phi}_x\dot{\phi}_ys_yc_y = -mgLs_xc_y \tag{3.53}$$

$$mL^2\ddot{\phi}_y - 2mL^2\dot{\phi}_x^2s_yc_y = -mgLc_xs_y \tag{3.54}$$

which can be written as

$$\ddot{\phi}_x = \frac{1}{c_y}(2\dot{\phi}_x\dot{\phi}_ys_y - \omega_0^2s_x) \tag{3.55}$$

$$\ddot{\phi}_y = \dot{\phi}_x^2s_yc_y - \omega_0^2c_xs_y \tag{3.56}$$

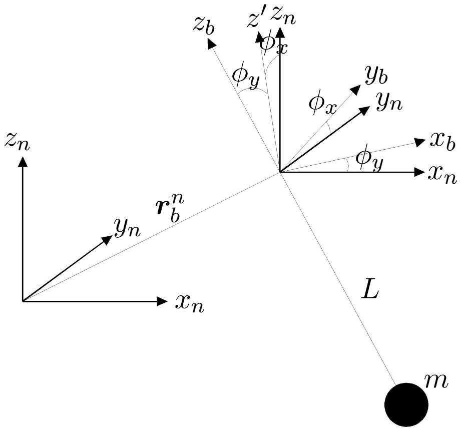

Figure 3.2.: Spherical Pendulum with Moving Attachment Point

3.10. Spherical Pendulum with Moving Attachment Point with Euler Angles

Now lets consider the spherical pendulum with a moving attachment point both in the xy plane in the z direction. Frame $\{n\}$ is still defined with the z axis pointing vertically upwards and the x and y axis makes the horizontal plane (Figure 3.2). Frame $\{b\}$ has its origin at the attachment point. The position of the attachment point in the coordinates of frame $\{n\}$ is $\boldsymbol{r}_b^n = [x_0, y_0, z_0]^{\mathrm{T}}$. The position of the point mass m is $\boldsymbol{r}^n = \boldsymbol{r}_b^n + \boldsymbol{R}_b^n \boldsymbol{r}_r^b$ where $\boldsymbol{r}_r^b = [0, 0, -L]^{\mathrm{T}}$. The position of the point mass is given as

$$\boldsymbol{r}^n = \begin{bmatrix} x_0 \\ y_0 \\ z_0 \end{bmatrix} + \begin{bmatrix} c_y & 0 & s_y \\ s_x s_y & c_x & -s_x c_y \\ -c_x s_y & s_x & c_x c_y \end{bmatrix} \begin{bmatrix} 0 \\ 0 \\ -L \end{bmatrix} = \begin{bmatrix} x_0 - L s_y \\ y_0 + L s_x c_y \\ z_0 - L c_x c_y \end{bmatrix} \tag{3.57}$$

The velocity of the point mass is the derivative with respect to time of $\boldsymbol{r}^n$

$$\boldsymbol{v}^n = \begin{bmatrix} \dot{x}_0 - L c_y \dot{\phi}_y \\ \dot{y}_0 + L c_x c_y \dot{\phi}_x - L s_x s_y \dot{\phi}_y \\ \dot{z}_0 + L s_x c_y \dot{\phi}_x + L c_x s_y \dot{\phi}_y \end{bmatrix} \tag{3.58}$$

In the same way as in section 3.2 the Lagrange equations are derived from the energy equations. The kinetic energy for a spherical pendulum is found from

$\frac{1}{2}m(\boldsymbol{v}^n)^2$ and is

$$\begin{aligned}K =&\frac{1}{2}mL^2\left(\dot\phi_x^2 c_y^2 + \dot\phi_y^2\right) + \frac{1}{2}m(\dot x_0^2 + \dot y_0^2 + \dot z_0^2)\\ &- mL\dot x_0\dot\phi_y c_y + mL\dot y_0\left(\dot\phi_x c_x c_y - \dot\phi_y s_x s_y\right)\\ &+ mL\dot z_0\left(\dot\phi_x s_x c_y + \dot\phi_y c_x s_y\right)\end{aligned} \tag{3.59}$$

and the potential energy is

$$U = mgL(1 - c_x c_y) \tag{3.60}$$

The Lagrangian equations of motion is then found from (3.6)

$$\begin{aligned}\mathcal{L} =&\frac{1}{2}mL^2\left(\dot\phi_x^2 c_y^2 + \dot\phi_y^2\right) + \frac{1}{2}m(\dot x_0^2 + \dot y_0^2 + \dot z_0^2)\\ &- mL\dot x_0\dot\phi_y c_y + mL\dot y_0\left(\dot\phi_x c_x c_y - \dot\phi_y s_x s_y\right)\\ &+ mL\dot z_0\left(\dot\phi_x s_x c_y + \dot\phi_y c_x s_y\right) - mgL(1 - c_x c_y)\end{aligned} \tag{3.61}$$

The derivative with respect to time for ϕ_x is

$$\begin{aligned}\frac{\mathrm{d}}{\mathrm{d}t}\left(\frac{\partial\mathcal{L}}{\partial\dot\phi_x}\right) =&\frac{\mathrm{d}}{\mathrm{d}t}\left(mL^2\dot\phi_x c_y^2 - mL\dot y_0 c_x c_y + mL\dot z_0 s_x c_y\right)\\ =&mL^2\ddot\phi_x c_y^2 + mL\ddot y_0 c_x c_y - 2mL^2\dot\phi_x\dot\phi_y s_y c_y + mL\ddot z_0 s_x c_y\\ &- mL\dot y_0(\dot\phi_x s_x c_y + \dot\phi_y c_x s_y) + mL\dot z_0(\dot\phi_x c_x c_y - \dot\phi_y s_x s_y)\end{aligned} \tag{3.62}$$

and

$$\frac{\partial\mathcal{L}}{\partial\phi_x} = -mL\dot y_0(\dot\phi_x s_x c_y + \dot\phi_y c_x s_y) + mL\dot z_0(\dot\phi_x c_x c_y - \dot\phi_y s_x s_y) - mgLs_x c_y \tag{3.63}$$

From (3.7) the resulting equation of motion for ϕ_x is

$$mL^2\ddot\phi_x c_y^2 + mL\ddot y_0 c_x c_y + mL^2\ddot z_0 s_x c_y + 2mL^2\dot\phi_x\dot\phi_y s_y c_y - mgLs_x c_y = 0 \tag{3.64}$$

The same procedure for ϕ_y

$$\begin{aligned}\frac{\mathrm{d}}{\mathrm{d}t}\left(\frac{\partial\mathcal{L}}{\partial\dot\phi_y}\right) =&\frac{\mathrm{d}}{\mathrm{d}t}\left(mL^2\dot\phi_y - mL\dot x_0 c_y - mL\dot y_0 s_x s_y + mL\dot z_0 c_x s_y\right)\\ =&mL^2\ddot\phi_y - mL\ddot x_0 c_y - mL\ddot y_0 s_x s_y + mL\ddot z_0 c_x s_y\\ &+ mL\dot x_0\dot\phi_y s_y - mL\dot y_0(\dot\phi_x c_x s_y + \dot\phi_y s_x c_y) + mL\dot z_0(\dot\phi_x s_x s_y - \dot\phi_y c_x c_y)\end{aligned} \tag{3.65}$$

and

$$\begin{aligned}\frac{\partial \mathcal{L}}{\partial \phi_y} =& - mL^2\dot{\phi}_x^2 s_y c_y + mL\dot{x}_0\dot{\phi}_y s_y \\ & - mL\dot{y}_0(\dot{\phi}_x c_x s_y + \dot{\phi}_y s_x c_y) + mL\dot{z}_0(\dot{\phi}_x s_x s_y - \dot{\phi}_y c_x c_y) \\ & - mgLc_x s_y\end{aligned} \tag{3.66}$$

This gives the resulting equation of motion for ϕ_y

$$mL^2\ddot{\phi}_y - mL\ddot{x}_0 c_y - mL\ddot{y}_0 s_x s_y + mL^2\ddot{z}_0 c_x s_y + mL^2\dot{\phi}_x^2 s_y c_y + mgLc_x s_y = 0 \tag{3.67}$$

which gives the following expressions for $\ddot{\phi}_x$ and $\ddot{\phi}_y$

$$\ddot{\phi}_x = \frac{1}{c_y}\left(2\dot{\phi}_x\dot{\phi}_y s_y - \frac{\ddot{y}_0 c_x}{L} - \frac{\ddot{z}_0 s_x}{L} - \omega_0^2 s_x\right) \tag{3.68}$$

$$\ddot{\phi}_y = -\dot{\phi}_x^2 s_y c_y + \frac{\ddot{x}_0 c_y}{L} + \frac{\ddot{y}_0 s_x s_y}{L} - \frac{\ddot{z}_0 c_x s_y}{L} - \omega_0^2 c_x s_y \tag{3.69}$$

For a moving attachment point in the xy plane ($\dot{z} = 0$) makes the expressions

$$\ddot{\phi}_x = \frac{1}{c_y}\left(2\dot{\phi}_x\dot{\phi}_y s_y - \frac{\ddot{y}_0 c_x}{L} - \omega_0^2 s_x\right) \tag{3.70}$$

$$\ddot{\phi}_y = -\dot{\phi}_x^2 s_y c_y + \frac{\ddot{x}_0 c_y}{L} + \frac{\ddot{y}_0 s_x s_y}{L} - \omega_0^2 c_x s_y \tag{3.71}$$

3.11. Damping

In order to damp the oscillations a damping controller is defined using the accelerations of the attachment point $(\ddot{x}_0, \ddot{y}_0, \ddot{z}_0)$, under the assumption that $\boldsymbol{r}_0^n$ is fixed, as

$$\ddot{x}_0 = -2\zeta\omega_0 L\dot{\phi}_y - \frac{1}{c_y}\ddot{y}_0 s_x s_y \tag{3.72}$$

$$\ddot{y}_0 = 2\zeta\omega_0 L\dot{\phi}_x \tag{3.73}$$

3.12. Spherical Pendulum with Varying Rope Length

The position of the point mass is the same as in section 3.10

$$\boldsymbol{r}^n = \begin{bmatrix} x_0 - Ls_y \\ y_0 + Ls_x c_y \\ z_0 - Lc_x c_y \end{bmatrix} \tag{3.74}$$

since the rope length L is varying as a function of time, it has to be implemented in the velocity expression

$$\boldsymbol{v}^n = \begin{bmatrix} \dot{x}_0 - Lc_y\dot{\phi}_y - \dot{L}s_y \\ \dot{y}_0 + Lc_xc_y\dot{\phi}_x - Ls_xs_y\dot{\phi}_y + \dot{L}s_xc_y \\ \dot{z}_0 + Ls_xc_y\dot{\phi}_x + Lc_xs_y\dot{\phi}_y - \dot{L}c_xc_y \end{bmatrix} \tag{3.75}$$

The kinetic energy is found to be

$$\begin{aligned} K =& \frac{1}{2}mL^2(\dot{\phi}_x^2c_y^2 + \dot{\phi}_y^2) + \frac{1}{2}m\dot{L}^2 + \frac{1}{2}m(\dot{x}_0^2 + \dot{y}_0^2 + \dot{z}_0^2) \\ &- mL\dot{x}_0\dot{\phi}_yc_y + mL\dot{y}_0(\dot{\phi}_xc_xc_y - \dot{\phi}_ys_xs_y) \\ &+ mL\dot{z}_0(\dot{\phi}_xs_xc_y + \dot{\phi}_yc_xs_y) - \frac{1}{2}m\dot{L}(\dot{x}_0s_y - \dot{y}_0s_xc_y + \dot{z}_0c_xc_y) \end{aligned} \tag{3.76}$$

The potential energy is still $U = mgL(1 - c_xc_y)$. The Lagrangian is found using the same procedure as before.

$$\begin{aligned} \mathcal{L} =& \frac{1}{2}mL^2(\dot{\phi}_x^2c_y^2 + \dot{\phi}_y^2) + \frac{1}{2}m\dot{L}^2 + \frac{1}{2}m(\dot{x}_0^2 + \dot{y}_0^2 + \dot{z}_0^2) \\ &- mL\dot{x}_0\dot{\phi}_yc_y + mL\dot{y}_0(\dot{\phi}_xc_xc_y - \dot{\phi}_ys_xs_y) + mL\dot{z}_0(\dot{\phi}_xs_xc_y + \dot{\phi}_yc_xs_y) \\ &- \frac{1}{2}m\dot{L}(\dot{x}_0s_y - \dot{y}_0s_xc_y + \dot{z}_0c_xc_y) - mgL(1 - c_xc_y) \end{aligned} \tag{3.77}$$

The derivative with respect to time for ϕ_x is going to be the same as without the varying rope length.

$$\begin{aligned} \frac{\mathrm{d}}{\mathrm{d}t}\left(\frac{\partial \mathcal{L}}{\partial \dot{\phi}_x}\right) =& \frac{\mathrm{d}}{\mathrm{d}t}\left(mL^2\dot{\phi}_xc_y^2 + mL\dot{y}_0c_xc_y + mL\dot{z}_0s_xc_y\right) \\ =& mL^2\ddot{\phi}_xc_y^2 + mL\ddot{y}_0c_xc_y + mL\ddot{z}_0s_xc_y - mL\dot{y}_0(\dot{\phi}_xs_xc_y + \dot{\phi}_yc_xs_y) \\ &+ mL\dot{z}_0(\dot{\phi}_xc_xc_y - \dot{\phi}_ys_xs_y) - 2mL^2\dot{\phi}_x\dot{\phi}_ys_yc_y \\ &+ m\dot{L}(\dot{y}_0c_xc_y + \dot{z}_0s_xc_y) + 2mL\dot{L}\dot{\phi}_xc_y^2 \end{aligned} \tag{3.78}$$

and

$$\begin{aligned} \frac{\partial \mathcal{L}}{\partial \phi_x} =& - mL\dot{y}_0(\dot{\phi}_xs_xc_y + \dot{\phi}_yc_xs_y) + mL\dot{z}_0(\dot{\phi}_xc_xc_y - \dot{\phi}_ys_xs_y) \\ &+ m\dot{L}(\dot{y}_0c_xc_y + \dot{z}_0s_xc_y) - mgLs_xc_y \end{aligned} \tag{3.79}$$

the resulting equation of motion is

$$\begin{aligned} mL^2\ddot{\phi}_xc_y^2 + mL\ddot{y}_0c_xc_y + mL\ddot{z}_0s_xc_y - 2mL^2\dot{\phi}_x\dot{\phi}_ys_yc_y \\ +2mL\dot{L}\dot{\phi}_xc_y^2 + mgLs_xc_y = 0 \end{aligned} \tag{3.80}$$

For ϕ_y is the derivative with respect to time the same,

$$\begin{aligned}\frac{\mathrm{d}}{\mathrm{d}t}\left(\frac{\partial\mathcal{L}}{\partial\dot{\phi}_y}\right) =&\frac{\mathrm{d}}{\mathrm{d}t}\left(mL^2\dot{\phi}_y - mL\dot{x}_0c_y - mL\dot{y}_0s_xs_y + mL\dot{z}_0c_xs_y\right)\\ =&mL^2\ddot{\phi}_y - mL\ddot{x}_0c_y - mL\ddot{y}_0s_xs_y + mL\ddot{z}_0c_xs_y\\ &+ mL\dot{x}_0\dot{\phi}_ys_y - mL\dot{y}_0(\dot{\phi}_xc_xs_y + \dot{\phi}_ys_xc_y) - mL\dot{z}_0(\dot{\phi}_xs_xs_y - \dot{\phi}_yc_xc_y)\\ &- m\dot{L}(\dot{x}_0c_y + \dot{y}_0s_xs_y - \dot{z}_0c_xs_y) + 2mL\dot{L}\dot{\phi}_y\end{aligned} \tag{3.81}$$

and

$$\begin{aligned}\frac{\partial\mathcal{L}}{\partial\phi_y} =& - mL^2\dot{\phi}_x^2s_yc_y + mL\dot{x}_0\dot{\phi}_ys_y\\ &- mL\dot{y}_0(\dot{\phi}_xc_xs_y + \dot{\phi}_ys_xc_y) - mL\dot{z}_0(\dot{\phi}_xs_xs_y - \dot{\phi}_yc_xc_y)\\ &- m\dot{L}(\dot{x}_0c_y + \dot{y}_0s_xs_y - \dot{z}_0c_xs_y) - mgLc_xs_y\end{aligned} \tag{3.82}$$

which gives the resulting equation of motion for ϕ_y

$$\begin{aligned}mL^2\ddot{\phi}_y - mL\ddot{x}_0c_y - mL\ddot{y}_0s_xs_y + mL\ddot{z}_0c_xs_y\\ +mL^2\dot{\phi}_x^2s_yc_y + 2mL\dot{L}\dot{\phi}_y + mgLc_xs_y = 0\end{aligned} \tag{3.83}$$

which gives the following expressions for $\ddot{\phi}_x$ and $\ddot{\phi}_y$

$$\ddot{\phi}_x =\frac{1}{c_y}\left(2\dot{\phi}_x\dot{\phi}_ys_y - \frac{1}{L}\ddot{y}_0c_x - \frac{1}{L}\ddot{z}_0s_x - \omega_0^2s_x\right) - \frac{2}{L}\dot{L}\dot{\phi}_x \tag{3.84}$$

$$\begin{aligned}\ddot{\phi}_y =& - \dot{\phi}_x^2s_yc_y + \frac{1}{L}\ddot{x}_0c_y + \frac{1}{L}\ddot{y}_0s_xs_y - \frac{1}{L}\ddot{z}_0c_xs_y\\ &- \frac{2e}{L}\dot{L}\dot{\phi}_y - \omega_0^2c_xs_y\end{aligned} \tag{3.85}$$

3.13. Lyapunov Stability Analysis for a Spherical Pendulum

The stability of the system is ensured for the spherical pendulum, as in section 3.5. Consider the energy function $V = K+U$ where the motion of the attachment point is assumed to be an exogenous variable (independent from the other variables in the system). The function becomes

$$V = \frac{1}{2}mL^2\left(\dot{\phi}_x^2c_y^2 + \dot{\phi}_y^2\right) + mgL(1 - c_xc_y) \tag{3.86}$$

The time derivative of the function is

$$\begin{aligned}\dot{V} = {} & \dot{\phi}_x(mL^2\ddot{\phi}_x c_y^2) + \dot{\phi}_y(mL^2\ddot{\phi}_y) - mL^2\dot{\phi}_x^2\dot{\phi}_y s_y c_y \\ & + mgL(\dot{\phi}_y c_x s_y + \dot{\phi}_x s_x c_y)\end{aligned} \tag{3.87}$$

From (3.64) and (3.67) gives

$$mL^2\ddot{\phi}_x c_y^2 = mL\ddot{y}_0 c_x c_y + 2mL^2\dot{\phi}_x\dot{\phi}_y s_y c_y - mgLs_x c_y \tag{3.88}$$

and

$$mL^2\ddot{\phi}_y = -mL\ddot{x}_0 c_y - mL\ddot{y}_0 s_x s_y - mL^2\dot{\phi}_x^2 s_y c_y - mgLc_x s_y \tag{3.89}$$

which gives the expression for $\dot{V}$

$$\begin{aligned}\dot{V} = {} & \dot{\phi}_x(mL\ddot{y}_0 c_x c_y + 2mL^2\dot{\phi}_x\dot{\phi}_y s_y c_y - mgLs_x c_y) \\ & + \dot{\phi}_y(-mL\ddot{x}_0 c_y - mL\ddot{y}_0 s_x s_y - mL^2\dot{\phi}_x^2 s_y c_y - mgLc_x s_y) \\ & - mL^2\dot{\phi}_x^2\dot{\phi}_y s_y c_y + mgL(\dot{\phi}_x s_x c_y + \dot{\phi}_y c_x s_y)\end{aligned} \tag{3.90}$$

which gives the resulting

$$\dot{V} = mL\ddot{y}_0\dot{\phi}_x c_x c_y - mL\dot{\phi}_y(\ddot{x}_0 c_y + \ddot{y}_0 s_x s_y) \tag{3.91}$$

Replacing $\ddot{x}_0$ and $\ddot{y}_0$ with the damping expressions from (3.72) and (3.73) and get

$$\dot{V} = -2mL^2\zeta\omega_0(\dot{\phi}_x^2 c_x c_y + \dot{\phi}_y^2 c_y) \tag{3.92}$$

This means that $\dot{V}$ is negative for all $-\frac{\pi}{2} < \phi_x < \frac{\pi}{2}$ and $-\frac{\pi}{2} < \phi_y < \frac{\pi}{2}$, which means that the system is Lyapunov stable. Similarly to what was done in section 3.5 must LaSalle's invariance principle be checked. Let the set of trajectories $I = \{\boldsymbol{\phi}, \dot{\boldsymbol{\phi}} : \dot{V}(\boldsymbol{\phi}) = 0\}$, where $\boldsymbol{\phi} = [\phi_x, \phi_y]^{\mathrm{T}}$, which is the same as $I = \{\boldsymbol{\phi}, \dot{\boldsymbol{\phi}} : \dot{\boldsymbol{\phi}} = 0\}$ which means that there are no trajectories within I which again means that the equilibrium is asymptotically stable.

3.14. Additions to the Damping

Additional terms have to be inserted into (3.72) and (3.73) to ensure the system's ability to follow a trajectory. Two feedback loops as in are added. The updated damping becomes

$$\ddot{y}_0 = 2\zeta\omega_0 L\dot{\phi}_x + K_p(r_y - y_0) - K_d\dot{y}_0 \tag{3.93}$$

and

$$\ddot{x}_0 = -2\zeta\omega_0 L\dot{\phi}_y - \frac{\ddot{y}_0 s_x s_y}{c_y} + K_p(r_x - x_0) - K_d\dot{x}_0 \tag{3.94}$$

where K_p and K_d are proportional control gains, as in a P-regulator. r_x and r_y are trajectories in the x and y direction, respectively. Since the movement in the z direction does not affect the damping of the oscillations, a position and velocity can be used to control the attachment point's movement in that direction.

$$\ddot{z}_0 = K_p(r_z - z_0) - K_d\dot{z}_0 \tag{3.95}$$

For the rope length a simple position loop system is used

$$\dot{L} = K_p(r_L - L) \tag{3.96}$$

where L is the current rope length, while r_L is the desired rope length.

The additions to the damping equation takes the difference between the desired position and the velocity of the attachment point into consideration when determining the acceleration. The first loop, referred to as the position loop, of (3.93) and (3.94) takes the difference in position and multiplies it with the proportional control gain K_p. The second loop, referred to as the velocity loop, takes the velocity and multiplies it with another control gain K_d. In practice this means that the gains determine how much the difference in position, and velocity should affect the acceleration of the attachment point. The position loop (e.g. $K_p(x_0 - r_x)$) works well when the difference between x_0 and r_x is large, but struggles to follow the reference when it changes rapidly. The velocity loop (e.g. $K_d\dot{x}_0$) takes the velocity of the attachment point into account. If the velocity is large the acceleration is reduced to provide overshooting.

3.15. Velocity as Input

In practice it is not possible to use the acceleration as an input [17]. The desired velocity v_x and v_y are therefore used. The alternative accelerations are given by the formula

$$a_{x0} = \frac{(v_x - \dot{x}_0)}{T_v} \tag{3.97}$$

$$a_{y0} = \frac{(v_y - \dot{y}_0)}{T_v} \tag{3.98}$$

$$a_{z0} = \frac{(v_z - \dot{z}_0)}{T_v} \tag{3.99}$$

T_v is here a time constant as used in [11]. It is paramount that these acceleration are as close to similar as possible.

Chapter 4.

Knuckle Boom Crane

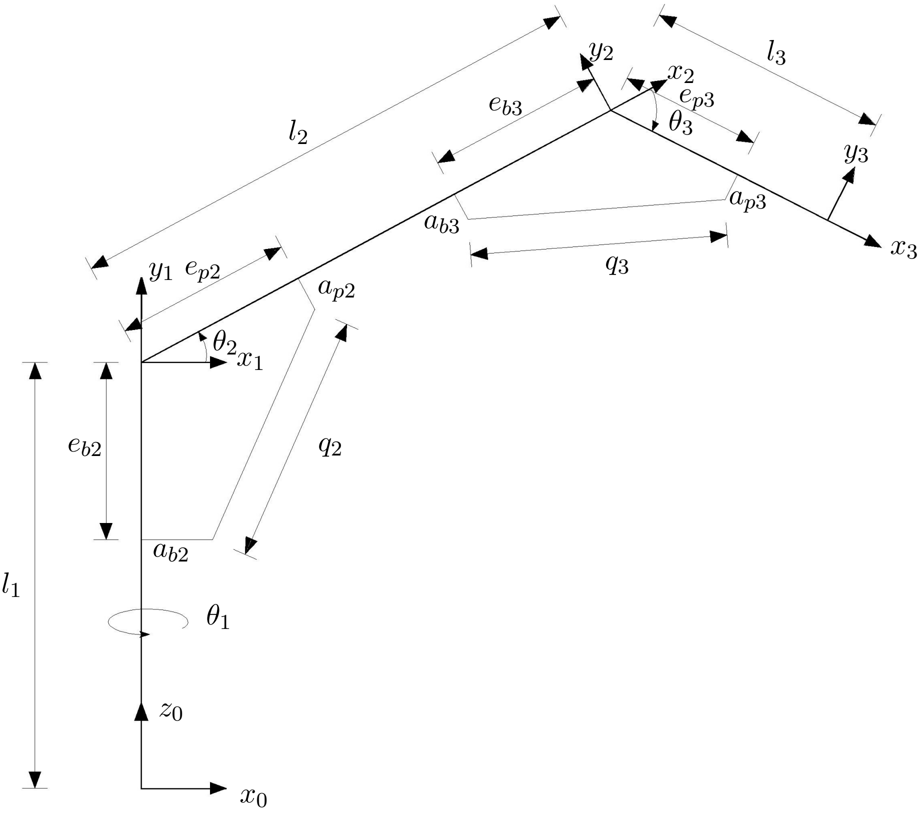

Figure 4.1.: Description of Crane

Link	a_i	θ_i	d_i	θ_i
1	0	$\frac{\pi}{2}$	l_1	θ_1^*
2	l_2	0	0	$\theta_2(q_2)^*$
3	l_3	0	0	$\theta_3(q_3)^*$

Table 4.1.: Denavit-Hartenberg parameters of knuckle boom crane

4.1. Description of Crane

The knuckle boom crane is a 3 DOF crane consisting of three joints, all rotational, see Figure 4.1. The first joint is a slewing joint that makes the crane rotate about the vertical axis with an angle θ_1. The second joint is rotational with the joint variable θ_2. The joint rotates due to the extension of a linear actuator. θ_2 is depending on the length of the linear actuator q_2. The third joint is similar to the second with joint variable $\theta_3(q_3)$. This is similar to what was presented in [6] and [23].

Considering the crane without the linear actuators the system can be described using Denavit-Hartenberg convention. The joint variables $\boldsymbol{q}$ is $[\theta_1, \theta_2(q_2), \theta_3(q_3)]$ and the forward kinematics is given by its parameters and is generally presented as in Table 4.1. The position and orientation of the crane tip can be described using the Homogeneous Transformation Matrix. Here the parameters describing the transformation from one joint to another, for the knuckle boom crane the matrices are found using Equation 2.14

$$\boldsymbol{T}_1^0 = \begin{bmatrix} c_1 & 0 & s_1 & 0 \\ s_1 & 0 & -c_1 & 0 \\ 0 & 1 & 0 & l_1 \\ 0 & 0 & 0 & 1 \end{bmatrix} \tag{4.1}$$

$$\boldsymbol{T}_2^1 = \begin{bmatrix} c_2 & -s_2 & 0 & c_2 l_2 \\ s_2 & c_2 & 0 & s_2 l_2 \\ 0 & 0 & 1 & 0 \\ 0 & 0 & 0 & 1 \end{bmatrix} \tag{4.2}$$

$$\boldsymbol{T}_3^2 = \begin{bmatrix} c_3 & -s_3 & 0 & c_3 l_3 \\ s_3 & c_3 & 0 & s_3 l_3 \\ 0 & 0 & 1 & 0 \\ 0 & 0 & 0 & 1 \end{bmatrix} \tag{4.3}$$

In order to find the position and orientation of the attachment point of the knuckle boom crane in the coordinates of frame $\{0\}$, the homogeneous transformation matrix from frame {0} to frame {3} is found from a the composite transformation matrix

$$\boldsymbol{T}_3^0 = \boldsymbol{T}_1^0 \boldsymbol{T}_2^1 \boldsymbol{T}_3^2 \tag{4.4}$$

which is an expression for the position and orientation of the attachment point in the coordinates of frame {0}.

$$\boldsymbol{T}_2^0 = \boldsymbol{T}_1^0 \boldsymbol{T}_2^1 = \begin{bmatrix} c_1c_2 & -c_1s_2 & s_1 & c_1c_2l_2 \\ s_1c_2 & -s_1s_2 & -c_1 & s_1c_2l_2 \\ s_2 & c_2 & 0 & s_2l_2 + l_1 \\ 0 & 0 & 0 & 1 \end{bmatrix} \tag{4.5}$$

$$\boldsymbol{T}_3^0 = \boldsymbol{T}_2^0 \boldsymbol{T}_3^2 = \begin{bmatrix} c_1c_2c_3 - c_1s_2s_3 & -c_1c_2s_3 - c_1s_2c_3 & s_1 & c_1c_2c_3l_3 - c_1s_2s_3l_3 + c_1c_2l_2 \\ s_1c_2c_3 - s_1s_2s_3 & -s_1c_2s_3 - s_1s_2c_3 & -c_1 & s_1c_2c_3l_3 - s_1s_2s_3l_3 + s_1c_2l_2 \\ s_2c_3 + c_2s_3 & -s_2s_3 + c_2c_3 & 0 & s_2c_3l_3 + c_2s_3l_3 + s_2l_2 + l_1 \\ 0 & 0 & 0 & 1 \end{bmatrix} \tag{4.6}$$

For simplicity, the notation $s_i = \sin\theta_i$ and $c_i = \cos\theta_i$ is used. As described in section 2.5 is the joint axis z in the coordinates of frame 0, the three first elements in the thirds column in $\boldsymbol{T}_i^0$. Which gives

$$\boldsymbol{z}_0 = [0, 0, 1]^{\mathrm{T}}, \quad \boldsymbol{z}_1 = \boldsymbol{z}_2 = \boldsymbol{z}_3 = [s_1, -c_1, 0]^{\mathrm{T}} \tag{4.7}$$

and the position vector of the origin of frame i in the coordinates of frame 0 is the first three elements of the last column of $\boldsymbol{T}_i^0$

$$\begin{aligned} \boldsymbol{p}_0 &= [0, 0, 0]^{\mathrm{T}} \\ \boldsymbol{p}_1 &= [0, 0, l_1]^{\mathrm{T}} \\ \boldsymbol{p}_2 &= [c_1c_2l_2,\ s_1c_2l_2,\ s_2l_2 + l_1]^{\mathrm{T}} \\ \boldsymbol{p}_3 &= [c_1c_2c_3l_3 - c_1s_2s_3l_3 + c_1c_2l_2,\ s_1c_2c_3l_3 - s_1s_2s_3l_3 \\ &\quad + s_1c_2l_2,\ s_2c_3l_3 + c_2s_3l_3 + s_2l_2 + l_1]^{\mathrm{T}} \end{aligned} \tag{4.8}$$

4.2. Jacobian

For this particular system, with three rotary joints is the Jacobian given, from Equation 2.17, as

$$\boldsymbol{J} = \begin{bmatrix} \boldsymbol{J}_P \\ \boldsymbol{J}_O \end{bmatrix} = \begin{bmatrix} \boldsymbol{z}_0 \times (\boldsymbol{p_3} - \boldsymbol{p_0}) & \boldsymbol{z}_1 \times (\boldsymbol{p_3} - \boldsymbol{p_1}) & \boldsymbol{z}_2 \times (\boldsymbol{p_3} - \boldsymbol{p_2}) \\ \boldsymbol{z}_0 & \boldsymbol{z}_1 & \boldsymbol{z}_2 \end{bmatrix} \tag{4.9}$$

which with the a z vectors inserted becomes

$$\boldsymbol{J} = \begin{bmatrix} \boldsymbol{J_P} \\ \boldsymbol{J_O} \end{bmatrix} = \begin{bmatrix} \boldsymbol{z}_0 \times (\boldsymbol{p_3} - \boldsymbol{p_0}) & \boldsymbol{z}_1 \times (\boldsymbol{p_3} - \boldsymbol{p_1}) & \boldsymbol{z}_2 \times (\boldsymbol{p_3} - \boldsymbol{p_2}) \\ 0 & s_1 & s_1 \\ 0 & -c_1 & -c_1 \\ 1 & 0 & 0 \end{bmatrix} \tag{4.10}$$

It is seen that the three rows at the bottom is not linearly independent, and with the crane's 3 DOFs is only $\boldsymbol{J_P}$ considered. The velocity of the end-effector in the coordinates of frame 0 is therefore

$$\dot{\boldsymbol{p}}_e = \boldsymbol{J_P}\dot{\boldsymbol{q}} = \begin{bmatrix} \boldsymbol{z}_0 \times (\boldsymbol{p_3} - \boldsymbol{p_0}) & \boldsymbol{z}_1 \times (\boldsymbol{p_3} - \boldsymbol{p_1}) & \boldsymbol{z}_2 \times (\boldsymbol{p_3} - \boldsymbol{p_2}) \end{bmatrix} \begin{bmatrix} \dot{\theta}_1 \\ \dot{\theta}_2 \\ \dot{\theta}_3 \end{bmatrix} \tag{4.11}$$

The derivation of the Jacobian is found in section A.1.

The relationship between the derivative of the joint angles and the velocity of the end-effector is $\dot{\boldsymbol{p}}_e = \boldsymbol{J_P}\dot{\boldsymbol{q}}$. When given the velocity of the end-effector, the derivative of the joint angles is found using the inverse Jacobian

$$\dot{\boldsymbol{q}} = \boldsymbol{J}_p^{-1}\dot{\boldsymbol{P}}_e \tag{4.12}$$

4.3. Defining the Angles θ_2 and θ_3

For the second link, θ_2 is found from using the law of cosine on the triangle made by b_{21}, b_{22} and q_2 (Figure 4.2) where b_{21} and b_{22} are used to divide the geometry into three triangles. b_{21} is the hypotenuse of the triangle with catheti a_{b2} and e_{b2} and b_{22} is the hypotenuse of the triangle with catheti a_{p2} and e_{p2}. From the left figure in Figure 4.2 it is seen that

$$\theta_2^* = \pi - \theta_2 - \beta_2 - \gamma_2 \tag{4.13}$$

where $\theta_2 = \arctan \frac{a_{b2}}{e_{b2}}$, $\beta_2 = \arctan \frac{a_{p2}}{e_{p2}}$. Due to the use of the Denavit-Hartenberg convention is the angle θ_2 to be zero when the two arms make a 90 deg angle between them. θ_2 is therefore defined as

$$\begin{aligned} \theta_2 =& \frac{\pi}{2} - \theta_2^* \\ =& \theta_2 + \beta_2 + \gamma_2 - \frac{\pi}{2} \end{aligned} \tag{4.14}$$

The law of cosine is applied to find γ_2 using the triangle made by b_{21}, b_{22} and q_2.

$$q_2^2 = b_{21}^2 + b_{22}^2 - 2b_{21}b_{22}\cos\gamma_2 \tag{4.15}$$

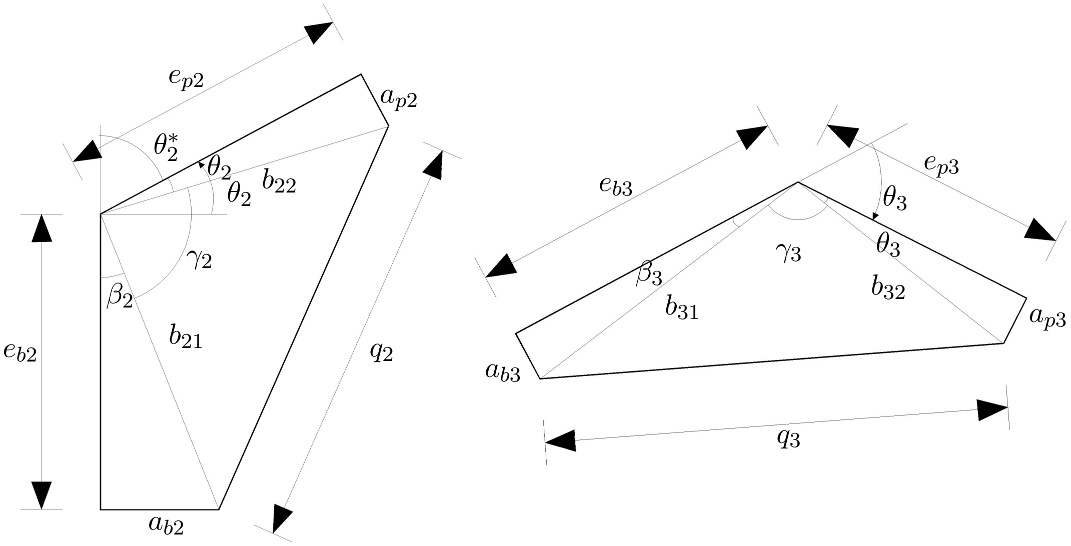

Figure 4.2.: Shoulder Joint

solving for γ_2 gives

$$\gamma_2 = \arccos \frac{q_2^2 - b_{21}^2 - b_{22}^2}{-2b_{21}b_{22}} \tag{4.16}$$

which gives the following expression for θ_2

$$\theta_2 = \theta_2 + \beta_2 + \arccos \frac{q_2^2 - b_{21}^2 - b_{22}^2}{-2b_{21}b_{22}} - \frac{\pi}{2} \tag{4.17}$$

The third link is similar to the second, the angle is to be zero when it is parallel to the second link. The expression for θ_3 becomes

$$\theta_3 = \theta_3 + \beta_3 + \gamma_3 - \pi \tag{4.18}$$

γ_3 is found in the same way as for γ_2 and is

$$\gamma_3 = \arccos \frac{q_3^2 - b_{31}^2 - b_{32}^2}{-2b_{31}b_{32}} \tag{4.19}$$

and

$$\theta_3 = \theta_3 + \beta_3 + \arccos \frac{q_3^2 - b_{31}^2 - b_{32}^2}{-2b_{31}b_{32}} - \pi \tag{4.20}$$

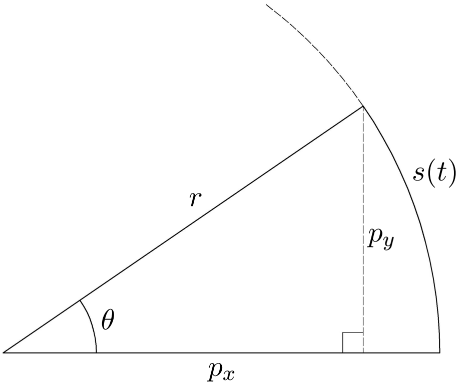

Figure 4.3.: Arc length

Solving for q_2 and q_3 gives the expression for the linear actuators as a function of the angles θ_2 and θ_3

$$\begin{aligned}\frac{q_2^2 - b_{21}^2 - b_{22}^2}{-2b_{21}b_{22}} &= \cos\left(\theta_2 - \theta_2 - \beta_2 + \frac{\pi}{2}\right)\\ q_2^2 &= -2b_{21}b_{22}\cos\left(\theta_2 - \theta_2 - \beta_2 + \frac{\pi}{2}\right) + b_{21}^2 + b_{22}^2\\ q_2 &= \sqrt{-2b_{21}b_{22}\cos\left(\theta_2 - \theta_2 - \beta_2 + \frac{\pi}{2}\right) + b_{21}^2 + b_{22}^2}\end{aligned} \tag{4.21}$$

$$\begin{aligned}\frac{q_3^2 - b_{31}^2 - b_{32}^2}{-2b_{31}b_{32}} &= \cos\left(\theta_3 - \theta_3 - \beta_3 + \pi\right)\\ q_3^2 &= -2b_{31}b_{32}\cos\left(\theta_3 - \theta_3 - \beta_3 + \pi\right) + b_{31}^2 + b_{32}^2\\ q_3 &= \sqrt{-2b_{31}b_{32}\cos\left(\theta_3 - \theta_3 - \beta_3 + \pi\right) + b_{31}^2 + b_{32}^2}\end{aligned} \tag{4.22}$$

4.4. Trajectory planning

The planning of the trajectory of a robot arm, or in this case a crane, can be found using the joint variables determined by the end-effector position and orientation specified by the user. The expression in (2.31) can also be used to find an analytic expression for the arc length s of the path. The arc goes from value $s = 0$ at $t = 0$ to the value $s = s_f$ at $t = t_f$. The expression then becomes

$$s\left(t\right) = \begin{cases} s_i + \frac{1}{2}\ddot{s}_c t^2 & 0 \leq t \leq t_c \\ s_i + \ddot{s}_c t_c\left(t - t_c/2\right) & t_c < t \leq t_f - t_c \\ s_f - \frac{1}{2}\ddot{s}_c\left(t_f - t\right)^2 & t_f - t_c < t \leq t_f. \end{cases} \tag{4.23}$$

With the acceleration defined as in (2.30) is set with an equal sign, gives $t_c = t_f - t_c$ which would make the expression of the arc length

$$s\left(t\right) = \begin{cases} s_i + \frac{1}{2}\ddot{s}_c t^2 & 0 \leq t \leq t_c \\ s_f - \frac{1}{2}\ddot{s}_c\left(t_f - t\right)^2 & t_c < t \leq t_f. \end{cases} \tag{4.24}$$

This finds a trajectory in the xy plane. For a given angle θ and a radius r the arc length is defined as $s = r\theta$. The position of a point on the arc is found using Figure 4.3, where it can be seen that the position in the x direction can be found from

$$\theta = \arccos\left(\frac{p_x}{r}\right) \tag{4.25}$$

which means that

$$s = r\theta = r\arccos\left(\frac{p_x}{r}\right) \tag{4.26}$$

which ultimately gives

$$p_x = r\cos\left(\frac{s}{r}\right) \tag{4.27}$$

the same derivation gives

$$p_y = r\sin\left(\frac{s}{r}\right) \tag{4.28}$$

In order to find a trajectory in the z direction, the parameter is simply changed to z in (4.29)

$$z\left(t\right) = \begin{cases} z_i + \frac{1}{2}\ddot{z}_c t^2 & 0 \leq t \leq t_c \\ z_f - \frac{1}{2}\ddot{z}_c\left(t_f - t\right)^2 & t_c < t \leq t_f. \end{cases} \tag{4.29}$$

The position vector then becomes

$$\boldsymbol{p} = \begin{bmatrix} p_x \\ p_y \\ z \end{bmatrix} = \begin{bmatrix} r\cos\left(\frac{s}{r}\right) \\ r\sin\left(\frac{s}{r}\right) \\ z \end{bmatrix} \tag{4.30}$$

Chapter 5.

Simulations

5.1. About the Simulations

When tuning K_p and K_d a trial and error approach has been used. Starting with both values set to zero and then attempting to find a value that damps both the angles ϕ_x, ϕ_y and follows the trajectory r_x and r_y adequately. Initial angles are set to $\phi_x = 5$ deg and $\phi_y = -10$ deg. The trajectories are initially set as constants, meaning that the attachment point is moved to constant x and y values. These values are set to $r_x = 2.5$ m and $r_y = -2.5$ m. The damping ratio is initially set to $\zeta = 0.7$. The rope length is set to $L = 1$ m. The duration of the simulations is 100 s. Note that all dotted lines are trajectories and are not named in the plots.

In Figure 5.1 the program is run with both parameters equal to zero to see how the systems work without taking the attachments point's position or velocity into consideration.

In Figure 5.2-Figure 5.4 different constant values for the gains are used to see how the added damping will affect the system. The values used are $K_p = 10$ and $K_d = 10$, $K_p = 5$ and $K_d = 5$, $K_p = 0.5$ and $K_d = 0.5$ (notice that the time span is longer for Figure 5.4 than for the previous plots). How a difference in the parameters will affect the system is also of interest, therefore, $K_p = 0.75$ and $K_d = 0.25$, $K_p = 0.25$ and $K_d = 0.75$ are also tested and displayed in Figure 5.5 and Figure 5.6.

To ensure the controller's robustness towards change in rope lengths, periods and frequencies. some of these parameters are included in the control gains. In Figure 5.7 a new parameter ω_{XY} is introduced and it is defined as $\omega_0/10$ (remember that $\omega_0 = \sqrt{\frac{g}{L}}$). The damping coefficients are then set as $K_p = \omega_{XY}^2$ and $K_d = 2\zeta\omega_{XY}$. The numerical value of these coefficients will for all practical rope lengths and periods be between 0 and 1.

Figure 5.8 shows the impact the damping ratio ζ has on both the damping of the oscillations and also the converging towards the trajectory of the motion in the x and y direction.

To further test the controller's ability to damp the oscillations while following a trajectory, are cyclical trajectories applied in section 5.3. The trajectories are set to $r_x = \frac{1}{2}\sin(0.15t)$ and $r_y = \frac{1}{2}\cos(0.15t)$. The period for these trajectories are $\approx 40\,\mathrm{s}$ and gives a consistent movement of the attachment point.

In section 3.15 a velocity loop is introduced and the acceleration resulting from this loop is compared to the acceleration exiting from the controller. Figure 5.10 shows the comparisons of the two accelerations. In Figure 5.11 the motion of the end-effector in x and y direction is depicted for both accelerations. The time constant is set to $T_v = 0.3$.

Until now, the attachment point has been moving in the xy plane. Figure 5.12 shows the damping of the oscillations alongside the motion of the end-effector in the x, y and z direction. In section 5.6 the variation of the rope length is added. In Figure 5.13 and Figure 5.15 the rope length goes from 2.5 m to 0.1 m and from 0.1 m to 2.5 m respectively. In Figure 5.14 the gain for the rope length loop is doubled to ensure a quicker reaching of the desired rope length and to test how this effects the tasks given.

The simulations thus far have been executed in Matlab. For the rest of the simulations, Simulink has been used in order to simulate a complete system with the knuckle boom crane's end-effector as the attachment point.

For a more practical situation, a planned trajectory is applied using the theory from section 2.6. Forward kinematics found from using the Denavit-Hartenberg convention from section 2.4, gives the initial position of the end-effector given the initial joint angles θ_1, θ_2, and θ_3. The path the end-effector is instructed to take is a quarter-circle in the xy plane. Two situations are looked at: one where the crane moves in the z direction, section 5.7, and one where the crane moves in the xy plane and hoisting of the cable stands for the movement in the z direction, section 5.8. For both situations, the movement in the z direction is done before the motion in the xy plane begins. Four different scenarios are simulated within each of the two situations. $t_f = 100$ s and $t_s = 20$ s; $t_f = 100$ s and $t_s = 10$ s; $t_f = 50$ s and $t_s = 10$ s and $t_f = 50$ s and $t_s = 20$ s, where t_f and t_s is defined as in section 2.6. The initial movement in the z direction is set to be finished at t_s. The planar movement is set to be finished at $t_f - t_s$ before the lowering of the point mass is done before t_f. For example, when $t_f = 100$ s and $t_s = 20$ s, will the system use the first 20 s to rise the payload, the next 60 s to move the payload to its desired position in the xy plane, before lowering the payload to its final position for the last 20 s.

The path of the end-effector for each simulation is plotted in Figure 5.16 and Figure 5.21.

Figure 5.17-Figure 5.20 consist of nine plots where the motion, velocity, and acceleration of the end-effector in the x, y and z direction are shown in addition to the damping of the angles ϕ_x and ϕ_y. Initial conditions are $L = 1$ m, $\phi_x = 5$ deg, $\phi_y = -10$ deg, $\theta_1 = 0$ deg, $\theta_2 = 45$ deg and $\theta_3 = 45$ deg. The crane is instructed to rise 1.5 m before t_s and lower 1.5 m before t_f.

Figure 5.22-Figure 5.25 consist of seven plots where the motion, velocity and acceleration of the end-effector in the x and y direction in addition to the rope length and the damping of angles phi_x and ϕ_y. The initial conditions are similar to the ones above, but this time it is the rope length that is instructed to rise and lower 1.5 m and $L_0 = 1.6\,m$. (The rope length can not be zero).

Lastly the motion of the linear actuators q_2 and q_3 alongside the change in the joint variables θ_1, θ_2 and θ_3 using the equations from section 4.3. These are shown in Figure 5.26-Figure 5.29 for the constant rope length and in Figure 5.30-Figure 5.33 for the varying rope length.

It should be noted that more values than the ones shown here were tested.

5.2. Constant Trajectories

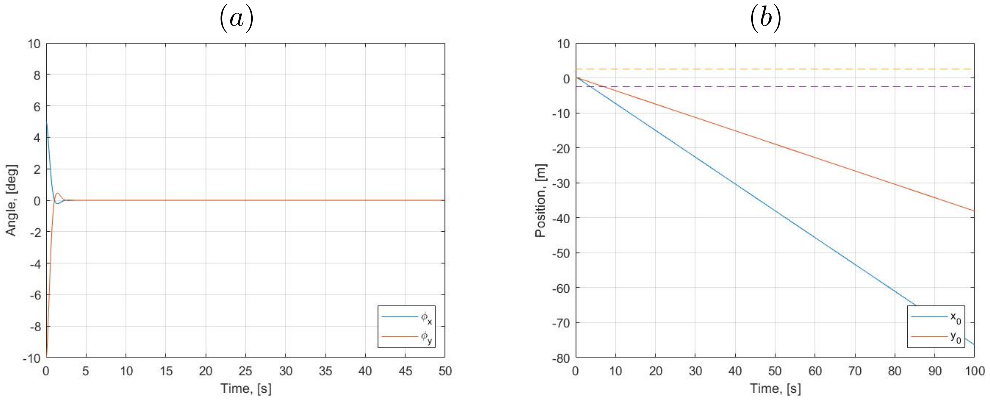

Figure 5.1.: Simulations when $K_p = 0$ and $K_d = 0$: (a) angles ϕ_x and ϕ_y and (b) motion of attachment point.

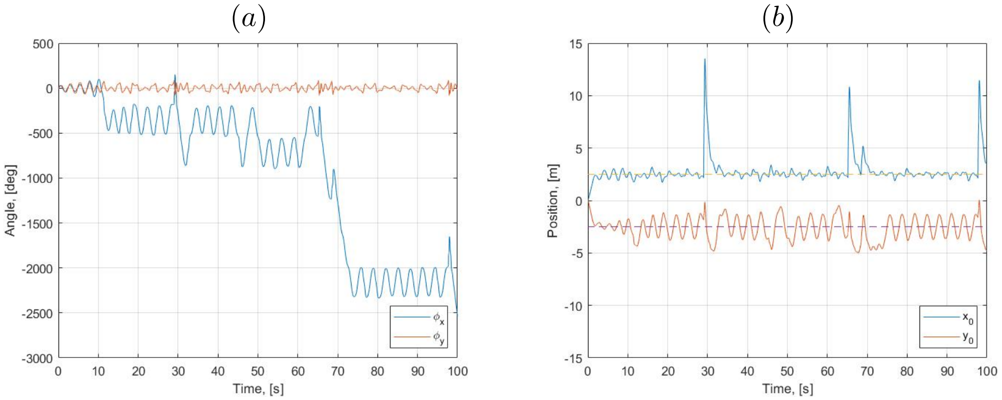

Figure 5.2.: Simulations when $K_p = 10$ and $K_d = 10$: (a) angles ϕ_x and ϕ_y and (b) motion of attachment point.

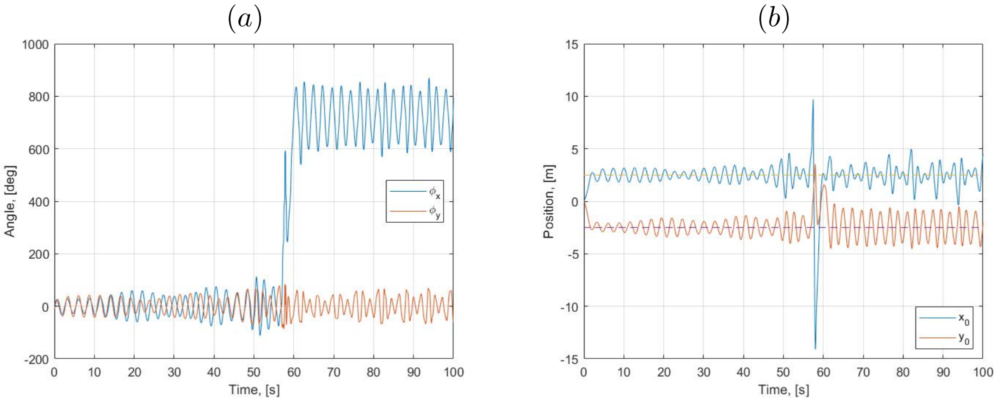

Figure 5.3.: Simulations when $K_p = 5$ and $K_d = 5$: (a) angles ϕ_x and ϕ_y and (b) motion of attachment point.

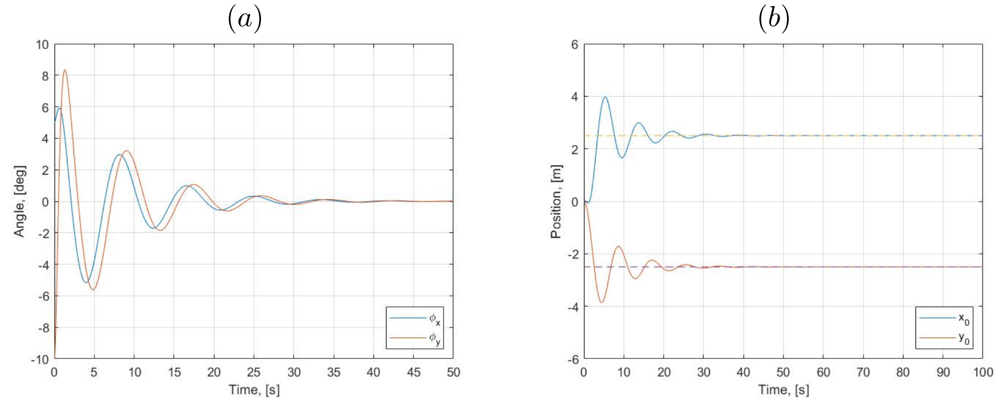

Figure 5.4.: Simulations when $K_p = 0.5$ and $K_d = 0.5$: (a) angles ϕ_x and ϕ_y and (b) motion of attachment point.

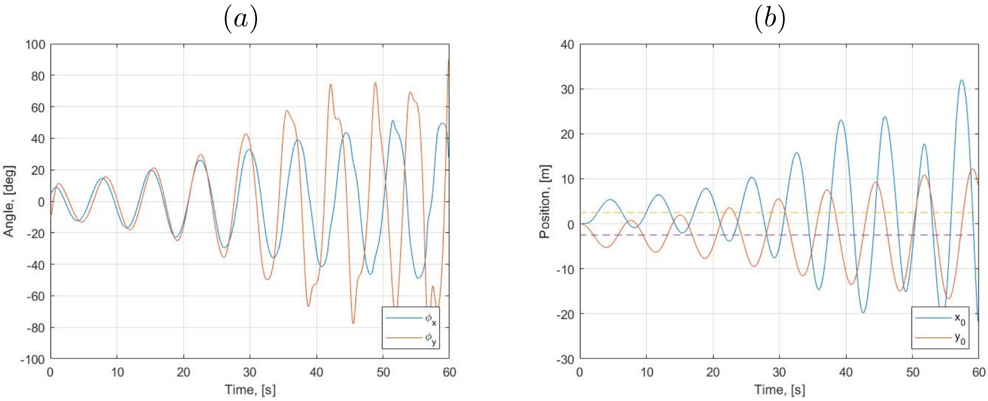

Figure 5.5.: Simulations when $K_p = 0.75$ and $K_d = 0.25$: (a) angles ϕ_x and ϕ_y and (b) motion of attachment point.

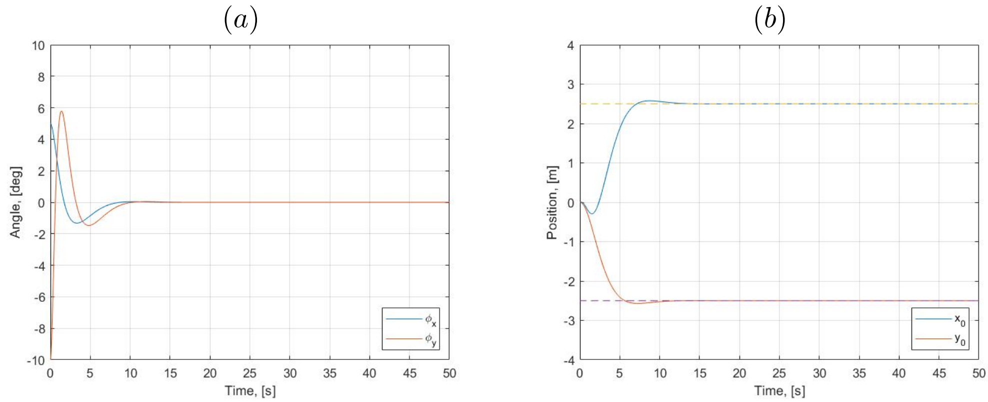

Figure 5.6.: Simulations when $K_p = 0.25$ and $K_d = 0.75$: (a) angles ϕ_x and ϕ_y and (b) motion of attachment point.

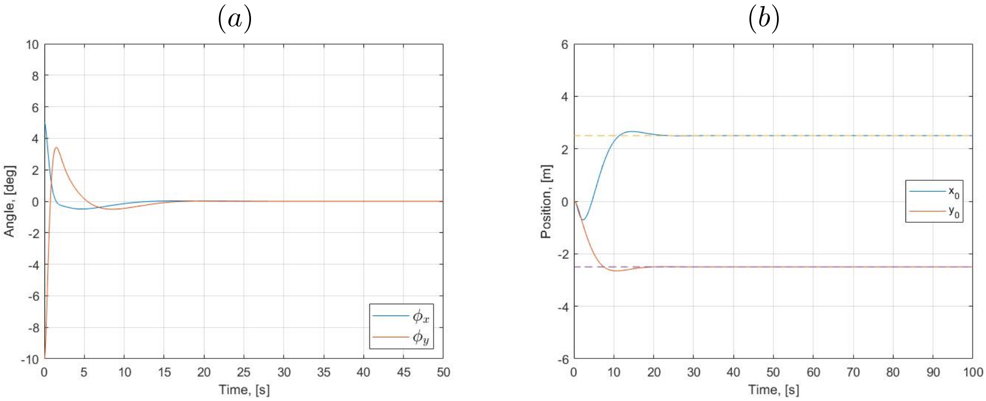

Figure 5.7.: Simulations when $K_p = \omega_{XY}^2$ and $K_d = 2\zeta\omega_{XY}$: (a) angles ϕ_x and ϕ_y and (b) motion of attachment point.

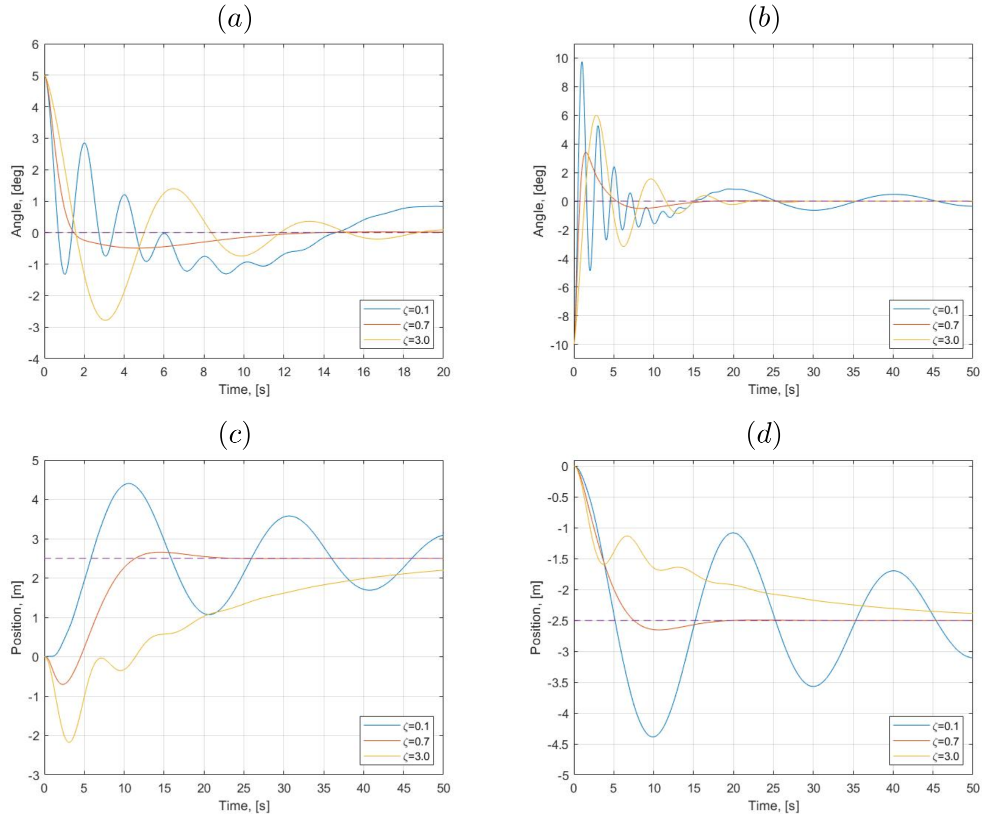

Figure 5.8.: Simulations of damping ratios $\zeta = 0.1$, $\zeta = 0.7$ and $\zeta = 3$: (a) angle ϕ_x (b) angle ϕ_y (c) motion of attachment point in the x direction and (d) in the x direction.

5.3. Cyclical Trajectories

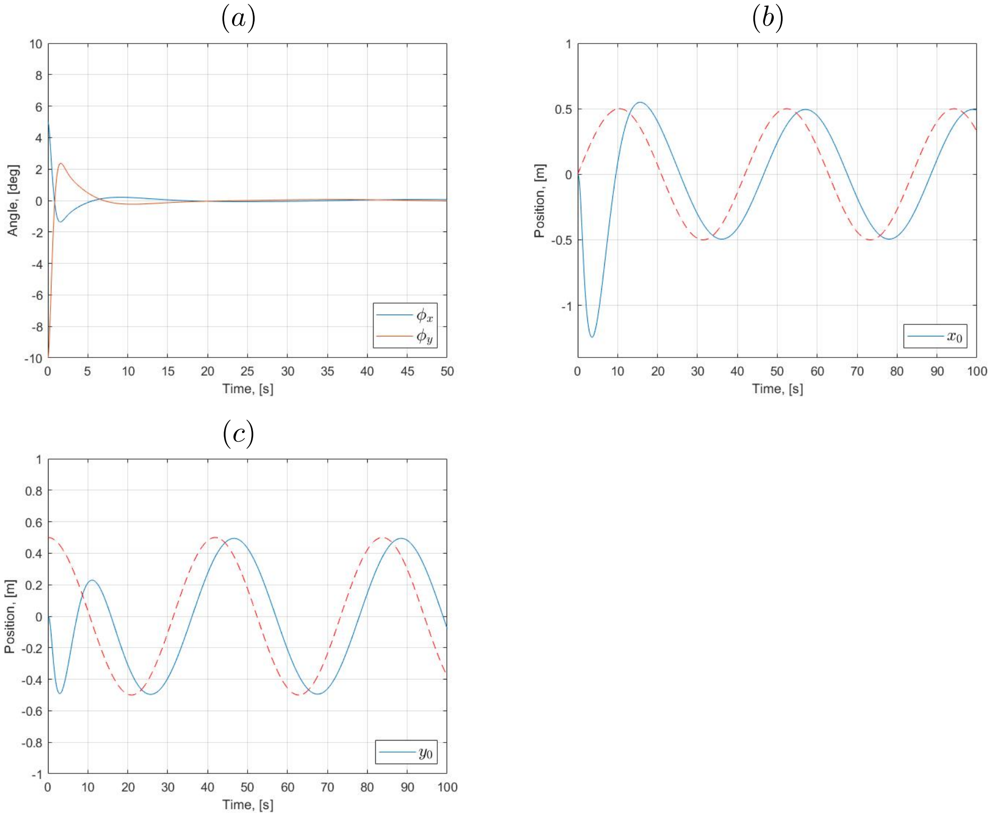

Figure 5.9.: Simulations with cyclical trajectories $r_x = 0.5\sin(0.15t)$ and $r_y = 0.5\cos(0.15t)$ for $K_p = \omega_{XY}^2$ and $K_d = 2\zeta\omega_{XY}$: (a) angles ϕ_xnd ϕ_y, (b) motion in the x direction and (c) in the y direction

5.4. Velocity as Input

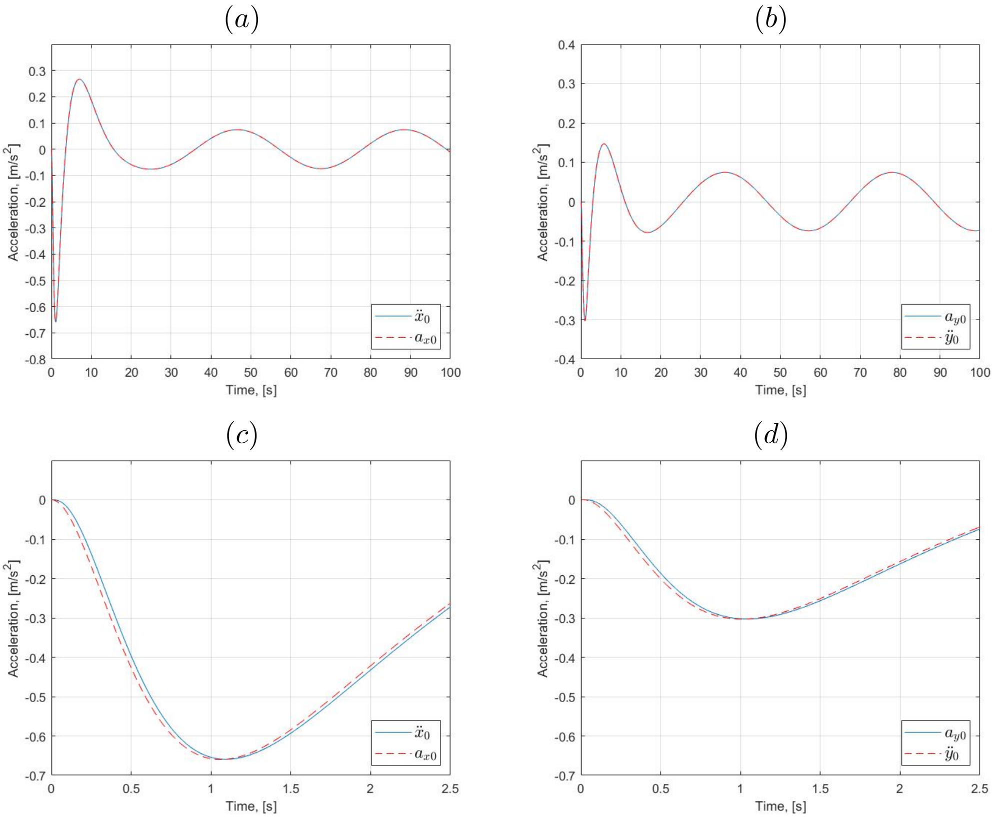

Figure 5.10.: Simulations where the acceleration in the velocity loop is compared to the acceleration out the controller: (a) acceleration in the x direction, (b) acceleration in the y direction, (c) a zoomed plot of the acceleration in x direction and (d) in the y direction.

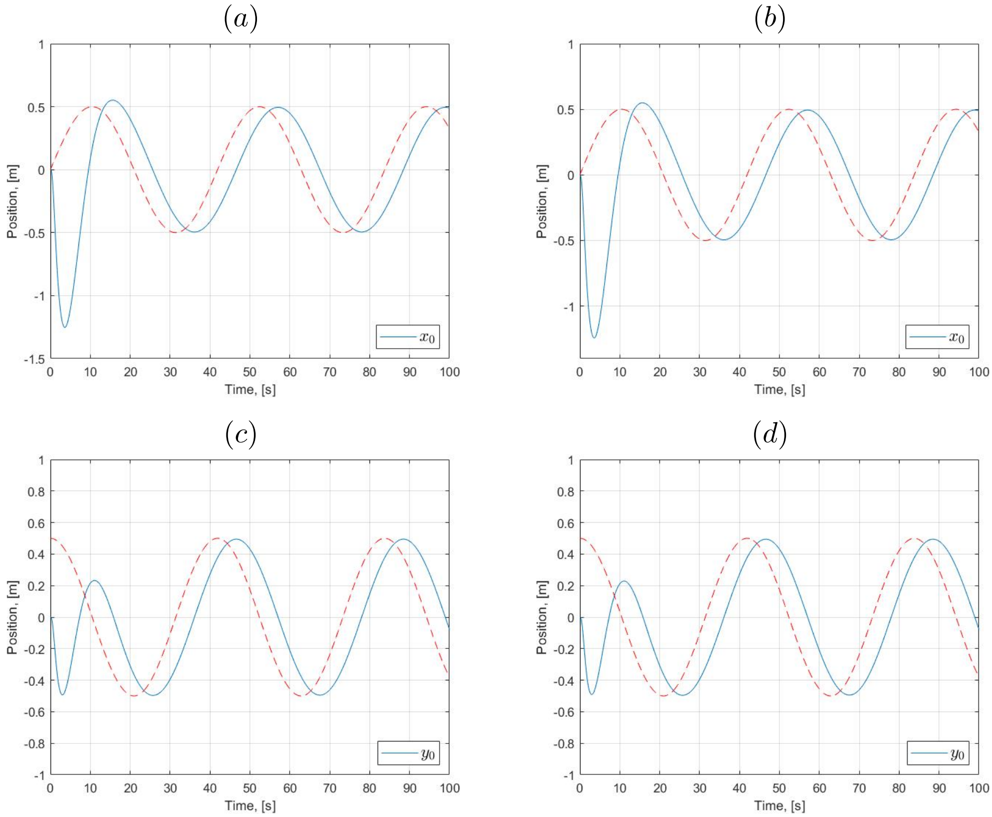

Figure 5.11.: A comparison of the attachment point's motion using the two accelerations: (a) the acceleration out of the controller in the x direction, (b) the acceleration from the velocity loop in the x direction, (c) the acceleration out of the controller in the y direction and (d) in the y direction

5.5. Moving Attachment Point in x, y and z Direction

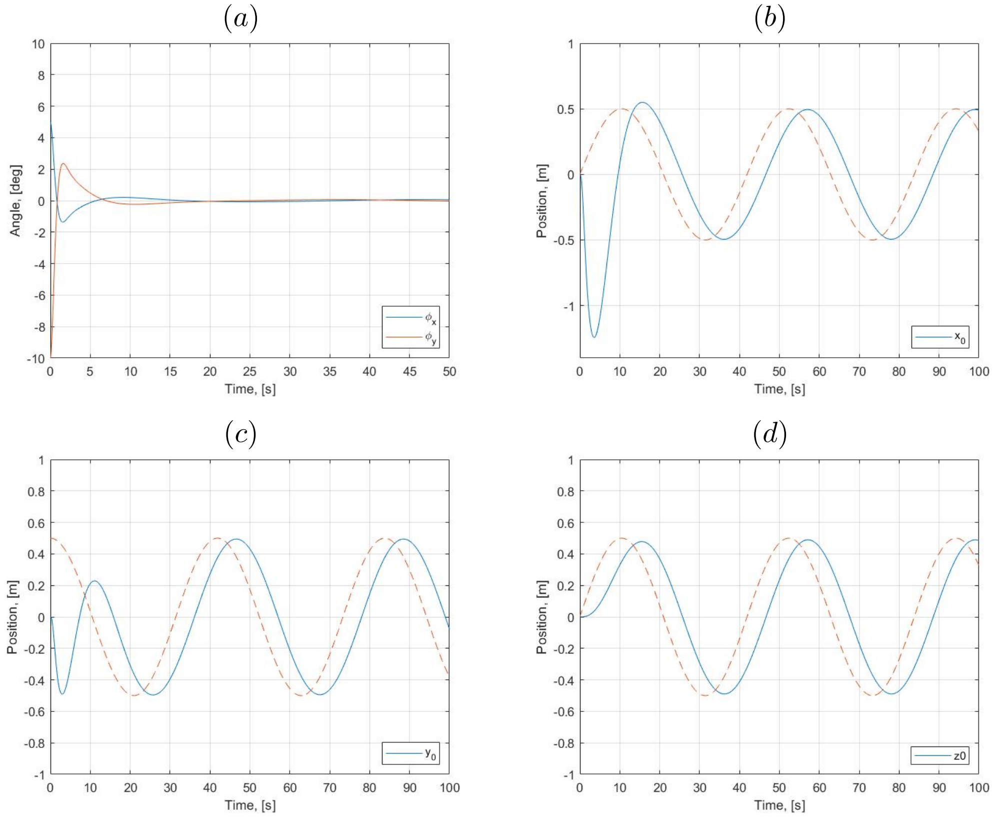

Figure 5.12.: Simulations when attachment point is moving in 3D: (a) angles ϕ_x and ϕ_y, and motion of attachment point in the (b)x direction, (c) y direction and (d) z direction with cyclical trajectories.

5.6. Moving Attachment Point and Varying Rope Length

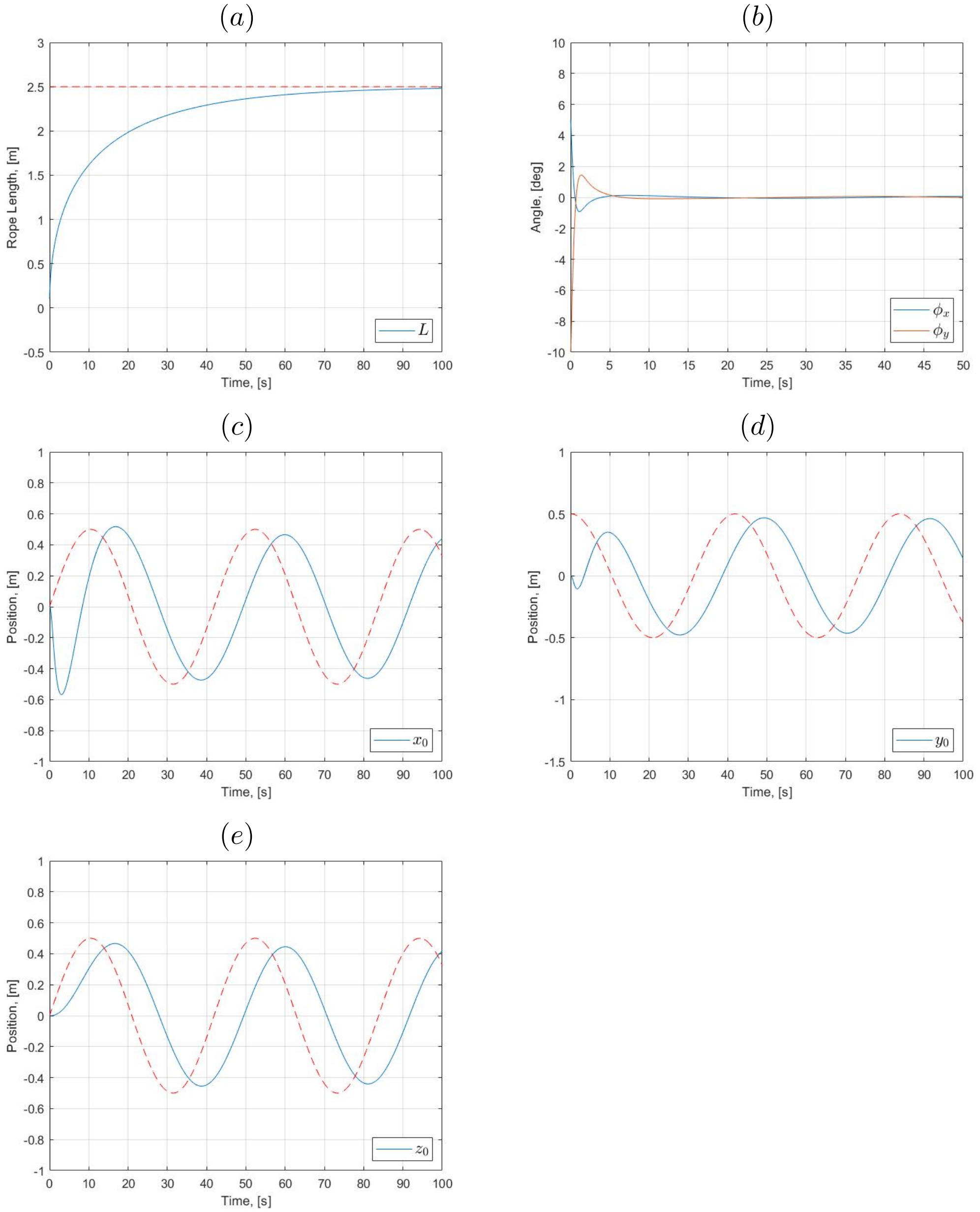

Figure 5.13.: Simulations for increasing rope length and cyclical trajectories: (a) rope length, (b) angles ϕ_x and ϕ_y, (c) motion in the x direction, (d) motion in the y direction, and (e) motion in the z direction.

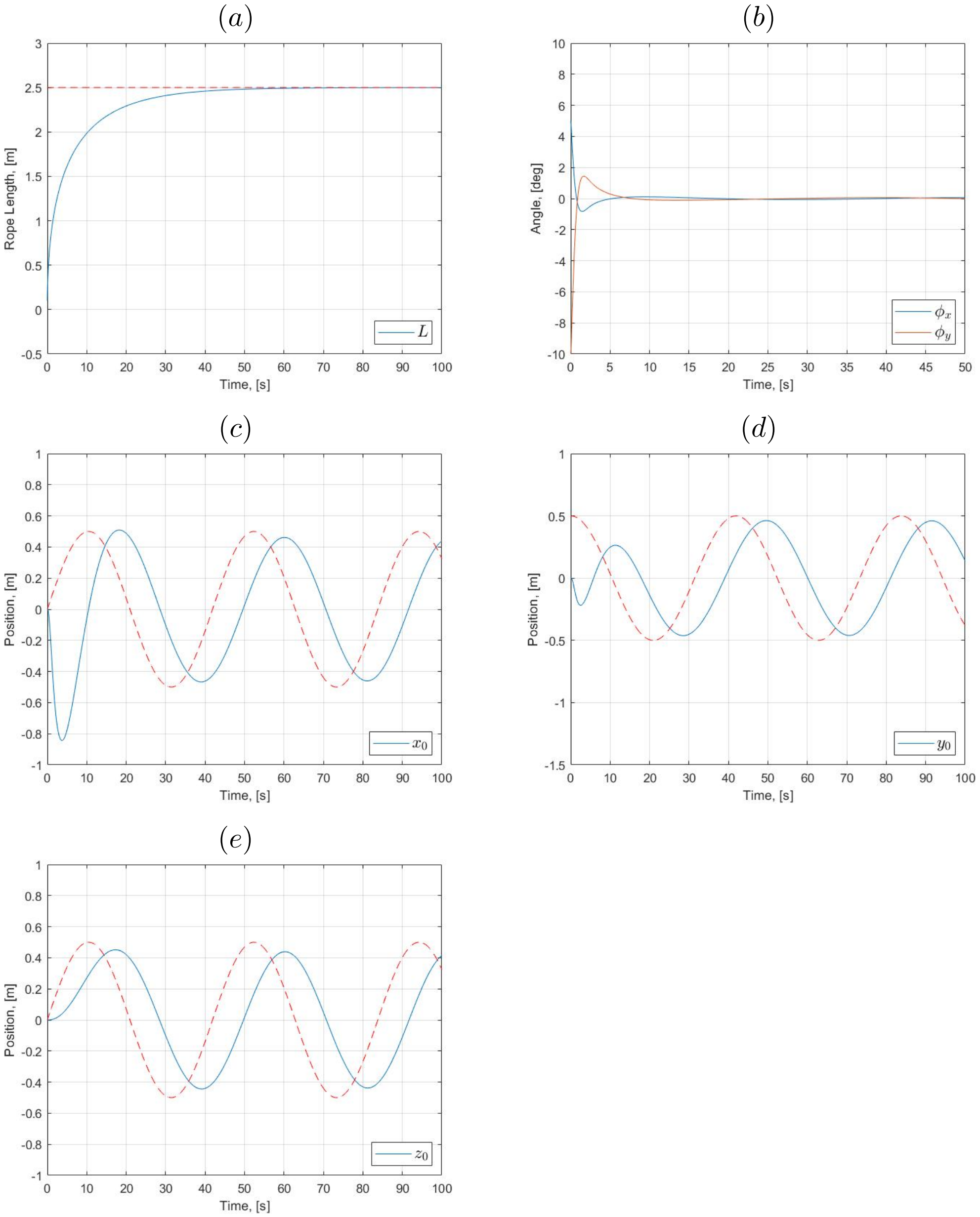

Figure 5.14.: Simulations for increasing rope length and cyclical trajectories with change damping: (a) rope length, (b) angles ϕ_x and ϕ_y, (c) motion in the x direction, (d) motion in the y direction, and (e) motion in the z direction.

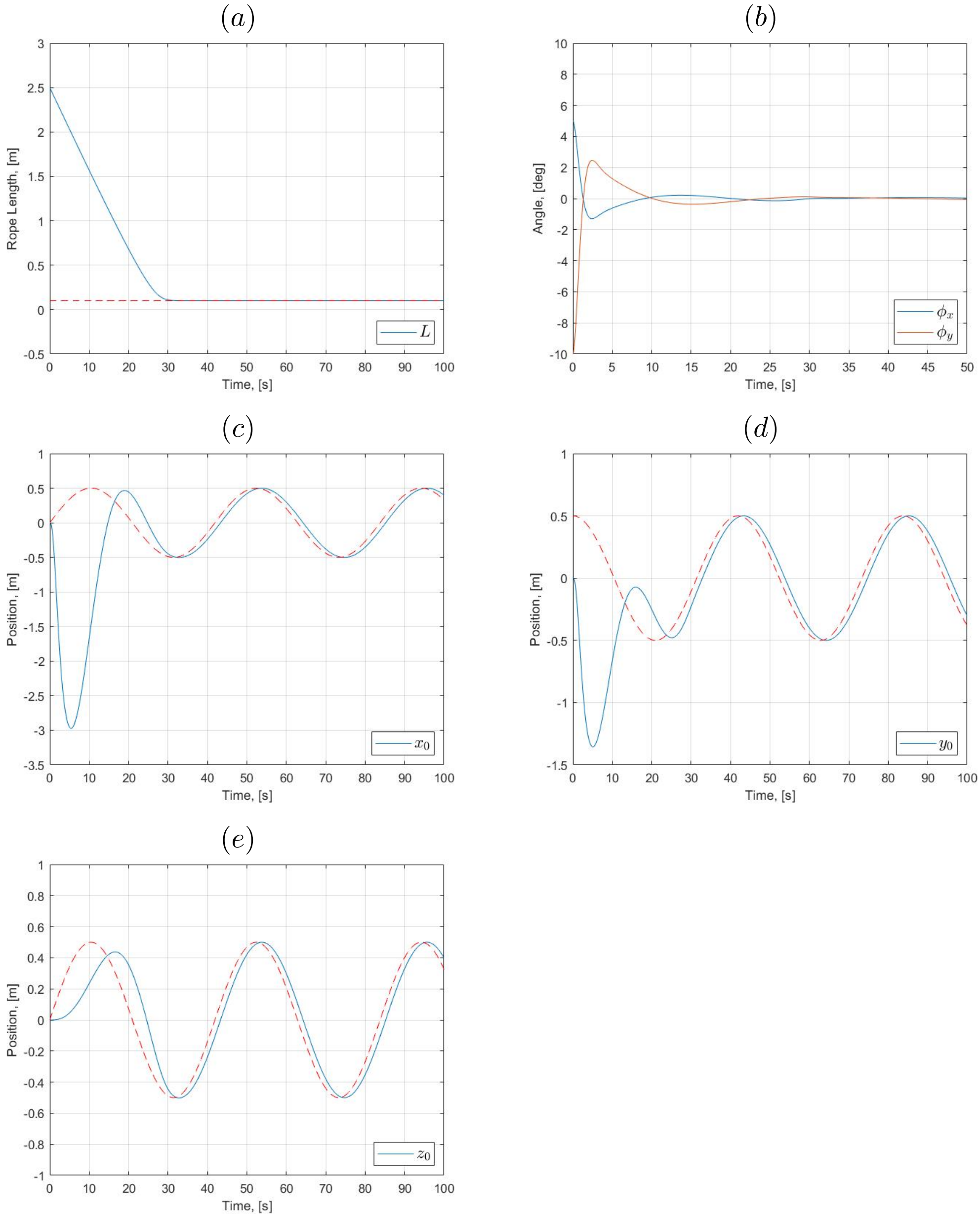

Figure 5.15.: Simulations for decreasing rope length and cyclical trajectories: (a) rope length, (b) angles ϕ_x and ϕ_y, (c) motion in the x direction, (d) motion in the y direction, and (e) motion in the z direction.

5.7. Planned Trajectory - Constant Rope Length

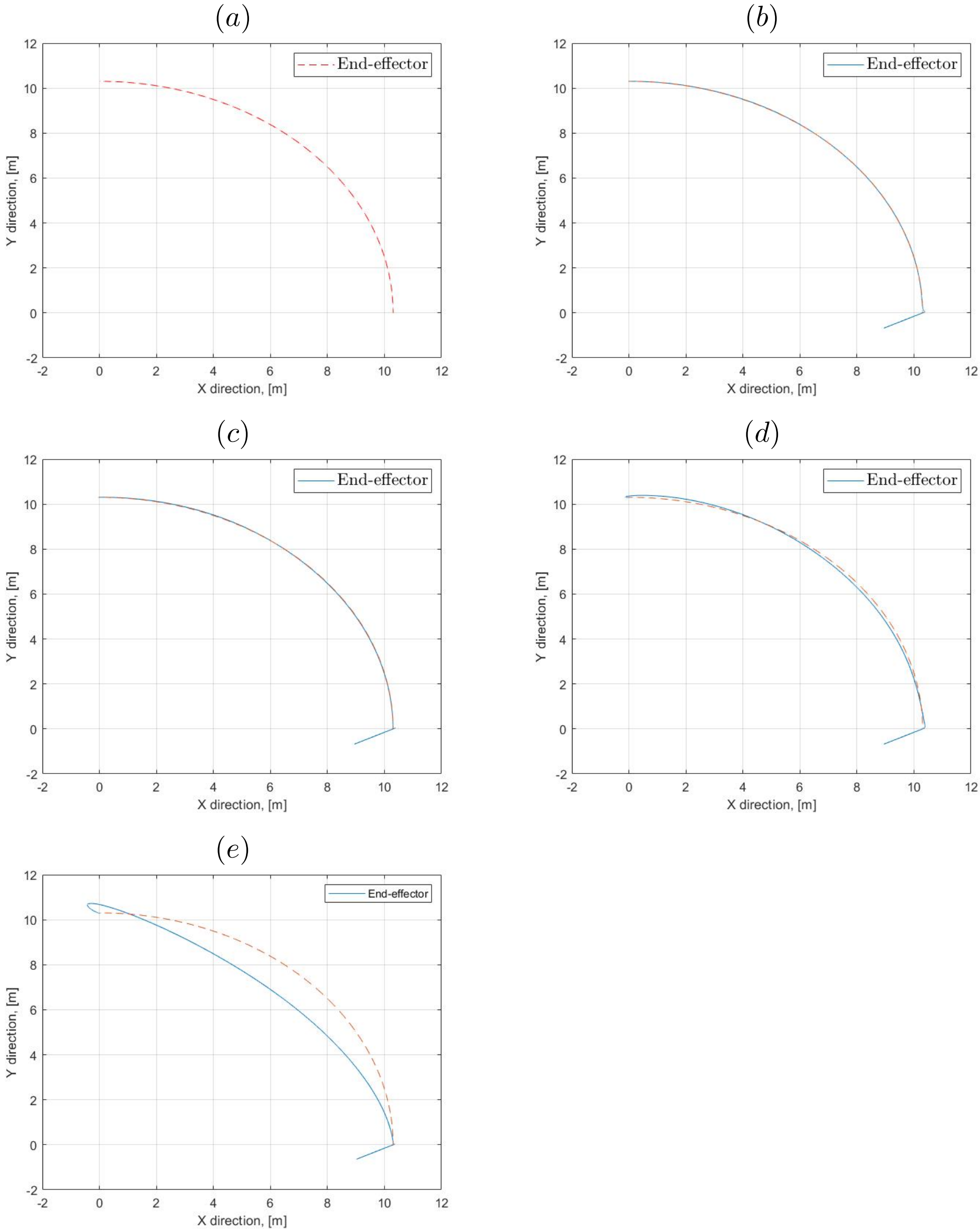

Figure 5.16.: Simulation for the planned trajectory when the rope length is constant: (a) trajectory of end-effector, (b) motion of end-effector when $t_f = 100\,\text{s}$ and $t_s = 10\,\text{s}$, (c) $t_f = 100\,\text{s}$ and $t_s = 20\,\text{s}$, (d) $t_f = 50\,\text{s}$ and $t_s = 10\,\text{s}$, and (e) $t_f = 50\,\text{s}$ and $t_s = 20\,\text{s}$

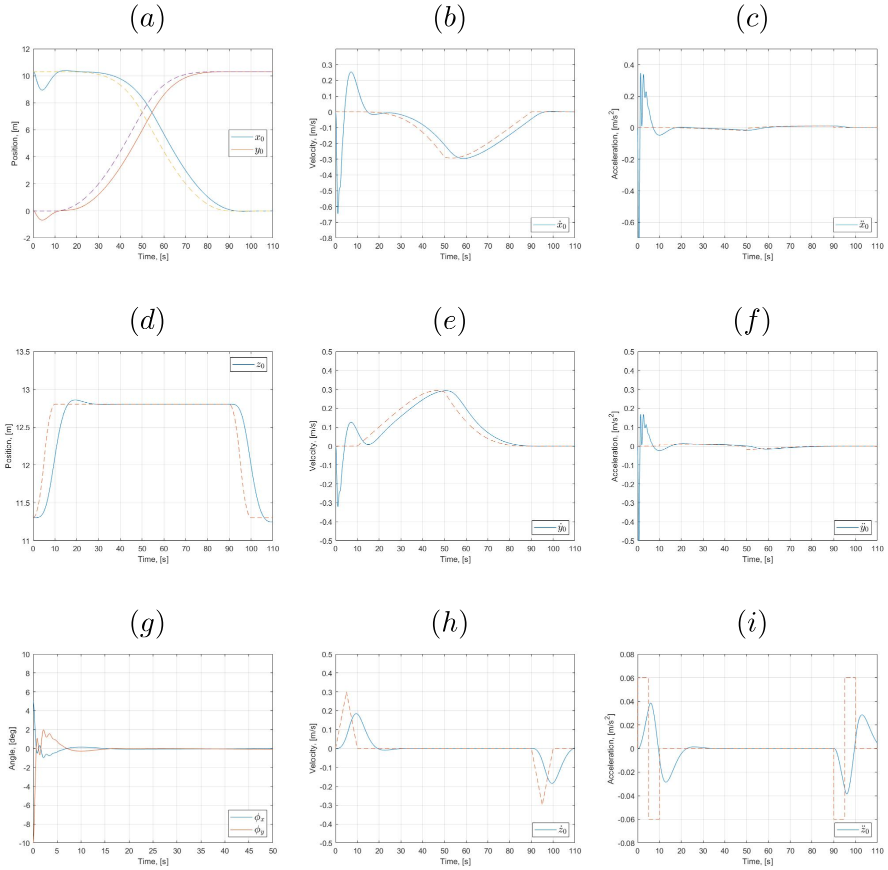

Figure 5.17.: Simulations for $t_f = 100\,\mathrm{s}$ and $t_s = 10\,\mathrm{s}$ with constant rope length: (a) motion of end-effector in the x and y direction, (b) velocity in the x direction, (c) acceleration in the x direction, (d) motion of end-effector in z direction, (e) velocity in the y direction,(f) acceleration in the y direction, (g) angles ϕ_x and ϕ_y, (h) velocity in the z direction, and (i) acceleration in the z direction

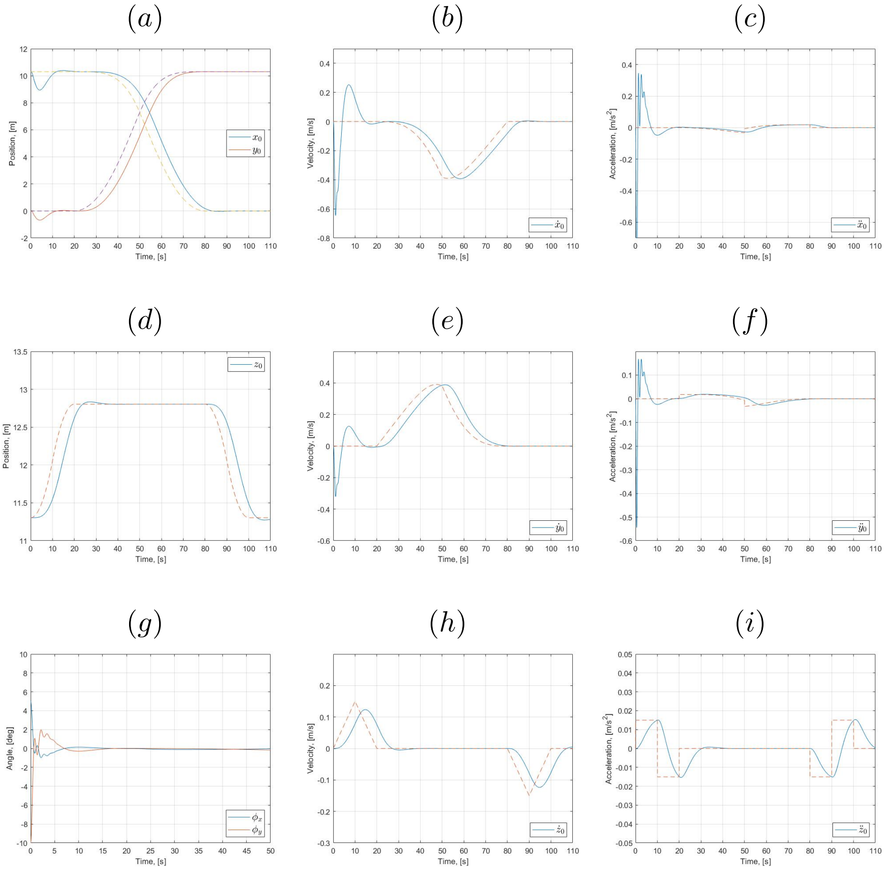

Figure 5.18.: Simulations for$t_f = 100\,$s and $t_s = 20\,$s with constant rope length: (a) motion of end-effector in the x and y direction, (b) velocity in the x direction, (c) acceleration in the x direction, (d) motion of end-effector in z direction, (e) velocity in the y direction,(f) acceleration in the y direction, (g) angles ϕ_x and ϕ_y, (h) velocity in the z direction, and (i) acceleration in the z direction

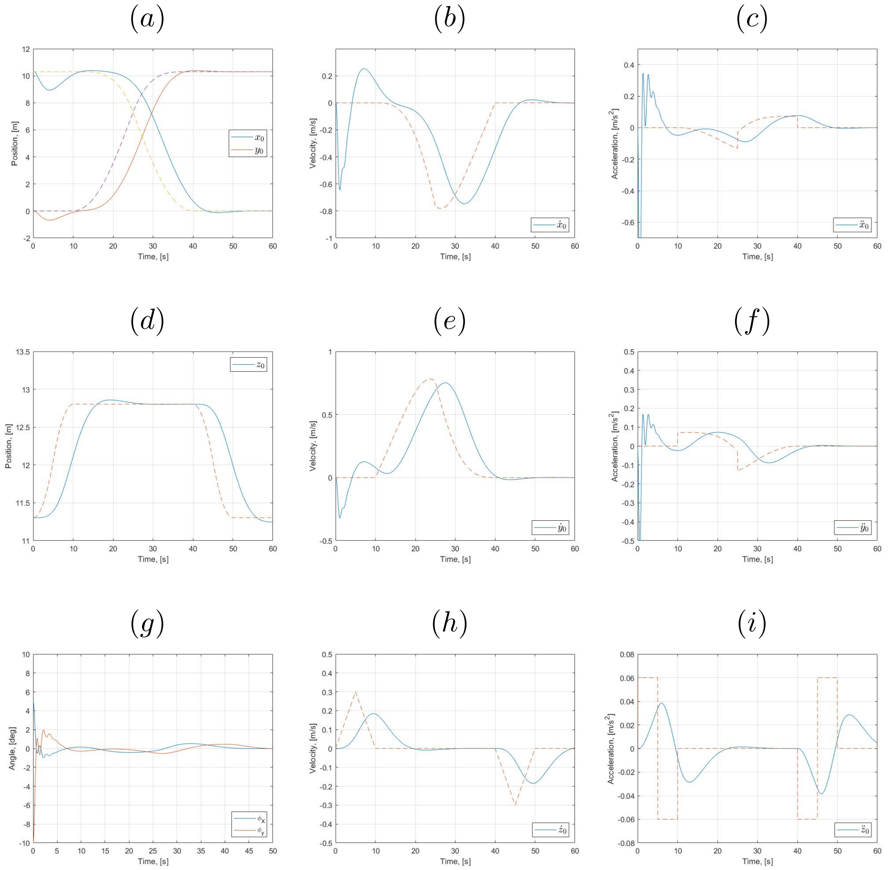

Figure 5.19.: Simulations for$t_f = 50\,\text{s}$ and $t_s = 10\,\text{s}$ with constant rope length: (a) motion of end-effector in the x and y direction, (b) velocity in the x direction, (c) acceleration in the x direction, (d) motion of end-effector in z direction, (e) velocity in the y direction,(f) acceleration in the y direction, (g) angles ϕ_x and ϕ_y, (h) velocity in the z direction, and (i) acceleration in the z direction

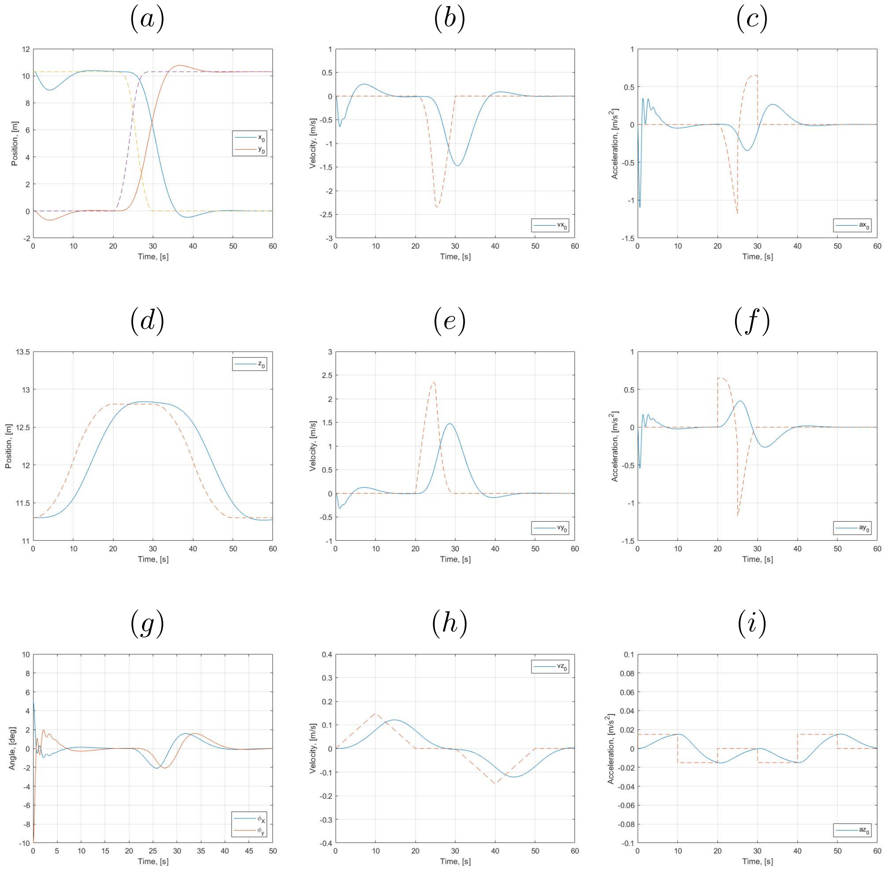

Figure 5.20.: Simulations fort$_f = 50\,$s and $t_s = 20\,$s with constant rope length: (a) motion of end-effector in the x and y direction, (b) velocity in the x direction, (c) acceleration in the x direction, (d) motion of end-effector in z direction, (e) velocity in the y direction,(f) acceleration in the y direction, (g) angles ϕ_x and ϕ_y, (h) velocity in the z direction, and (i) acceleration in the z direction

5.8. Planned Trajectory - Varying Rope Length

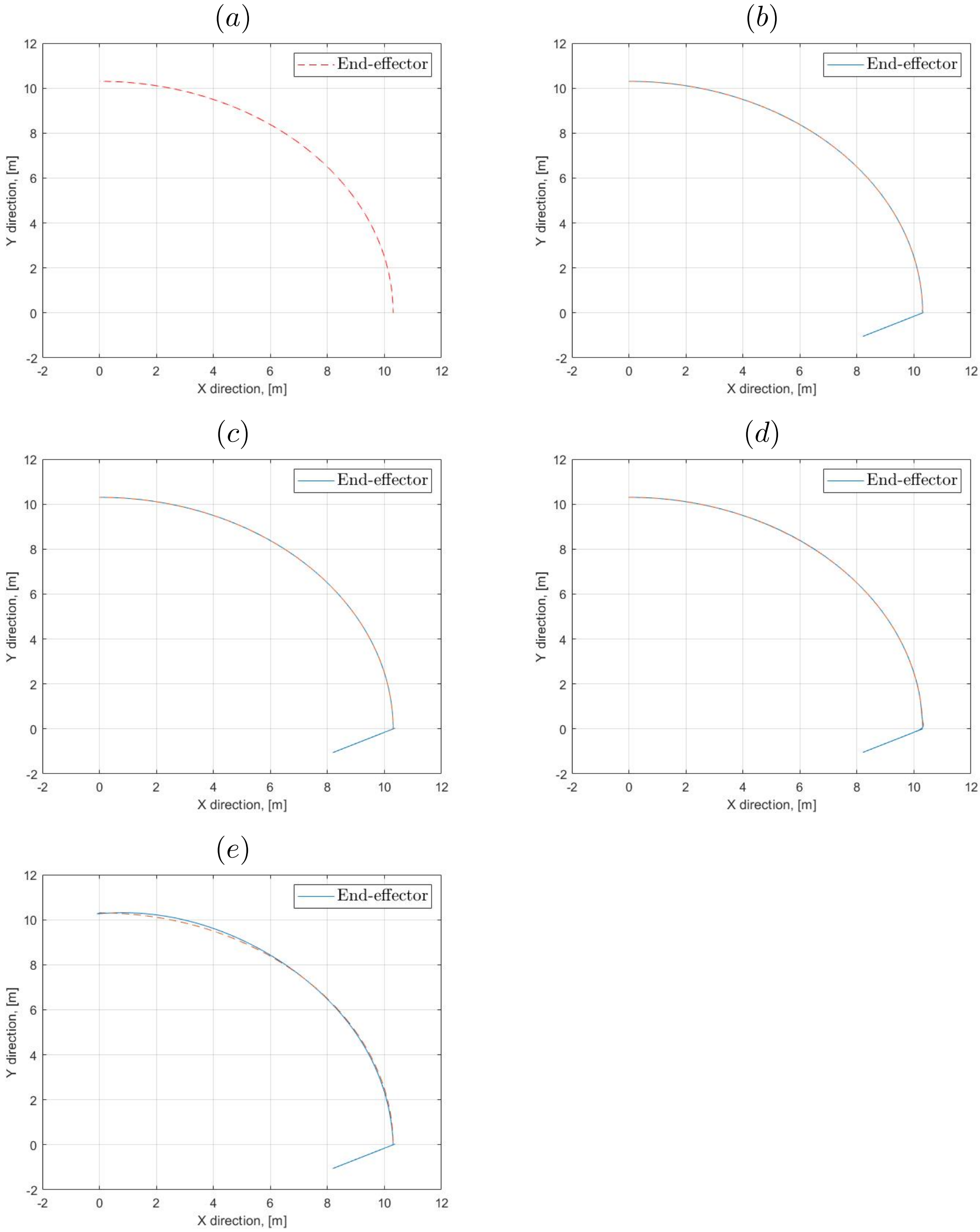

Figure 5.21.: Simulation for the planned trajectory when the rope length is varying: (a) trajectory of end-effector, (b) motion of end-effector when $t_f = 100\,\text{s}$ and $t_s = 10\,\text{s}$, (c) $t_f = 100\,\text{s}$ and $t_s = 20\,\text{s}$, (d) $t_f = 50\,\text{s}$ and $t_s = 10\,\text{s}$, and (e) $t_f = 50\,\text{s}$ and $t_s = 20\,\text{s}$

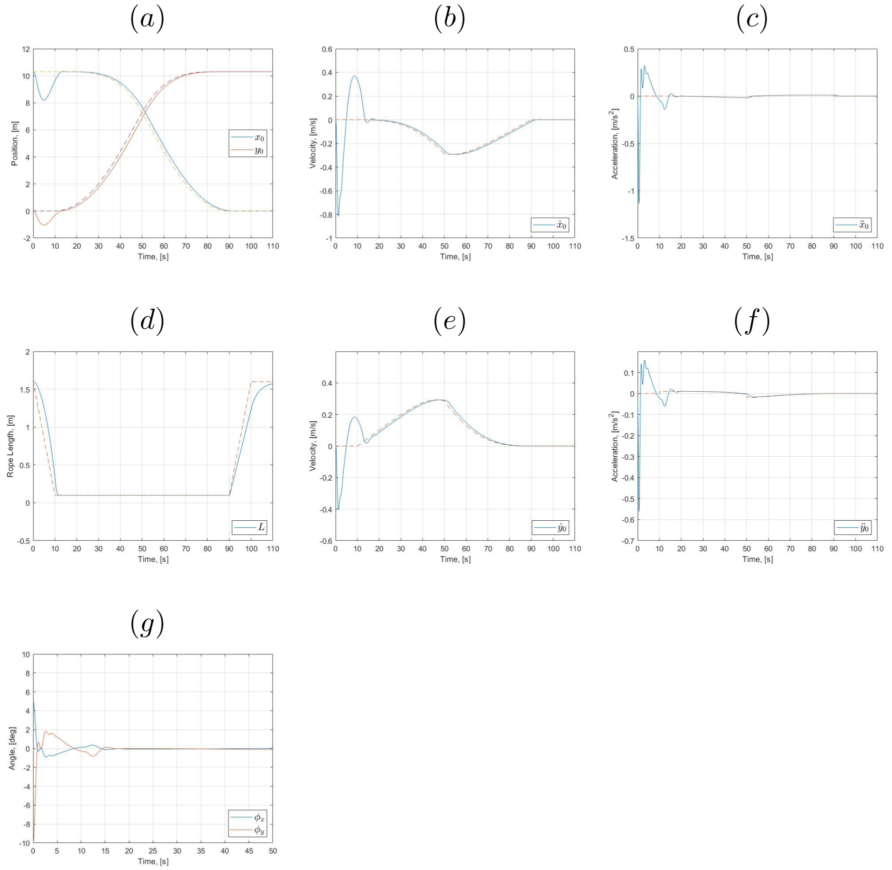

Figure 5.22.: Simulations for$t_f = 100\,\text{s}$ and $t_s = 10\,\text{s}$ with varying rope length: (a) motion of end-effector in the x and y direction, (b) velocity in the x direction, (c) acceleration in the x direction, (d) motion of end-effector in z direction, (e) velocity in the y direction,(f) acceleration in the y direction, (g) angles ϕ_x and ϕ_y

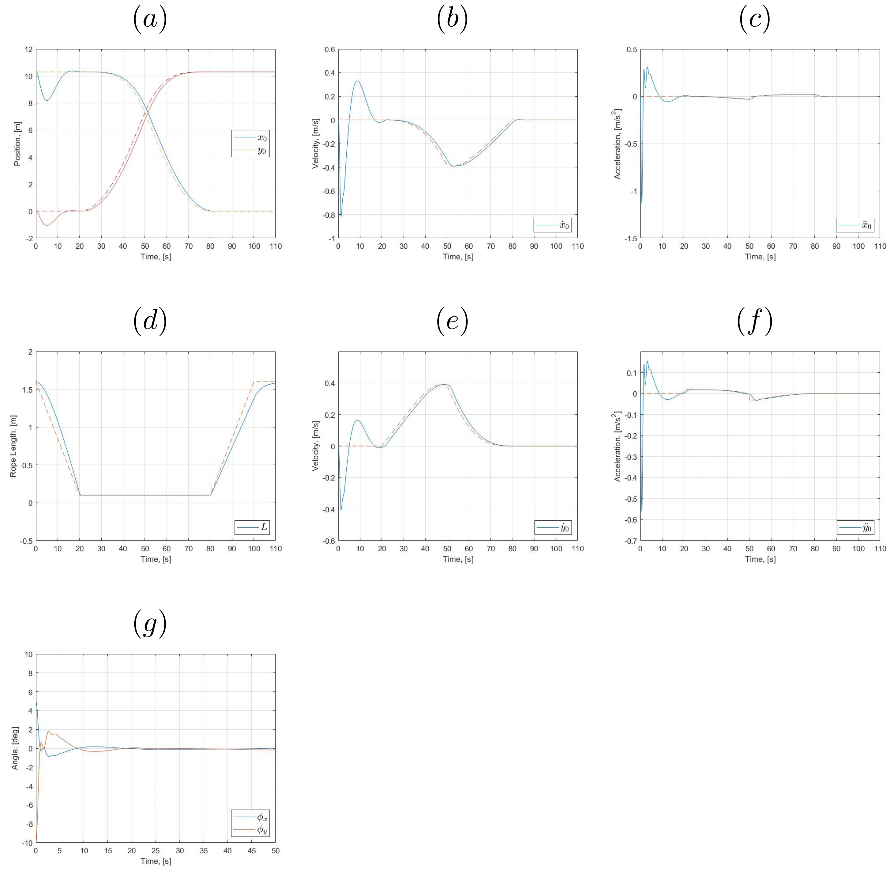

Figure 5.23.: Simulations for$t_f = 100\,\text{s}$ and $t_s = 20\,\text{s}$ varying rope length: (a) motion of end-effector in the x and y direction, (b) velocity in the x direction, (c) acceleration in the x direction, (d) motion of end-effector in z direction, (e) velocity in the y direction,(f) acceleration in the y direction, (g) angles ϕ_x and ϕ_y

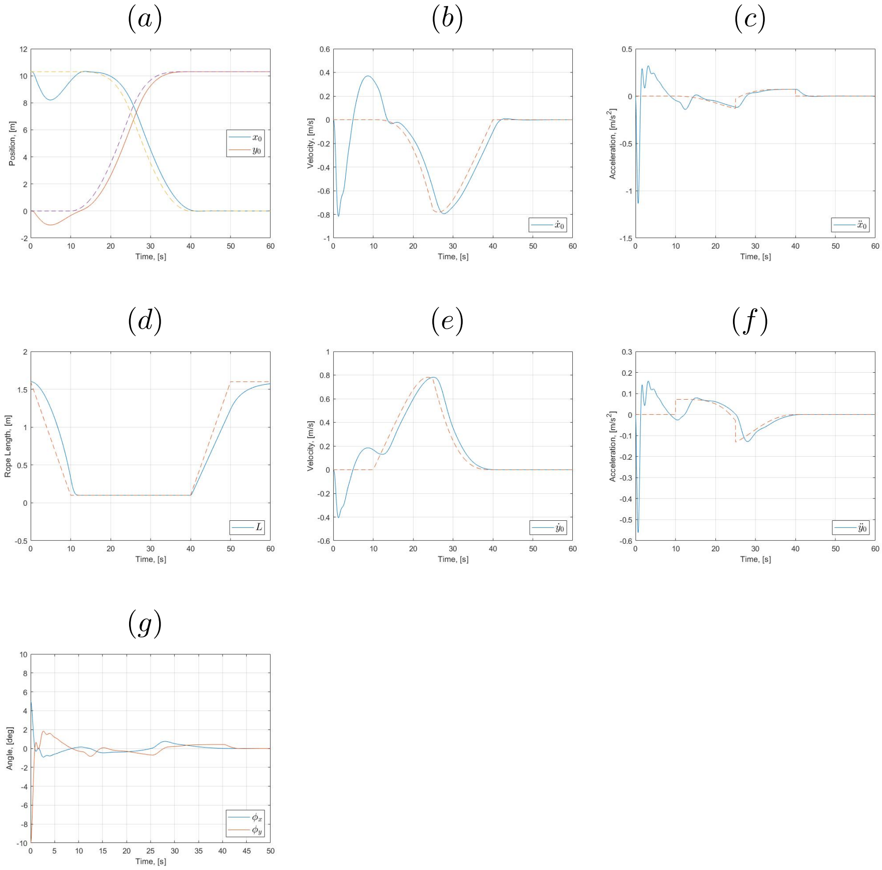

Figure 5.24.: Simulations for$t_f = 50\,\mathrm{s}$ and $t_s = 10\,\mathrm{s}$ with varying rope length: (a) motion of end-effector in the x and y direction, (b) velocity in the x direction, (c) acceleration in the x direction, (d) motion of end-effector in z direction, (e) velocity in the y direction,(f) acceleration in the y direction, (g) angles ϕ_x and ϕ_y

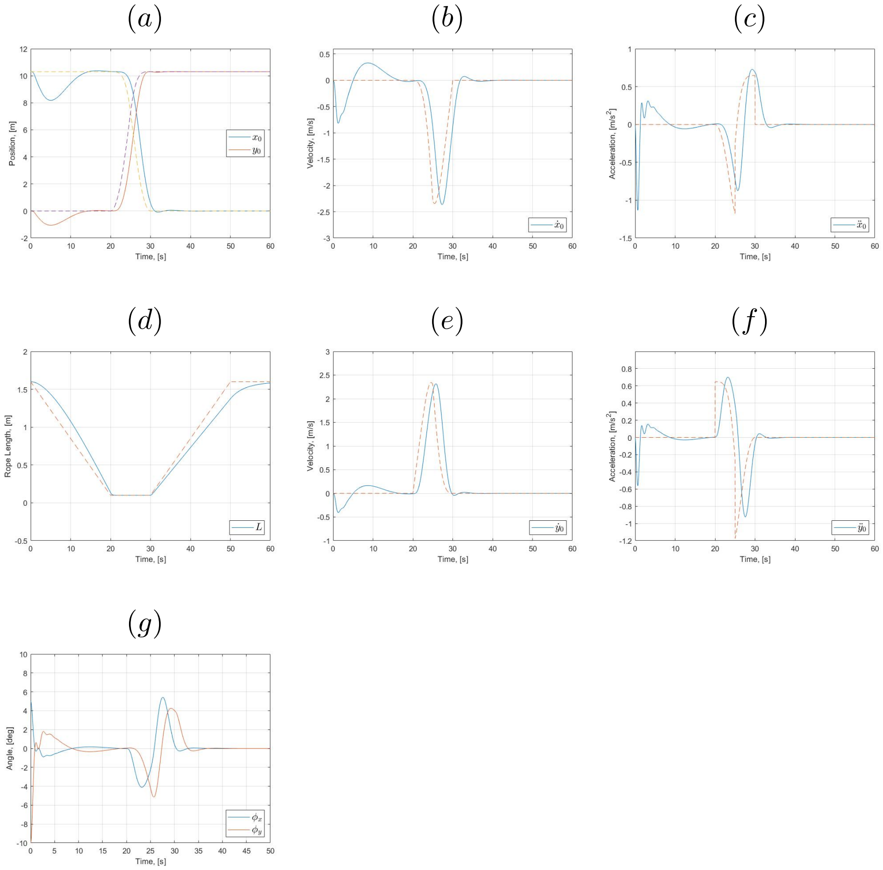

Figure 5.25.: Simulations for$t_f = 50\,$s and $t_s = 20\,$s with varying rope length: (a) motion of end-effector in the x and y direction, (b) velocity in the x direction, (c) acceleration in the x direction, (d) motion of end-effector in z direction, (e) velocity in the y direction,(f) acceleration in the y direction, (g) angles ϕ_x and ϕ_y

5.9. Actuators - Constant Rope Length

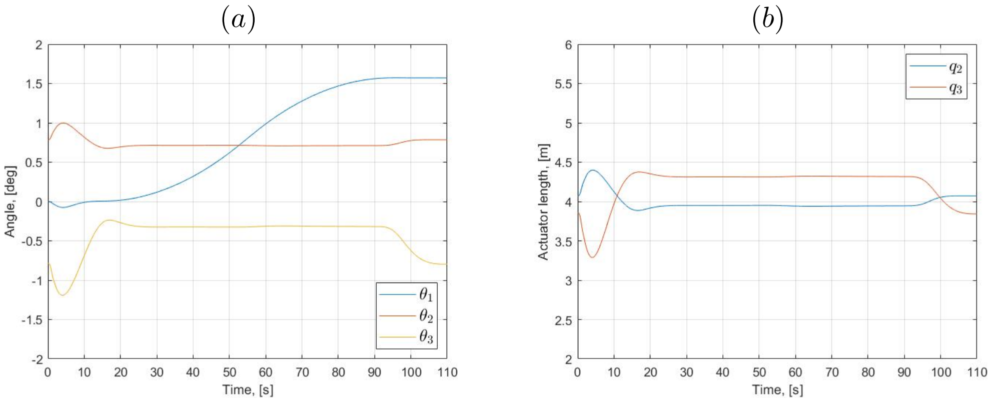

Figure 5.26.: Simulations of actuators when rope length is constant and $t_f = 100\,\mathrm{s}$ and $t_s = 10\,\mathrm{s}$: (a) angles θ_1, θ_2 and θ_3 and (b) the resulting motion in the linear actuators of the knuckle boom crane.

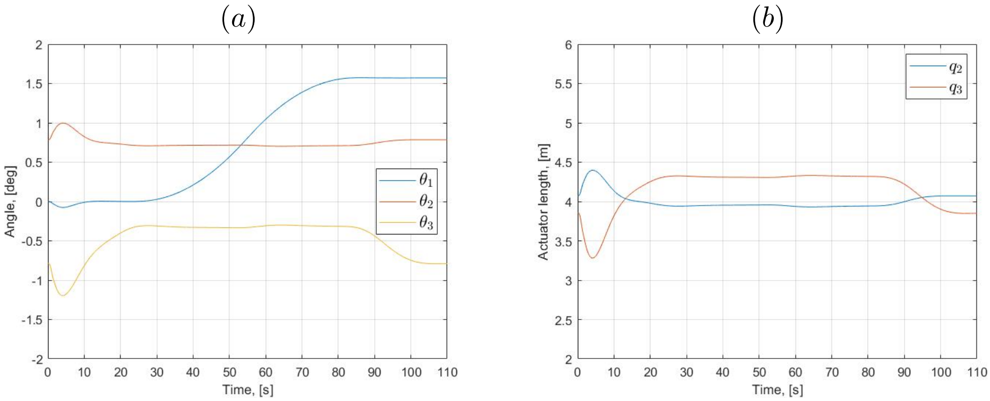

Figure 5.27.: Simulations of actuators when rope length is constant and $t_f = 100\,\mathrm{s}$ and $t_s = 20\,\mathrm{s}$: (a) anglesθ_1, θ_2 and θ_3 and (b) the resulting motion in the linear actuators of the knuckle boom crane.

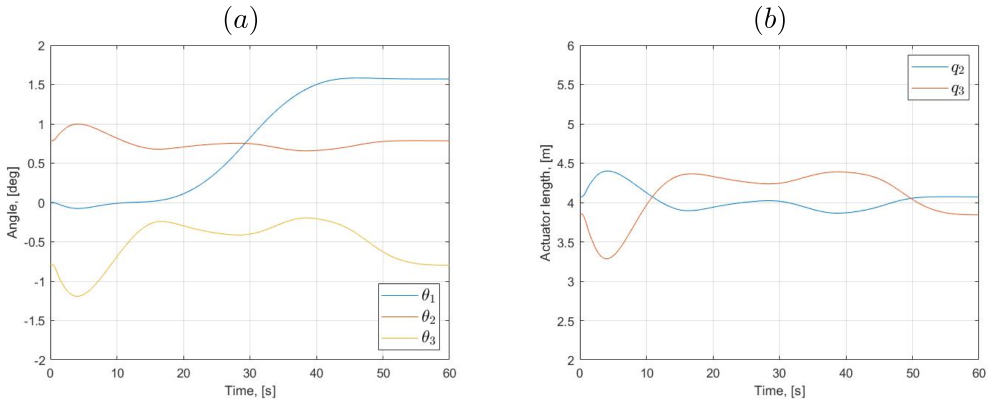

Figure 5.28.: Simulations of actuators when rope length is constant and $t_f = 50\,\mathrm{s}$ and $t_s = 10\,\mathrm{s}$: (a) angles θ_1, θ_2 and θ_3 and (b) the resulting motion in the linear actuators of the knuckle boom crane.

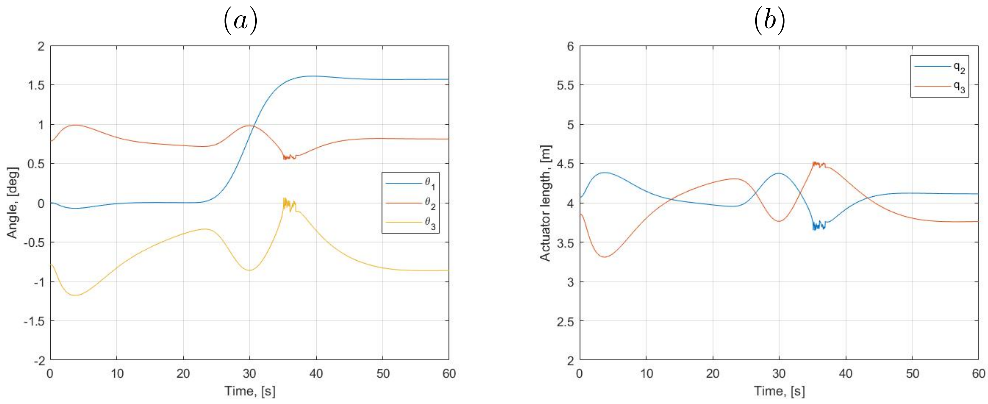

Figure 5.29.: Simulations of actuators when rope length is constant and $t_f = 50\,\mathrm{s}$ and $t_s = 20\,\mathrm{s}$: (a) angles θ_1, θ_2 and θ_3 and (b) the resulting motion in the linear actuators of the knuckle boom crane.

5.10. Actuators - Varying Rope Length

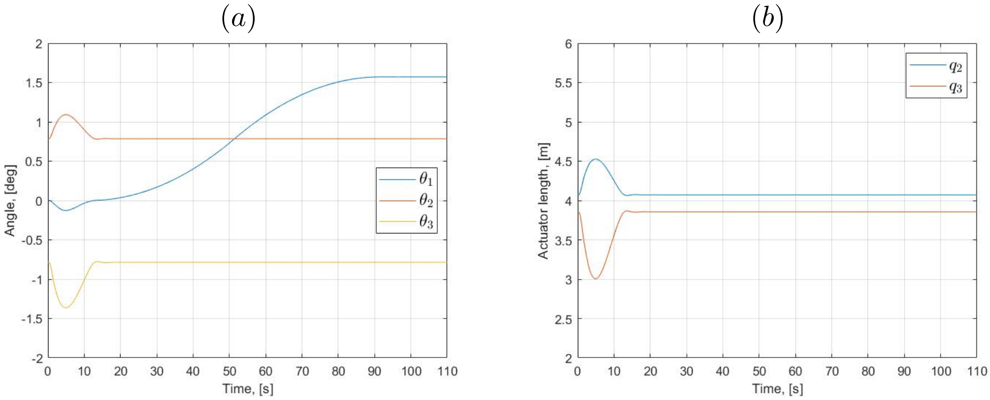

Figure 5.30.: Simulations of actuators when rope length is varying and $t_f = 100\,\mathrm{s}$ and $t_s = 10\,\mathrm{s}$: (a) angles θ_1, θ_2 and θ_3 and (b) the resulting motion in the linear actuators of the knuckle boom crane.

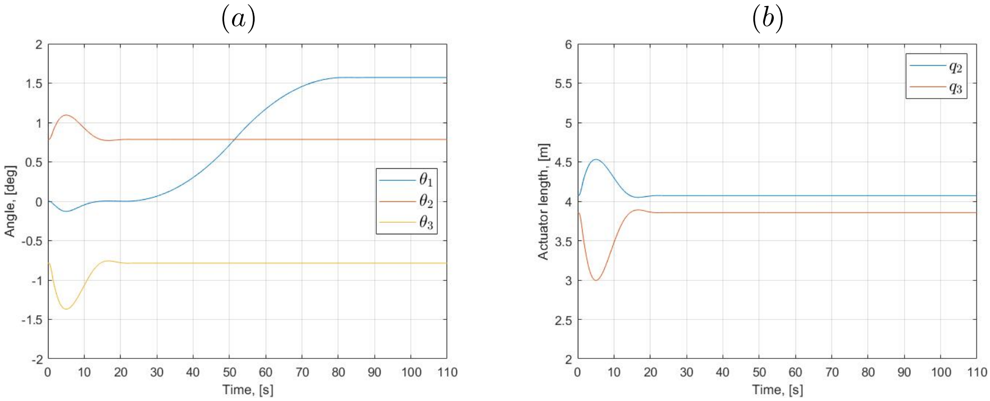

Figure 5.31.: Simulations of actuators when rope length is varying and $t_f = 100\,\mathrm{s}$ and $t_s = 20\,\mathrm{s}$: (a) angles θ_1, θ_2 and θ_3 and (b) the resulting motion in the linear actuators of the knuckle boom crane.

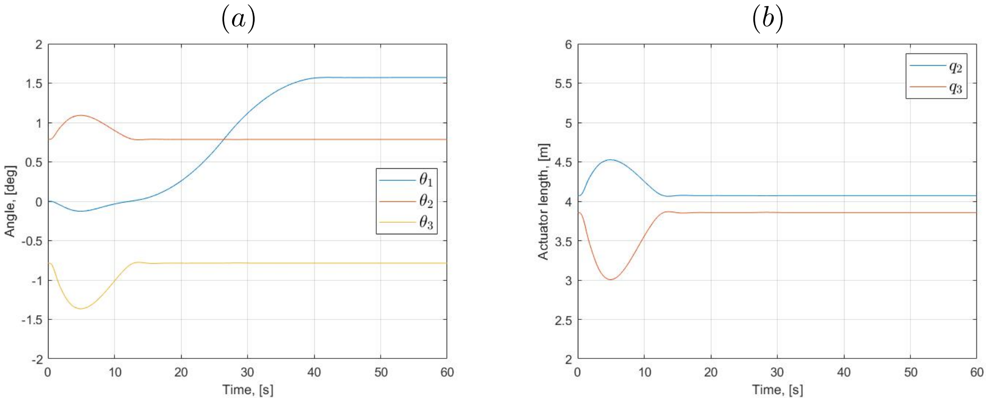

Figure 5.32.: Simulations of actuators when rope length is varying and $t_f = 50\,\mathrm{s}$ and $t_s = 10\,\mathrm{s}$: (a) angles θ_1, θ_2 and θ_3 and (b) the resulting motion in the linear actuators of the knuckle boom crane.

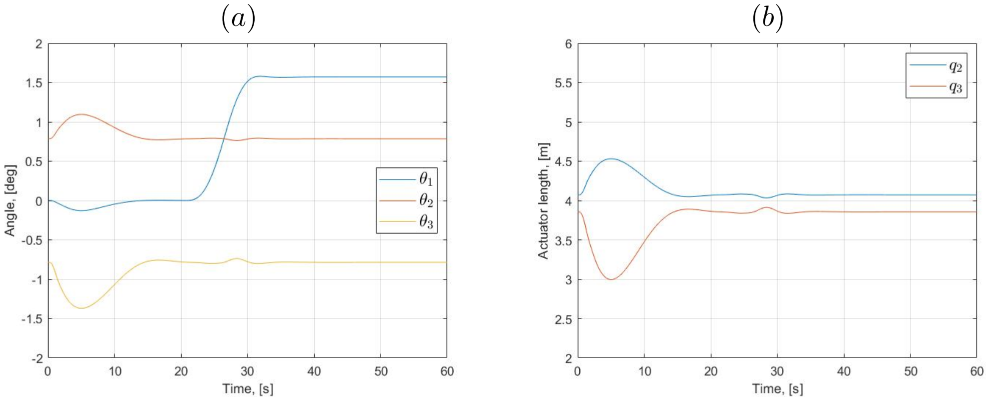

Figure 5.33.: Simulations of actuators when rope length is varying and $t_f = 50\,\mathrm{s}$ and $t_s = 20\,\mathrm{s}$: (a) angles θ_1, θ_2 and θ_3 and (b) the resulting motion in the linear actuators of the knuckle boom crane.

Chapter 6.

Discussion

6.1. Constant Trajectories

The system's ability to follow the desired path as well as stabilizing the payload based on the control gains K_p and K_d is shown in section 5.2. Both gains are inactive and the system only damps the oscillations, which is seen in Figure 5.1, where the angels ϕ_x and ϕ_y are damped within five seconds, while the position of the attachment point is nowhere near the trajectories. Without any constraints on where the attachment can move, the attachment point will drift off since its only assignment is to damp the oscillations.

When the gains are set to $K_p = 10$ and $K_d = 10$ does the system not follow the trajectories, nor damps the oscillations. From Figure 5.2 is seen that the high gains overrule the damping of the oscillation and are also overshooting the attempt to follow the trajectory of the attachment point. It is obvious that this solution is not feasible for any practical matter. There is progress When the gains are lowered to $K_p = 5$ and $K_d = 5$ in Figure 5.3, even though the ϕ_x takes off after 60 s, and none of the angels nor position converges towards their respective trajectories, the oscillate around the desired values, which is an improvement.

Further, the gains are lowered to below 1, and the contours of a functional system can be seen in Figure 5.4. Both of the angles and the position converge towards their trajectories and are more or less stable after 45 s. It is seen that ϕ_y has a bigger amplitude which is logical given its initial value is greater than for ϕ_x.

When examining the situation where the gains are not equal to each other a tendency is shown in Figure 5.5 and Figure 5.6. When $K_p > K_d$ the oscillations amplifies gradually, leading to a non-functioning system. According to section 3.14, the term $K_d\dot{x}_0$ slows down the acceleration when the velocity is high. This does not affect the system now, and the main contributor to the acceleration is the difference between the desired and the actual position of the attachment point. when $K_p < K_d$ the result is more satisfactory, and the oscillations and position converge within 10 s which is an improvement from when the gains were equal.

As mentioned in section 5.1, to ensure a robust system concerning varying rope lengths, periods and frequencies are the variables L and ω_0 included, through ω_{XY} into the damping equations. If Figure 5.7 is compared to Figure 5.6 the positions of the attachment point converging faster for $K_p = 0.25$ and $K_d = 0.75$ than for $K_p = \omega_{XY}^2$ and $K_d = 2\zeta\omega_{XY}$. The angles are stable at approximately the same time, but the amplitude is greater for the previous values. It is logical that a quick converging of the position excites larger oscillations of the pendulum. It might be more desirable for the system to have a smooth converging, than for it to reach the equilibrium as rapidly as possible.

In section 3.3 the assets of the damping ratio were described and Figure 5.8 shows that for positions are reacting according to the theory. For $\zeta = 0.1$ the system is clearly underdamped and oscillating with a slowly decreasing amplitude. For $\zeta = 3.0$ the system is overdamped and the positions never reach their trajectories. Both of these values of ζ result in undesired oscillations of the pendulum. The chosen $\zeta = 0.7$ is slightly overshooting the positions and has small oscillations of the payload, but is quickly in a stable state.

6.2. Cyclical Trajectories

More is required of the controller when the cyclical trajectory of the attachment point is inserted. Figure 5.9 shows that both angles ϕ_x and ϕ_y converge at about 15 s which is similar to when the trajectories were constant. When the desired position of the attachment point was constant at 2.5 m a longer change in position was demanded so that the converging occurs after a similar duration is not surprising. Worth noting is that the angles do not oscillate after the initial stabilization. For the attachment point's position, it is clear that the stabilization of the pendulum is requiring unwanted motion in the first 10 s where the position is over 1 m away from its desired location in the x direction, and about 1 m away in the y direction. It should also be noted that there is a 10 s delay which is due to processing time and should be taken into account when applying to a physical system.

6.3. Velocity as Input

In section 3.15 an alternative way of determining the acceleration of the attachment point was introduced, and the comparison of the two is shown in Figure 5.10. It shows that the two accelerations coincide within a reasonable amount of accuracy, and the zoomed plots in Figure 5.10 show that the difference is about 1/100 s. The resulting plots of the attachment point's motion are shown in Figure 5.11. The differences are unnoticeable which confirms that it is a feasible alternative to the actual acceleration.

6.4. Moving Attachment Point in x, y and z Direction

In section 5.5 the working space of the attachment point is extended to a three dimensional motion. The motion in the z direction seems to have little to none impact on the systems ability to follow the trajectory in the x and y direction. In Equation 3.84 and Equation 3.85 the term that includes the acceleration in the z direction is $\frac{1}{L}\ddot{z}_0 s_x s_y$ and $\frac{1}{L}\ddot{z}_0 c_x s_y$. With the angles ϕ_x and ϕ_y being close to zero makes the values of s_x and s_y close to zero which results in the impact on the system minimal.

6.5. Moving Attachment Point and Varying Rope Length

Another addition to the system is the varying rope length. In Figure 5.13 change in rope length from 0.1 m to 2, 5 m is tested. Similarly to the adding of 3D motion, seems the system to take little effect of this change, other than that the amplitude of the motion in all directions is slightly less than their respective trajectories. It seems that the control gains for the rope length are too small to reach the desired rope length within a time that is satisfactory, so in Figure 5.14 the gain is doubled, and the system reaches $L = 2.5\,\mathrm{m}$ after about 40 s. The controller is now struggling slightly more to follow the trajectory for the first part of the simulation but is still not far off. Again must the a compromise be regarding what is most important of reaching the desired rope length or following the trajectory closely.

When the rope length decreases instead of increases, shown in Figure 5.15, the trajectory is initially harder to follow, but when the system has caught opp with the trajectory follows it very closely. The motion, will initially cause a bigger offset in the angles and therefore a bigger impact on the position of the attachment point, when the rope length is large.

6.6. Planned Trajectory - Constant Rope Length

For a more practical approach with a planned trajectory is tested. With a constant rope length initially shown in Figure 5.16-Figure 5.20. It is seen from Figure 5.16 that the system is able to follow that trajectory within a few seconds when $t_f = 100\,\mathrm{s}$, but not as well when $t_f = 50\,\mathrm{s}$. The controller is instructed to move along the trajectory within the time defined. When $t_f = 50\,\mathrm{s}$ and $t_s = 20\,\mathrm{s}$ is the time this path has to be made 10 s, which is not enough. And the last figure in Figure 5.16 confirms that.

In Figure 5.13 it could be seen that the system struggled with the first seconds where all the movement happens at the same time. The instruction the system is receiving, is therefore, to raise the crane before starting on the trajectory in the xy plane. When the total duration of the simulation is set to $t_f = 100\,\mathrm{s}$, shown in Figure 5.17 and Figure 5.18 the system is able to follow the trajectories in the x, y, and z direction. It seems as the initial angles of ϕ_x and ϕ_y are demanding some drastic changes in the velocity and acceleration which might be a problem when integrating the controller in a physical system.

When $t_f = 50$, Figure 5.19 and Figure 5.20, it is seen that the system is finding difficulties reaching the desired velocity and acceleration, but the motion is also here not far from the trajectories.

6.7. Planned Trajectory - Varying Rope Length

Instead of using the crane to move the payload in the z direction, hoisting is attempted in section 5.8. As expected is the initial disturbances more crucial here, given that the rope length is 0.5 m longer than in section 5.7. From Figure 5.22 and Figure 5.23 it is shown that after the rope length has reached its desired value, the trajectory is followed by only a small error. It seems as if this approach is superior to the previous if the situations where $t_f = 50\,\mathrm{s}$. The hoisting itself does not cause much noise to the damping of the oscillations, and after it is hoisted to its desired length, it follows the trajectory well.

6.8. Actuators

For implementing this on a physical crane, the motion of the joint angles θ_1, θ_2 and θ_3 are plotted in section 5.9. It is desirable and crucial that the plots are smooth. When the rope length is constant is it seen from Figure 5.26-Figure 5.29 that both the joint variables and linear actuators are moving smoothly except for when $t_f = 50\,\mathrm{s}$ and $t_s = 20\,\mathrm{s}$. It is not surprising that the action demanded by the actuators are more present when the hoisting is done by the crane than when it is done by varying the rope length, as seen in Figure 5.30-Figure 5.33. The actuators should ideally be constant when the rope length is varying, which is not the case. This means that the system uses the actuators actively to stabilize the payload.

Chapter 7.

Simulink Implementation

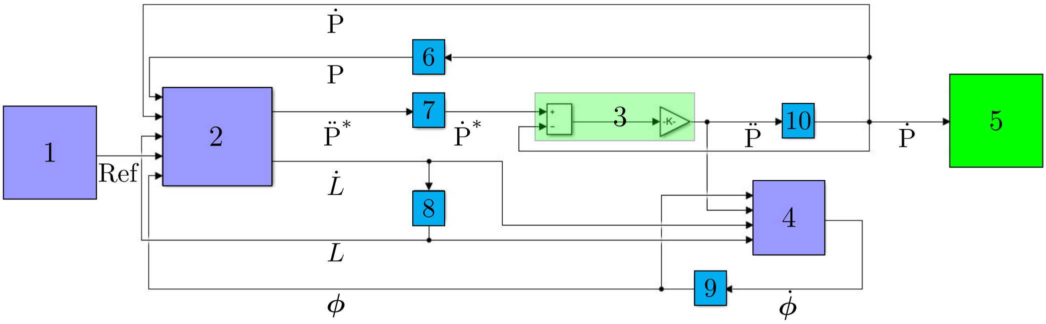

Figure 7.1.: Flowchart of Simulink system: (1) trajectory, (2) controller, (3) velocity loop, (4) spherical pendulum, (5) actuator, and (5-9) integrators. (The variables are placed under their respective lines.)

For the simulations, Simulink was used with build-in Matlab functions. The system is depicted in Figure 7.1. The blue boxes are Matlab functions, the green boxes are subsystems and the cyan boxes are integrals. Note that an asterisk is used for the acceleration and velocity that goes into the velocity loop, while the acceleration and resulting velocity out of the velocity loop is without the asterisk.

All Matlab functions and the can be found in the section A.2

7.1. Matlab Functions

7.1.1. Trajectory

The desired trajectory of the end-effector is found using the theory from section 2.6. The function, which can be found in subsection A.2.1, has the following inputs, which corresponds to the variables used in Chapter 4.

- Time, t
- Trajectory time, t_f
- Start time, t_s
- Distance from base to end-effector
- Angle of trajectory, θ
- Initial position of end-effector

and outputs the motion and velocity of the end-effector. The refernece to the rope length is included in the output via an external "repeating sequence" block or a step function.

7.1.2. Controller

The controller function (subsection A.2.2) takes in the following inputs

- Position of end-effector, P
- Velocity of end-effector, $\dot{\mathrm{P}}$
- Rope length, L
- Reference from "Trajectory", Ref
- The angles ϕ_x and ϕ_y, and their derivatives $\dot{\phi}_x$ and $\dot{\phi}_y$, $\boldsymbol{\phi}$

and outputs the acceleration of the end-effector, $\ddot{\mathrm{P}}^* = [\ddot{x}_0, \ddot{y}_0, \ddot{z}_0]^\mathrm{T}$, and the derivative of the rope length, $\dot{L}$, applying the damping equations from section 3.14. The initial values are set to $g = 9.81$, $\omega_0 = \sqrt{(g/L)}$, $\zeta = 1/\sqrt{2}$ and $\omega_{XY} = \omega_0/10$ as described in Chapter 5.

7.1.3. Spherical Pendulum

The function for the spherical (subsection A.2.3) has the following inputs

- Angles ϕ_x and ϕ_y, $\boldsymbol{\phi}$
- Acceleration of the end-effector, $\ddot{\mathrm{P}}$
- Rope length, L
- Derivative of the rope length, $\dot{L}$

Length	l_1	l_2	l_3					
Value, m	6.0	7.5	5.0					
Offset	a_{b2}	a_{p2}	a_{b3}	a_{p3}	e_{b2}	e_{p2}	e_{b3}	e_{p3}
Value, m	2.5	2.5	2.5	2.0	1.0	0.5	0.4	0.4

Table 7.1.: System parameters of knuckle boom crane

The output from this function is a vector

$$\dot{\boldsymbol{\phi}} = \begin{bmatrix} \dot{\phi}_x \\ \ddot{\phi}_x \\ \dot{\phi}_y \\ \ddot{\phi}_y \end{bmatrix} \tag{7.1}$$

where $\ddot{\phi}_x$ and $\ddot{\phi}_y$ are defined as in Equation 3.84 and Equation 3.85.

7.2. Subsystems

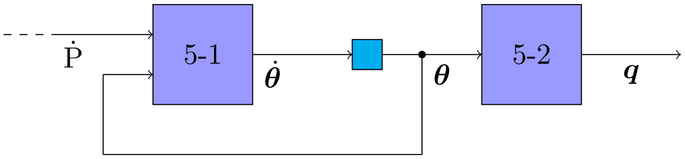

Figure 7.2.: Subsystem 5: (5-1) joint angle function, (5-2) is the actuator function.

Block 3 in Figure 7.1 is the velocity loop mentioned in section 3.15. The output from the controller, $\ddot{\mathrm{P}}^*$ is run through an integrator block and the resulting velocity $\dot{\mathrm{P}}^*$ fed into an adding block which subtracts the velocity $\dot{\mathrm{P}}$ and divides the sum by the time constant, $T_v = 0.3$ which is a preset value.

Block 5 consists of two Matlab functions as shown in Figure 7.2. The first (subsection A.2.4) one takes in the velocity of the end-effector, as in Equation 4.12, $\dot{\mathrm{P}}$, and the joint angles $\boldsymbol{\theta} = [\theta_1, \theta_2, \theta_3]^{\mathrm{T}}$ being fed back in a closed loop. The output is the derivative of the joint angle $\dot{\boldsymbol{\theta}}$ which is run through an integrator before being fed back. The joint angle vector is then the input in the second function in the subsystem (subsection A.2.5) which uses the equations from section 4.3. θ_1 is not used in this function, and the output is a vector $\boldsymbol{q} = [q_2, q_3]^{\mathrm{T}}$, which is the position of the linear actuators in the crane. The lengths of the system parameters are taken from [6] and are shown in Table 7.1.

Chapter 8.

Conclusion and Future Work

In this thesis, the stabilization of a spherical crane with a moving attachment point has been simulated by using Lagrangian kinematics and Euler angles. The simulations were done in Simulink and Matlab. The objective of the paper was to test a controller's ability to ensure both the stability and the desired position of the payload.

Several values of the control gains, K_p and K_d were tested in the simulations. Values between 0 and 1 were established as the best solution after extensive testing, and in order to define a system that is applicable for more than the specific initial values tested here, the values $K_p = \omega_{XY}^2$ and $K_d = 2\zeta\omega_{XY}$ were found to produce an output that was satisfactory. With these values of the control gains, was the system able to keep the angles close to equilibrium and followed the trajectory efficiently.

It is clear that when choosing the parameters one has to compromise between damping the payload oscillations and the ability to follow the trajectory. In practice, a crane in the right position can not lower an oscillating load. Therefore it is more crucial to damp the oscillation than to reach the desired position quickly. With the values found in this project, the oscillations are damped rapidly and the attachment point reaches the trajectory in a smooth fashion.

When applied to a practical scenario where the system tasks were split into three parts: Rising the payload 1.5 m, move the payload in a quarter-circular path, and ultimately lowering it 1.5 m. Various time spans were tested, and the joint angles and motion of the linear actuators were plotted to see if the output would be feasible for a physical crane. The system's outputs were satisfactory and the actuators were moving smoothly except for when the total duration of the simulation was 50 s, and the rise and lowering were executed by hoisting of the rope. The duration of the rise and lowering was 20 s which left 10 s to move the end-effector in the xy plane.

Another objective was to explore the opportunity to use a velocity loop to represent the acceleration of the end-effector using desired velocities v_x, v_y and v_z. The acceleration found using the loop was close the actual accelerations of the attachment point $\ddot{x}_0$ and $\ddot{y}_0$, and would be a natural par of the controller.

In order to get closer to a real-life situation, disturbances like wind or a moving base could be implemented to further test the controller's robustness. The rope in this thesis is considered stiff and mass-less. A crane with a heavy payload can behave like a double pendulum, which also could be interesting to use to test the controller. Knuckle boom cranes are, as mentioned in the introduction, used to do heavy lifting, usually outside. A good extension would be to simulate a payload with a certain geometry, for instance, a container. Together with a wind model could this be a very relevant task.

For the instances where a high-frequency oscillations occurred could it be possible to apply a low-pass filter to avoid potential challenges with implementing the controller to a physical crane, which is the most natural step - to implement the controller in a practical system and to see if the simulations match the practical experiments. In order to do so, the angles ϕ_x and ϕ_y must be measured. A possible solution could be computer vision for the detection, which is another potential extension to this thesis.

There are a lot of parameters included in this model, and choices had to be made regarding which parameters to test and which to leave constant. The time constant T_v used in the velocity loop was not tuned to find an optimal value. In order to ensure an acceleration as close to the theoretical value as possible would be a natural extension to this system. More situations and more trajectories could be tested, to further test the robustness of the controller.

References

[1] Department of Aerospace Engineering. *Frequency Response of Second-Order Systems*. URL: https://www.aero.iitb.ac.in/~bhat/frequency.html.

[2] M. A. Ahmad, R. E. Samin, and M. A. Zawawi. "Comparison of Optimal and Intelligent Sway Control for a Lab-Scale Rotary Crane System". In: *2010 Second International Conference on Computer Engineering and Applications*. Vol. 1. Mar. 2010, pp. 229–234. DOI: 10.1109/ICCEA.2010.52.

[3] David G. Alciatore and Michael B. Histand. *Introduction to Mechatronics and Measurement Systems*. 4th ed. McGraw-Hill, 2003.

[4] M.K. Bak, M.R. Hansen, and H.R. Karimi. "Robust Tool Point Control for Offshore Knuckle Boom Crane". In: *IFAC Proceedings Volumes* 44.1 (2011). 18th IFAC World Congress, pp. 4594–4599. ISSN: 1474-6670. DOI: https://doi.org/10.3182/20110828-6-IT-1002.03004. URL: http://www.sciencedirect.com/science/article/pii/S1474667016443326.

[5] Morten K. Bak and Michael R. Hansen. "Analysis of Offshore Knuckle Boom Crane - Part One: Modeling and Parameter Identification". In: *Modeling, Identification and Control* 34.4 (2013), pp. 157–174. DOI: 10.4173/mic.2013.4.1.

[6] Andrej Cibicik and Olav Egeland. "Dynamic modelling and force analysis of a knuckle boom crane using screw theory". In: *Mechanism and Machine Theory*. Vol. 133. 2019, pp. 179–194.

[7] Herbert Goldstein. *Classical Mechanics*. 3rd. Addison-Wesley, 2001. ISBN: 0201316110.

[8] Mahmud Iwan Solihin, Wahyudi, and Ari Legowo. "Fuzzy-tuned PID Anti-swing Control of Automatic Gantry Crane". In: *Journal of Vibration and Control*. Vol. 16. IEEE, Jan. 2010, pp. 127–145.

[9] Luc Jaulin. *Automation for robotics*. ISTE : Wiley, 2015. ISBN: 1119081424.

[10] Hassan K. Khalil. *Nonlinear Systems*. 3rd ed. Pearson, 2002.

[11] Karl Lukas Knierim, Kai Krieger, and Sawodny Oliver. "Flatness Based Control of a 3-DOF Overhead Crane with Velocity Controlled Drives". In: *IFAC Proceedings Volumes*. Vol. 43. Jan. 2010, pp. 363–368.

[12] J. L. Lagrange. *Mécanique Analytique.* 1811.

[13] L. M. Lyapunov. “The General Problem of the Stability of Motion”. Doctoral dissertation. Univ. Kharkov, 1892.

[14] Richard M. Murray, S. Shankar Sastry, and Li Zexiang. *A Mathematical Introduction to Robotic Manipulation.* 1st. Boca Raton, FL, USA: CRC Press, Inc., 1994. ISBN: 0849379814.

[15] R.M.T. Raja Ismail, M.A. Ahmad, M.S. Ramli, and F.R.M. Rashidi. “Nonlinear dynamic modelling and analysis of a 3-D overhead gantry crane system with system parameters variation”. In: *International Journal of Simulation: Systems, Science and Technology* 11.2 (2010). cited By 4, pp. 9–16. URL: `https://www.scopus.com/inward/record.uri?eid=2-s2.0-84855237094&partnerID=40&md5=0aed9fbc42dd85d6b31057e7602ee72a`.

[16] Liyana Ramli, Z. Mohamed, Auwalu M. Abdullahi, H.I. Jaafar, and Izzuddin M. Lazim. “Control strategies for crane systems: A comprehensive review”. English. In: *Mechanical Systems and Signal Processing* 95.C (2017), pp. 1–23. DOI: `10.1016/j.ymssp.2017.03.015`.

[17] Florentin Rauscher, Samuel Nann, and Sawodny Oliver. “Motion Control of an Overhead Crane Using a Wireless Hook Mounted IMU”. In: *2018 Annual American Control Conference (ACC).* IEEE, June 2018.

[18] Bruno Siciliano, Lorenzo Sciavicco, Luigi Villani, and Giuseppe Oriolo. *Robotics: modelling, planning and control.* Springer Science & Business Media, 2010.

[19] William Singhose, Lisa Porter, Michael Kenison, and Eric Kriikku. “Effects of hoisting on the input shaping control of gantry cranes”. In: *Control Engineering Practice* 8.10 (2000), pp. 1159–1165. ISSN: 0967-0661. DOI: `https://doi.org/10.1016/S0967-0661(00)00054-X`. URL: `http://www.sciencedirect.com/science/article/pii/S096706610000054X`.

[20] K. Song and Y. F. Xue. “Design of control system for knuckle boom crane”. English. In: *Mechanical Systems and Signal Processing* 624.C (2014), pp. 433–438.

[21] Jesper Kirk Sørensen, Michael R. Hansen, and Morten K. Ebbesen. “Numerical and Experimental Study of a Novel Concept for Hydraulically Controlled Negative Loads”. In: *Modeling, Identification and Control* 37.4 (2016), pp. 195–211. DOI: `10.4173/mic.2016.4.1`.

[22] Bajd Tadej, Mihelj Matjaž, and Munih Marko. *Introduction to Robotics.* Springer Netherlands : Imprint: Springer, 2013. ISBN: 9400761015.

[23] Geir O. Tysse, Andrej Cibicik, and Olav Egeland. “Vision-based control of a knuckle boom crane with online cable length estimation (In review)”. In: *IEEE/ASME Transactions on Mechatronics, (2019)* ().

[24] Lifu Wang, Hongbo Zhang, and Zhi Kong. “Anti-swing Control of Overhead Crane Based on Double Fuzzy Controllers”. In: *The 27th Chinese Control and Decision Conference (2015 CCDC)*. IEEE, July 2015, pp. 981–986.

[25] Tzu-Sung Wu, Mansour Karkoub, Wen-Shyong Yu, Chien-Ting Chen, Ming-Guo Her, and Kuan-Wei Wu. “Anti-sway tracking control of tower cranes with delayed uncertainty using a robust adaptive fuzzy control”. In: *Fuzzy Sets and Systems* 290 (2016). Theme: Control Engineering and Applications, pp. 118–137. ISSN: 0165-0114. DOI: `https://doi.org/10.1016/j.fss.2015.01.010`. URL: `http://www.sciencedirect.com/science/article/pii/S0165011415000305`.

Appendix A.

Appendix

A.1. Derivation of the Jacobian

$$\boldsymbol{p}_3 - \boldsymbol{p}_0 = \boldsymbol{p}_3 = \begin{bmatrix} c_1c_2c_3l_3 - c_1s_2s_3l_3 + c_1c_2l_2 \\ s_1c_2c_3l_3 - s_1s_2s_3l_3 + s_1c_2l_2 \\ s_2c_3l_3 + c_2s_3l_3 + s_2l_2 + l_1 \end{bmatrix}$$

$$\boldsymbol{p}_3 - \boldsymbol{p}_1 = \begin{bmatrix} c_1c_2c_3l_3 - c_1s_2s_3l_3 + c_1c_2l_2 \\ s_1c_2c_3l_3 - s_1s_2s_3l_3 + s_1c_2l_2 \\ s_2c_3l_3 + c_2s_3l_3 + s_2l_2 \end{bmatrix}$$

$$\boldsymbol{p}_3 - \boldsymbol{p}_2 = \begin{bmatrix} c_1c_2c_3l_3 - c_1s_2s_3l_3 \\ s_1c_2c_3l_3 - s_1s_2s_3l_3 \\ s_2c_3l_3 + c_2s_3l_3 \end{bmatrix}$$

This gives the velocity in the respective directions

$$
\begin{aligned}
[\boldsymbol{z}_0 \times (\boldsymbol{p_3} - \boldsymbol{p_0})]\dot{\theta}_1 &= \begin{bmatrix} 0 & -1 & 0 \\ 1 & 0 & 0 \\ 0 & 0 & 0 \end{bmatrix} \begin{bmatrix} c_1c_2c_3l_3 - c_1s_2s_3l_3 + c_1c_2l_2 \\ s_1c_2c_3l_3 - s_1s_2s_3l_3 + s_1c_2l_2 \\ s_2c_3l_3 + c_2s_3l_3 + s_2l_2 + l_1 \end{bmatrix} \dot{\theta}_1 \\
&= \begin{bmatrix} -s_1c_2c_3l_3 + s_1s_2s_3l_3 - s_1c_2l_2 \\ c_1c_2c_3l_3 - c_1s_2s_3l_3 + c_1c_2l_2 \\ 0 \end{bmatrix} \dot{\theta}_1 \\
[\boldsymbol{z}_1 \times (\boldsymbol{p_3} - \boldsymbol{p_1})]\dot{\theta}_2 &= \begin{bmatrix} 0 & 0 & -c_1 \\ 0 & 0 & -s_1 \\ c_1 & s_1 & 0 \end{bmatrix} \begin{bmatrix} c_1c_2c_3l_3 - c_1s_2s_3l_3 + c_1c_2l_2 \\ s_1c_2c_3l_3 - s_1s_2s_3l_3 + s_1c_2l_2 \\ s_2c_3l_3 + c_2s_3l_3 + s_2l_2 \end{bmatrix} \dot{\theta}_2 \\
&= \begin{bmatrix} -c_1(s_2c_3l_3 + c_2s_3l_3 + s_2l_2) \\ -s_1(s_2c_3l_3 + c_2s_3l_3 + s_2l_2) \\ c_1(c_1c_2c_3l_3 - c_1s_2s_3l_3 + c_1c_2l_2) + s_1(s_1c_2c_3l_3 - s_1s_2s_3l_3 + s_1c_2l_2) \end{bmatrix} \dot{\theta}_2 \\
[\boldsymbol{z}_2 \times (\boldsymbol{p_3} - \boldsymbol{p_2})]\dot{\theta}_3 &= \begin{bmatrix} 0 & 0 & -c_1 \\ 0 & 0 & -s_1 \\ c_1 & s_1 & 0 \end{bmatrix} \begin{bmatrix} c_1c_2c_3l_3 - c_1s_2s_3l_3 \\ s_1c_2c_3l_3 - s_1s_2s_3l_3 \\ s_2c_3l_3 + c_2s_3l_3 \end{bmatrix} \dot{\theta}_3 \\
&= \begin{bmatrix} -c_1(s_2c_3l_3 + c_2s_3l_3) \\ -s_1(s_2c_3l_3 + c_2s_3l_3) \\ c_1^2(c_2c_3l_3 - s_2s_3l_3) + s_1^2(c_2c_3l_3 - s_2s_3l_3) \end{bmatrix} \dot{\theta}_3 \\
&= \begin{bmatrix} -c_1l_3(s_2c_3 + c_2s_3) \\ -s_1l_3(s_2c_3 + c_2s_3) \\ l_3(c_2c_3 - s_2s_3) \end{bmatrix} \dot{\theta}_3
\end{aligned}
$$

A.2. Matlab Files

A.2.1. Trajectory Function

```matlab
function [x,y,z,dx,dy,dz] = Trajectory(tf,t,ts,r,ang,p0)
%For the xy plane
s=0;
ds=0;
tf1=tf-2*ts;
t1=t-ts;
sf=r*ang;
ddsc=4*sf/tf1^2;
tc=tf1/2-0.5*sqrt((tf1^2*ddsc-4*sf)/ddsc);
if t1 <= 0
    s =0;
    ds =0;
elseif t1 <= tc
    s=0.5*ddsc*t1^2;
    ds=ddsc*t1;
elseif t1 <= tf1
    s=sf-0.5*ddsc*(tf1-t1)^2;
    ds=ddsc*(tf1-t1);
else
    s=sf;
    ds=0;
end

%For the z direction
tf2=ts;
z=p0(3);
zi=z;
dz=0;
zf=p0(3)+1.5;
ddzc=4*abs(zf-zi)/tf2^2;
tc=tf2/2-0.5*sqrt((tf2^2*ddzc-4*(zf-zi))/ddzc);
if t <= 0
    z =zi;
    dz =0;
elseif t <= tc
    z=zi+0.5*ddzc*t^2;
    dz=ddzc*t;
elseif t <= tf2-tc
```

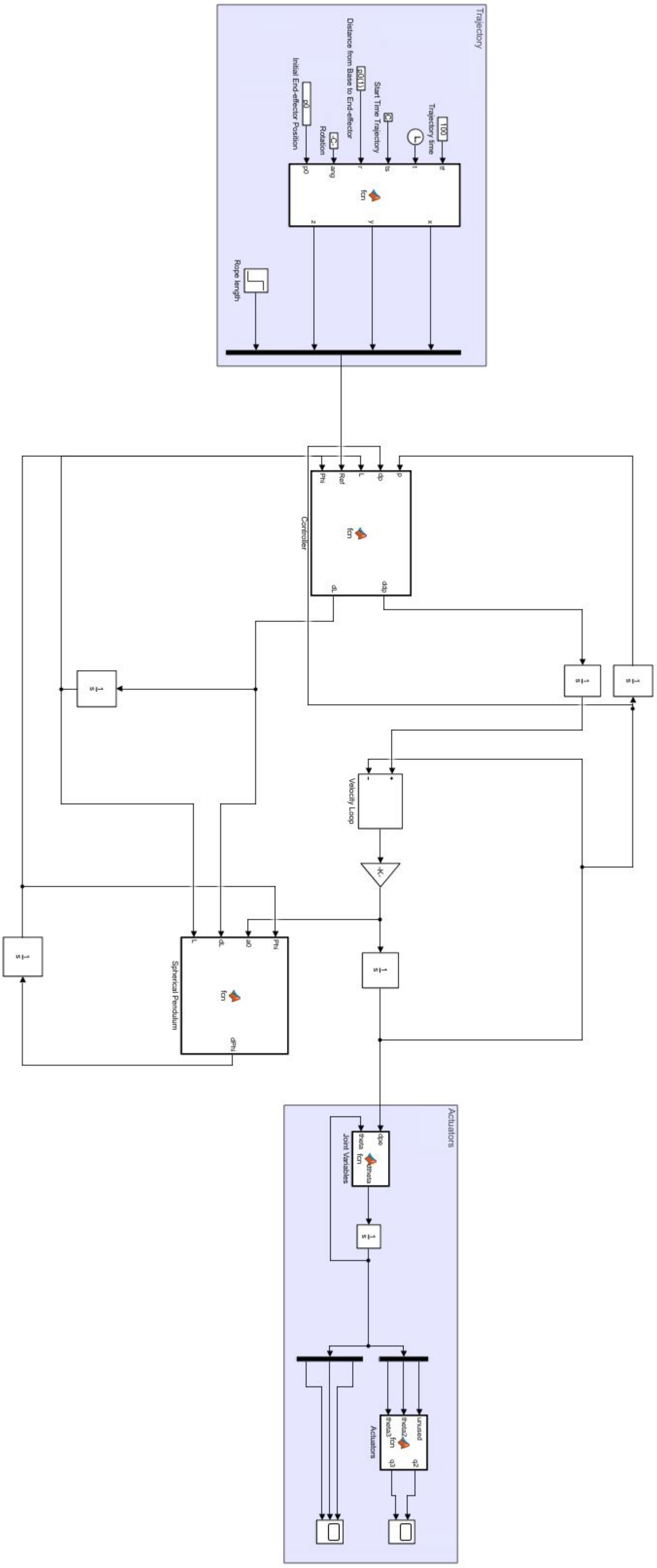

Figure A.1.: Simulink File

```
    z=ddzc*tc*(t-tc/2);
    dz=ddzc*t;
elseif t <= tf2
    z=zf-0.5*ddzc*(tf2-t)^2;
    dz=ddzc*(tf2-t);
else
    tf3=tf2;
    t3=t-(tf-ts);
    zi=p0(3)+1.5;
    dz=0;
    zf=p0(3);
    if t3 <= 0
        z =zi;
        dz =0;
    elseif t3 <= tc
        z=zi-0.5*ddzc*t3^2;
        dz=-ddzc*t3;
    elseif t3 <= tf3
        z=zf+0.5*ddzc*(tf3-t3)^2;
        dz=-ddzc*(tf3-t3);
    else
        z=zf;
        dz=0;
    end
end

%Transforming to position and velocity
p=[r*cos(s/r),r*sin(s/r),z]';
dpds=[-sin(s/r),cos(s/r)]';
dp=[dpds*ds;dz];

%Outputs
x=p(1);
y=p(2);
z=p(3);
dx=dp(1);
dy=dp(2);
dz=dz;
```

A.2.2. Contoller Function

```
function [ddp,dL] = Controller(p,dp,L,Lr,ref,Phi)

%inputs
phix = Phi(1); dphix = Phi(2);
phiy = Phi(3); dphiy = Phi(4);
x0 = p(1); dx0 = dp(1);
y0 = p(2); dy0 = dp(2);
z0 = p(3); dz0 = dp(3);


%Initial values
g = 9.81;
omega0 = 0.7;
zeta = 1/sqrt(2);
omegaXY = omega0*0.1;

%Control gains
Kp = omegaXY^2; Kd=2*zeta*omegaXY;

rx = ref(1);
ry = ref(2);
rz = ref(3);

%Abbreviations
w0 = omega0;
sx = sin(phix);
sy = sin(phiy);
cy = cos(phiy);

%Damping
ddy0 = 2*L*zeta*w0*dphix + Kp*(ry-y0) - Kd*dy0;
ddx0 = - 2*L*zeta*w0*dphiy - (1/cy)*sx*sy*ddy0 + Kp*(rx-x0
    ) - Kd*dx0;
ddz0 = Kp*(rz-z0) - Kd*dz0;

dL   = 4*Kp*(rL-L);
ddp=[ddx0,ddy0,ddz0]';
```

A.2.3. Spherical Pendulum Function

```
function dPhi = SphericalPendulum(Phi,ddp,dL,L)

%inputs
phix = Phi(1); dphix = Phi(2);
phiy = Phi(3); dphiy = Phi(4);


%Initial values
g = 9.81;
omega0 = sqrt(g/L);

%Abbreviations
w0 = omega0;
sx = sin(phix);
cx = cos(phix);
sy = sin(phiy);
cy = cos(phiy);

ddx0 = ddp(1);
ddy0 = ddp(2);
ddz0 = ddp(3);

%Equations of Motion
dPhi =  [dphix;
         (1/cy)*(-ddy0*cx/L - ddz0*sx/L ...
         + 2*dphix*dphiy*sy - 2/L*dL*dphix - w0^2*sx);
         dphiy;
         ddx0*cy/L + ddy0*sx*sy/L - ddz0*cx*sy/L ...
         - dphix^2*sy*cy - 2/L*dL*dphiy - w0^2*cx*sy];
```

A.2.4. Joint Angles Function

```
function dtheta = JointAngles(dp,q)
DH = [0, pi/2, 6, 0;
      7.5, 0, 0, 0;
      5, 0, 0, 0];
[J,~] = ForwKin(DH,q);
invJp = inv(J(1:3,1:3));
dtheta = invJp*dp;
```

A.2.5. Actuators Function

```
function [q2, q3] = Actuators(~,theta2,theta3)
a_b2 = 1.0;
a_p2 = 0.5;
e_b2 = 2.5;
e_p2 = 2.5;
b_21 = sqrt(a_b2^2+e_b2^2);
b_22 = sqrt(a_p2^2+e_p2^2);

a_b3 = 0.4;
a_p3 = 0.4;
e_b3 = 2.5;
e_p3 = 2.0;
b_31 = sqrt(a_b3^2+e_b3^2);
b_32 = sqrt(a_p3^2+e_p3^2);

alpha2 = atan(a_p2/e_p2);
beta2 = atan(a_b2/e_b2);

alpha3 = atan(a_p3/e_p3);
beta3  = atan(a_b3/e_b3);

q2 = sqrt(-2*b_21*b_22*cos(theta2-alpha2-beta2+pi/2) ...
     +b_21^2+b_22^2);
q3 = sqrt(-2*b_31*b_32*cos(theta3-alpha3-beta3+pi) ...
     +b_31^2+b_32^2);
```

A.2.6. Initial Simulink Function

```
%Denavit-Hartenberg Parameters
DH = [0, pi/2, 6, 0;
        7.5, 0, 0, 0;
        5, 0, 0, 0];

%Initial Angles
theta10 = 0;
theta20 = 45;
theta30 = -45;

theta_init=[theta10,theta20,theta30]'*pi/180;

%Jacobian and Transformation Matrix
[J,T]=ForwKin(DH,theta_init);

%Initial Position of End-effector
p0=T(1:3,4);

%Initial Rope Length
L0=1;
```

A.2.7. Complementary Functions

```
%Forward Kinematics
function [J, T] = ForwKin(DH, q)

%Transformation matrices
T01 = DH2T([DH(1,1:3),q(1)]);
T02 = T01*DH2T([DH(2,1:3), q(2)]);
T03 = T02*DH2T([DH(3,1:3), q(3)]);

%Position vectors
P0 = [0; 0; 0];
P1 = T01(1:3, 4);
P2 = T02(1:3, 4);
P3 = T03(1:3, 4);

%z vectors
Z0 = [0; 0; 1];
Z1 = T01(1:3, 3);
Z2 = T02(1:3, 3);

%Jacobian
J = [cross(Z0, P3-P0), cross(Z1, P3-P1), cross(Z2, P3-P2);
             Z0,               Z1,               Z2   ];

%Transformation Matrix
T = T03;
end
```

```
%Tranformation Matrix from Denavit-Hartenberg
function [T] = DH2T(DH)

%Denavit-Hartenberg Parameters
a = DH(1);
alpha = DH(2);
d = DH(3);
theta = DH(4);

%Transformation matrix
T = HRotZ(theta) * TranslZ(d) * TranslX(a) * HRotX(alpha);

end
```

```
%Rotation in Tranformation Matrix in the X Direction
function [T] = HRotX(angle)

T = [rotx(angle) [0 0 0]'; 0 0 0 1];

end
```

```
%Rotation in Tranformation Matrix in the Y Direction
function [T] = HRotY(angle)

T = [roty(angle) [0 0 0]'; 0 0 0 1];

end
```

```
%Rotation in Tranformation Matrix in the Z Direction
function [T] = HRotZ(angle)

T = [rotz(angle) [0 0 0]'; 0 0 0 1];

end
```

```
%Translation in the X Direction
function [T] = TranslX(x)

T = eye(4);
T(1,4) = x;

end
```

```
%Translation in the Y Direction
function [T] = TranslY(y)

T = eye(4);
T(2,4) = y;

end
```

```
%Translation in the Z Direction
function [T] = TranslZ(z)

T = eye(4);
T(3,4) = z;

end
```

```
%Rotation Matrix in the X Direction
function R = rotx(theta)

R = [1 0 0; ...
     0 cos(theta) -sin(theta); ...
     0 sin(theta) cos(theta)];

end
```

```
%Rotation Matrix in the Y Direction
function R = roty(theta)

R = [cos(theta) 0 sin(theta); ...
     0 1 0; ...
     -sin(theta) 0 cos(theta)];

end
```

```
%Rotation Matrix in the Z Direction
function R = rotz(theta)

R = [cos(theta) -sin(theta) 0; ...
     sin(theta) cos(theta) 0; ...
     0 0 1];

end
```

NTNU

Kunnskap for en bedre verden